

AD-A158 314

MULTI-DIMENSIONAL COMBUSTION INSTABILITY ANALYSIS OF
SOLID PROPELLANT ROCK. (U) ALABAMA UNIV IN HUNTSVILLE
DEPT OF MECHANICAL ENGINEERING T J CHUNG 15 MAY 85

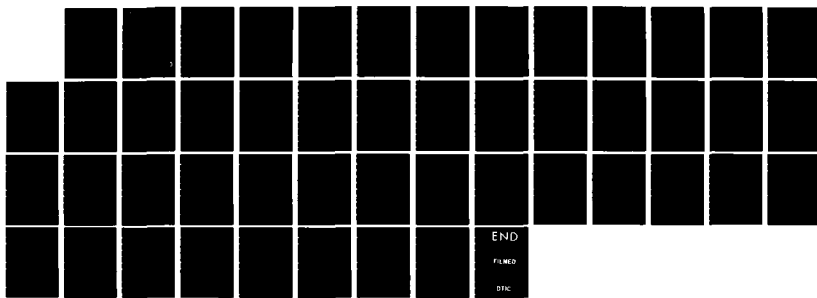
1/1

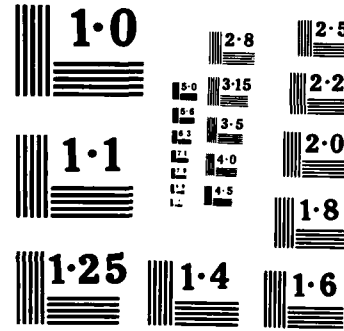
UNCLASSIFIED

AFOSR-TR-85-0567 AFOSR-83-0084

F/G 21/8.2

NL





NATIONAL BUREAU OF STANDARDS
MICROCOPY RESOLUTION TEST CHART

(2)

AFOSR-TR. 85-0567

MULTI-DIMENSIONAL COMBUSTION INSTABILITY ANALYSIS
OF SOLID PROPELLANT ROCKET MOTORS

AD-A158 314

T. J. Chung, Ph.D.
Department of Mechanical Engineering
The University of Alabama in Huntsville
Huntsville, Alabama 35899

May 14, 1985

FINAL REPORT
AFOSR83-0084

Prepared for
United States Air Force
Air Force Office of Scientific Research
Building 410
Bolling AFB, D. C. 20332

DTIC FILE COPY

Approved for public release;
distribution unlimited.

DTIC
ELECTE
AUG 26 1985
S D

85 8 21 044

UNCLASSIFIED

SECURITY CLASSIFICATION OF THIS PAGE

REPORT DOCUMENTATION PAGE

1a. REPORT SECURITY CLASSIFICATION UNCLASSIFIED		1b. RESTRICTIVE MARKINGS										
2a. SECURITY CLASSIFICATION AUTHORITY		3. DISTRIBUTION/AVAILABILITY OF REPORT Approved for public release; distribution is unlimited.										
2b. DECLASSIFICATION/DOWNGRADING SCHEDULE												
4. PERFORMING ORGANIZATION REPORT NUMBER(S)		5. MONITORING ORGANIZATION REPORT NUMBER(S) AFOSR-TR- 85-0567										
6a. NAME OF PERFORMING ORGANIZATION The University of Alabama in Huntsville	6b. OFFICE SYMBOL (If applicable)	7a. NAME OF MONITORING ORGANIZATION Air Force Office of Scientific Research										
6c. ADDRESS (City, State and ZIP Code) Huntsville, AL 35899		7b. ADDRESS (City, State and ZIP Code) Bolling Air Force Base, D.C. 20332-6448										
8a. NAME OF FUNDING/SPONSORING ORGANIZATION Air Force Office of Scientific Research	8b. OFFICE SYMBOL (If applicable)	9. PROCUREMENT INSTRUMENT IDENTIFICATION NUMBER AFOSR 83-0084										
8c. ADDRESS (City, State and ZIP Code) Bolling Air Force Base, D.C. 20332-6448		10. SOURCE OF FUNDING NOS. <table border="1"><tr><td>PROGRAM ELEMENT NO.</td><td>PROJECT NO.</td><td>TASK NO.</td><td>WORK UNIT NO.</td></tr><tr><td>61102F</td><td>2308</td><td>A1</td><td></td></tr></table>		PROGRAM ELEMENT NO.	PROJECT NO.	TASK NO.	WORK UNIT NO.	61102F	2308	A1		
PROGRAM ELEMENT NO.	PROJECT NO.	TASK NO.	WORK UNIT NO.									
61102F	2308	A1										
11. TITLE (Include Security Classification) MULTI-DIMENSIONAL COMBUSTION INSTABILITY ANALYSIS OF SOLID ROCKET MOTORS		12. PERSONAL AUTHOR(S) T.J. Chung										
13a. TYPE OF REPORT FINAL	13b. TIME COVERED FROM <u>15Mar83</u> TO <u>14Mar85</u>	14. DATE OF REPORT (Yr., Mo., Day) May 15, 1985	15. PAGE COUNT									
16. SUPPLEMENTARY NOTATION												
17. COSATI CODES <table border="1"><tr><td>FIELD</td><td>GROUP</td><td>SUB. GR.</td></tr><tr><td></td><td></td><td></td></tr><tr><td></td><td></td><td></td></tr></table>		FIELD	GROUP	SUB. GR.							18. SUBJECT TERMS (Continue on reverse if necessary and identify by block number) combustion instability, acoustic-hydrodynamic interaction, response function, particle damping	
FIELD	GROUP	SUB. GR.										
19. ABSTRACT (Continue on reverse if necessary and identify by block number) <p>Analytical models are developed for the multi-dimensional combustion instability analysis of solid propellant rocket motors. This research was motivated by the need for improvement of the current practice in combustion instability analysis. For example, the burning rates and response functions are affected by the extremely complex flowfield. The flow is three-dimensional or at least two-dimensional in axisymmetric geometries; vortex motions and turbulent flows must be adequately calculated; the coupling mechanism of acoustic and hydrodynamic wave oscillations and particle damping should be clarified. These flowfield phenomena, after all, are originated from the flame zone activities - oscillatory behavior of all field variables such as temperature, velocity, pressure, density of the gas, and fuel fractions. The response functions, which serve as boundary conditions for the flowfield, can be calculated from the first and second order perturbation eigenvalue analyses of the flame zone governing equations. The effect of velocity coupling appears, naturally, in the second order (nonlinear) solutions. All calculations are carried out using the finite</p>												
20. DISTRIBUTION/AVAILABILITY OF ABSTRACT UNCLASSIFIED/UNLIMITED <input checked="" type="checkbox"/> SAME AS RPT. <input type="checkbox"/> DTIC USERS <input type="checkbox"/>		21. ABSTRACT SECURITY CLASSIFICATION Unclassified										
22a. NAME OF RESPONSIBLE INDIVIDUAL LEONARD H CAVENY		22b. TELEPHONE NUMBER (Include Area Code) (202) 767-4937	22c. OFFICE SYMBOL AFOSR/NA									

UNCLASSIFIED

SECURITY CLASSIFICATION OF THIS PAGE

element method. Some of the findings are summarized below.

A consistent derivation of stability integrals for the growth constants associated with acoustic and vortical oscillations leads to various terms which have appeared for the first time. As a special, the flow turning terms arise as a consequence of integration by parts twice of the convective terms. The convection into the domain at a low frequency leads to the loss of energy, a trend reversed at a higher frequency, resulting in the gain of energy. This phenomenon is contrary to the case of surface convection, which is considered to be the effect of the turbulent mean flowfield. Unstable motions at low frequencies appear to be the result of turbulent flow, increasing in magnitude for large transition angles. There exists a combination of any acoustic frequency and any other vortical frequency which may produce a certain state of stable or unstable motion. Excitation of such frequencies may not be assured for all combinations. Stability boundaries, similar to those calculated by the Orr-Sommerfeld equation, are constructed for a given acoustic frequency, resulting in multiple islands. The effect of turbulent flow on stability boundaries is to expand their size and to move toward lower vortical frequencies, with large bay areas indicating stable regions for certain combinations of vortical frequencies and Reynolds numbers.

A rigorous formulation of the governing equations for particle damping involved in interactions of acoustic oscillations with vertical oscillations is derived. Simple examples of two-dimensional axisymmetric geometries are solved and compared with one-dimensional approximations. It is shown that there is a trend toward decreases in stability with a decrease in frequencies. However, the one-dimensional calculation overestimates the stability at higher frequencies. The optimum ranges of diameters for stability, however, are approximately the same in both cylindrical and one-dimensional geometries.

Based on the first and second order perturbation eigenvalue analyses of the flame zone, significant new results have been obtained. Calculations are based on impressed pressure waves and various radiative heat transfer parameters. Spatial distributions of field variables (pressure, density, velocity, temperature, and fuel fraction) indicate that the oscillatory behavior is pronounced at upstream and gradually diminishes toward downstream. Fluctuations of all field variables in the second order perturbation are relatively larger than those in the first order. Two-dimensional response functions are multi-peaked over all wave frequency ranges, and they also become negative as energy sinks. The combined effect of radiation and wave frequency upon response functions is significant at downstream for the first order system, whereas the effect observed at upstream and midstream is more pronounced in the second order perturbation as compared to the first order. Furthermore, the radiative heat transfer and the wave incidence angle are likely to influence the response functions along the parallel direction, as well as normal to the burning surface. Most important of all, the velocity coupled responses are exhibited in the second order perturbation as a nonlinear behavior.

MULTI-DIMENSIONAL COMBUSTION INSTABILITY ANALYSIS
OF SOLID PROPELLANT ROCKET MOTORS

T. J. Chung, Ph.D.
Department of Mechanical Engineering
The University of Alabama in Huntsville
Huntsville, Alabama 35899

May 14, 1985

FINAL REPORT
AFOSR83-0084

Prepared for
United States Air Force
Air Force Office of Scientific Research
Building 410
Bolling AFB, D. C. 20332

AIR FORCE OFFICE OF SCIENTIFIC RESEARCH (AFOSR)
NOTICE OF TECHNICAL APPROVAL
This technical report has been reviewed and approved for distribution to the public by AFOSR.
Distribution is unlimited.
MATTHEW J. KLEIN
Chief, Technical Information Division

ACKNOWLEDGEMENT

This research was sponsored by the Air Force Office of Scientific Research under contract AFOSR 83-0084 with Dr. Leonard Caveny as technical monitor. Many graduate students have assisted in various stages of the investigation. Among them are P.K. Kim, J.L. Sohn, and S.C. Chen.

TABLE OF CONTENTS

1. RESEARCH OBJECTIVES	1
1.1 Overall Objectives	1
1.2 Specific Objectives	1
2. MEAN FLOW CALCULATIONS AND INTERACTIONS OF UNSTEADY ACOUSTIC AND VORTICAL OSCILLATIONS IN AXISYMMETRIC CYLINDRICAL CAVITY	2
2.1 Summary	2
2.2 References	3
3. PARTICLE DAMPING EFFECTS ON COMBUSTION INSTABILITY	5
3.1 Summary	5
3.2 References	5
4. UNSTEADY RESPONSE OF BURNING SURFACE IN SOLID PROPELLANT COMBUSTION	7
4.1 Summary	7
4.2 References	8
APPENDIX 1	10
APPENDIX 2	22
APPENDIX 3	30

SECTION I

RESEARCH OBJECTIVES

1.1 Overall Objectives

The subject of combustion instability in solid propellant rocket motors has been studied by many investigators for the past thirty years. Today, stable motors are designed routinely and there seems to be little apparent concern over combustion instability. Looking into the history of the developmental process, however, one finds that more than half of all the motors developed have been found unstable. If new designs for more powerful motors are proposed, a prediction as to stability would be difficult unless trial and error procedures are repeated with costly experiments.

The current practice for the prediction of combustion instability is based on crude approximations. In most of the design calculations, one-dimensional analyses are predominantly used. Seldom are the mean flow calculations performed using the most modern technology - computational fluid dynamics. In the cavity of the solid propellant rocket motor are the extremely complicated fluid mechanics problems - compressible viscous flow, vortex shedding, turbulent boundary layers, particle damping (two phase flow), etc. In addition, oscillatory motions are prevalent, with acoustic and hydrodynamic wave oscillations coupled together. The boundary conditions for this flowfield are the unsteady responses of the flame zone distribution of field variables (velocity, pressure, density, temperature, and fuel fractions). The system may be linearly or nonlinearly unstable. Steep-fronted waves, erosive burning, and high amplitude responses as related to the velocity-coupling are the recent subjects of interest which are not fully understood. It is clear that the motor consists of both flame zone and cavity, and that these two regions should not be separated in the analysis. Obviously, this is beyond the current state of the art, but it is toward this goal that our overall objective must be intended.

Analytical or numerical models should be developed such that future high performance motors are designed using the computerized procedure. These models must be based on adequate multi-dimensional governing equations and numerical methods. The results should also be verified by experimental measurements. The final product should then be facilitated by an interactive computer graphics system displaying, for example, computed waterfall data from which suitable design decisions can be made.

1.2 Specific Objectives

The overall objective stated above represents our ultimate goal. The research performed during the two year period consists of (1) mean flow calculations and interactions of unsteady acoustic and vortical oscillations in an axisymmetric cylindrical cavity, (2) particle damping effects on combustion instability, and (3) unsteady response of the burning surface in solid propellant combustion.

It is anticipated that these investigations will contribute to the foundations on which further advancements can be made in the future.

SECTION 2

MEAN FLOW CALCULATIONS AND INTERACTIONS OF UNSTEADY
ACOUSTIC AND VORTICAL OSCILLATIONS IN
AXISYMMETRIC CYLINDRICAL CAVITY

2.1 Summary

The flowfield, such as occurs in solid propellant rocket motors, offers a fertile ground for fundamental research in fluid mechanics and heat transfer. Combustion induces not only the mean flowfield, but also acoustic pressure oscillations and possibly vortex fluctuations together with turbulent shear boundary layers. Furthermore, shock waves are commonplace in most instances. Obviously, a most rigorous analysis taking into account all of these phenomena would be difficult, if not impossible. However, with the advent of the electronic computer and the modern technology of numerical methods, it has become feasible to resolve hitherto unsolved problems.

Despite difficulties in analytical and numerical solutions to the complex physical phenomena in a rocket motor chamber, many researchers have contributed to the advancement of analysis and design of successful rocket motors. A large body of literature exists relative to this subject, the study of which has been pioneered by Crocco [1], Cantrell and Hart [2], Culick [3,4], and others. Flandro and Jacobs [5], among others, have noted that vortex shedding may lead to an instability in solid propellant rocket motors. It is quite possible that high speed mean flows also affect the stability [6] significantly.

The basic mathematical formulations of combustion instability were contributed by Culick [3,4]. Recently, it has been observed in both full-scale firings and cold flow simulations that interactions of acoustic and hydrodynamic (vortical) instability can be significant [7-13]. Although it can be argued that the hydrodynamic instability may not occur in high Reynolds numbers, the turbulent shear layer instabilities have been found to be affected by various combinations of Strouhal numbers and Reynolds numbers. The acoustic field may interact with vortex motions known as the "feedback" resulting in the vortex generated sound [14]. Some studies [15,16] indicate that the vortices may undergo "clipping", a phenomenon corresponding to the vortex disruption. It is also possible that lateral periodic motion of the vortex street known as "jitters" may lead to partial or complete escape of the vortices [15,16]. Whether these conditions prevail in large rocket motors in which flow separations at interface restrictors or inhibitors are likely to produce vortex motion must be clarified. No simple models, such as hyperbolic tangent velocity profile for the shear layer [11,17] and temporal or spatial growth theories [18, 19], appear to be adequate for the interactions of acoustic and vortical oscillations in a rocket chamber.

In the previous papers [20-22], finite element applications to the combustion instability analysis were discussed. Although a rigorous mathematical formulation of the stability integral was presented, the mean flow calculations did not include turbulent flows. Since the turbulent flowfield is involved in shear boundary layers and vortex motions, it is intended that this subject be considered in the mean flow calculations and, subsequently, in the stability integral. Shock waves will not be included in the present report.

The numerical results for certain combinations of acoustic and vortical frequencies indicate that stability boundaries for acoustics-coupled hydrodynamic oscillations are somewhat similar to the classical hydrodynamic stability boundaries, but they occur in the form of multiple islands. The turbulent flowfield appears to contribute toward instability, and this trend increases with larger transition angles of the rocket motor cross-section. Details of mathematical formulations, numerical calculations, and example problems are presented in Reference [23] or Appendix 1.

2.2 References

1. Crocco, L. and Chen, S.I., "Theory of Combustion Instability in Liquid Propellant Rocket Motors", AGARDograph No. 8, Butterworth Scientific Publication, London, 1956.
2. Cantrell, R.H. and Hart, R., "Interaction Between Sound and Flow in Acoustic Cavities: Mass, Momentum, and Energy Considerations", Journal of the Acoustical Society of America, Vol. 36, April, 1964, pp. 697-706.
3. Culick, F.E.C., "The Stability of One-Dimensional Motions in a Rocket Motor", Comb. Sci. and Tech., Vol. 7, 1973, pp. 165-175.
4. Culick, F.E.C., "Stability of Three-Dimensional Motions in a Combustion Chamber", Comb. Sci. and Tech., Vol. 10, 1975, pp. 109-124.
5. Flandro, G.A. and Jacobs, H.P., "Vortex Generated Sound in Cavities", Progress in Aeronautics and Astronautics, Vol. 37, AIAA, 1975, pp. 521-533.
6. Flandro, G.A., "Stability Prediction for Solid Propellant Rocket Motors with High Speed Mean Flow", AFRPL-TR-79-98, 1980.
7. Culick, F.E.C. and Magiawala, F., "Excitation of Acoustic Modes in a Chamber by Vortex Shedding", Journal of Sound and Vibration, Vol. 64, No. 3, 1979.
8. Flandro, G.A., "Influence of Vortex Shedding on Acoustic Instability in Solid Propellant Rockets", 16th JANNAF Combustion Meeting, Sept., 1979.
9. Brown, R.S. et. al, "Vortex Shedding Studies", AFRPL-TR-80-13, April, 1980.
10. Brown, R.S. et. al, "Vortex Shedding as an Additional Source of Acoustic Energy in Segmented Solid Propellant Rocket Motors", AIAA paper NO. 80-1092, AIAA/SAE/ASME 16th Joint Propulsion Conference, June, 1980.
11. Michalke, A., "On the Inviscid Instability of the Hyperbolic-Tangent Velocity Profile", Journal of Fluid Mechanics, Vol. 19, 1964, pp. 543-556.
12. Martin, W.W., Naudascher, E. and Padmanabhan, M., "Fluid Dynamic Excitation Involving Flow Instability", Proc. ASCE, Vol. 101, 1975.
13. Cumpsty, N.A. and Whitehead, D.S., "The Excitation of Acoustic Resonances by Vortex Shedding", Journal of Sound and Vibration, Vol. 18, No. 3, 1971.
14. Yates, J.E., "Interaction with and Production of Sound by Vortex Flows", AIAA Paper No. 77-1352, AIAA 16th Aerospace Conference, 1977.

15. Rockwell, D. and Knisely, C., "The Organized Nature of Flow Impingement Upon a Corner", Journal of Fluid Mechanics, Vol. 93, Pt. 3, 1979.
16. Rockwell, D. and Knisely, C., "Vortex - Edge Interaction: Mechanisms for Generating Low Frequency Components", Phys. Fluids, Vol. 23, 1980.
17. Michalke, A., "Vortex Formation in a Free Boundary Layer According to Stability Theory", Journal of Fluid Mechanics, Vol. 22, Pt. 2, 1965.
18. Michalke, A., "On Spatially Growing Disturbances in an Inviscid Shear Layer", Journal of Fluid Mechanics, Vol. 25, Pt. 4, 1966, pp. 521-554.
19. Freymuth, P. "On Transition in a Separated Laminar Boundary Layer", Journal of Fluid Mechanics, Vol. 25, Pt. 4, 1966, pp. 683-704.
20. Chung, T.J., Hackett, R.M. and Kim, J.Y., "A New Approach to Combustion Analysis for Solid Propellant Rocket Motors", 19th JANNAF Combustion Meeting, Oct. 4-7, 1982, Greenbelt, MD.
21. Chung, T.J., Hackett, R.M., Chan, S.C., Moon, K.J. and Sohn, J.L., "Three-Dimensional Vorticity-Pressure Interactions in Combustion Instability Analysis", 20th JANNAF Combustion Meeting, Monterey, CA, Oct. 16-20, 1983.
22. Chung, T.J. and Chan, S.C., "Particle Damping Effects on Combustion Instability", 22nd AIAA Aerospace Science Meeting, Reno, Nevada, Jan. 9-12, 1984.
23. Chung, T.J. and Sohn, J.L., "Interactions of Unsteady Acoustic and Vortical Oscillations in Axisymmetric Cylindrical Cavity", AIAA paper 84-1635, 1984.

SECTION 3

PARTICLE DAMPING EFFECTS ON COMBUSTION INSTABILITY

3.1 Summary

The study of acoustic energy losses due to aluminum particles in the solid propellant rocket motor combustion chamber has been carried out by a number of investigators. Epstein and Charhart [1] studied the absorption of sound in suspensions of non-interacting inert spherical particles and uniform temperatures. The validity of this investigation was subsequently substantiated by other researchers [2-4]. In a rocket motor, the particles are neither spherical nor inert and subjected to nonuniform temperature distributions [5].

Despite the extensive research on the subject of acoustic energy dissipation due to particle damping in the rocket motor [5-10], calculations of the stability integral arising from particle damping are limited to simple one-dimensional cases.

Thus, the purpose of the present study is to demonstrate the feasibility of mathematical formulations and numerical calculations via finite elements. Furthermore, interactions of particle damping with fluid viscosity and heat transfer are included. It is shown that additional boundary and domain terms arise from integrating by parts "twice" of the Green function stability integral containing the momentum equation.

Simple example problems of two-dimensional axisymmetric geometries are solved and compared with one-dimensional approximations. It is shown that there is a trend toward decrease in stability with a decrease in frequencies. However, the one-dimensional calculation overestimates the stability at higher frequencies. The optimum ranges of diameters for stability, however, are approximately the same in both cylindrical and one-dimensional geometries. For the first axial and tangential modes, however, the trends are significantly different from those of the axial mode. The two-dimensional cylindrical system is more stable than the one-dimensional system for all frequencies. There is an indication that optimum particle diameters shift toward larger sizes as the frequencies decrease. For further details, see Reference [13] or Appendix 2.

3.2 References

1. Epstein, P.S. and Carhart, R.R., "The Absorption of Sound in Suspensions and Emulsions", Journal of Acoustic Society of America, Vol. 25, No. 3, 1953, pp. 553-565.
2. Dobbins, R.A. and Tempkin, S., "Measurement of Particulate Acoustic Attenuation", AIAA Journal, Vol. 2, No. 6, 1964, pp. 1106-1111.
3. Tempkin, S. and Dobbins, R.A., "Measurements of Attenuation and Dispersion of Sound by an Aerosol", Journal of Acoustic Society of America, Vol. 40, No. 5, 1966, pp. 1016-1024.

4. Tempkin, S. and Dobbins, R.A., "Attenuation and Dispersion of Sound by Particulate Relaxation Processes", J. Acoustic Society of America, Vol. 40, 1966, pp. 317-324.
5. Culick, F.E.C., "T-Burner Testing of Metalized Solid Propellants", AFRPL-TR-74-28, Oct. 1974.
6. Levine, J.N. and Culick, F.E.C., "Numerical Analysis of Nonlinear Longitudinal Combustion Instability in Metalized Solid Propellant Rocket Motors", 9th JANNAF Combustion Meeting, Sept., 1972.
7. Culick, F.E.C. and Levine, J.N., "Comparison of Approximate and Numerical Analysis of Nonlinear Combustion Instability", AIAA 12th Aerospace Science Meeting, 1974, AIAA paper No. 74-201.
8. Culick, F.E.C., "Stability of Three-Dimensional Motions in a Combustion Chamber", Combustion Science and Technology, Vol. 10, 1975, pp. 109-124.
9. Derr, R.L., Kraeutle, K.J., Mathes, H.B. nad Dehority, G.L., "Combustion Instability Studies Using Metalized Solid Propellants: Part I, Experimental Verification of Particle Damping Theory", 12th JANNAF Meeting, 1975, CPIA No. 273, Vol. II, pp. 155-165.
10. Kraeutle, K.J. and Derr, R.L., "Combustion Instability Studies Using Metallized Solid Propellants: Additional Experimental Evidence for the Validity of Particle Damping Theory", 13th JANNAF Combustion Meeting, Vol. II, Dec., 1976.
11. Chung, T.J., Hackett, R.M. and Kim, J.Y., "Recent Advances in Combustion Instability of Solid Propellant Rocket Motors", AIAA Journal, in press.
12. Chung, T.J., Finite Element Analysis in Fluid Dynamics, McGraw-Hill, 1978.
13. Chung, T.J. and Chan, S.C., "Particle Damping Effects on Combustion Instability", AIAA paper 84-0373, 1984.

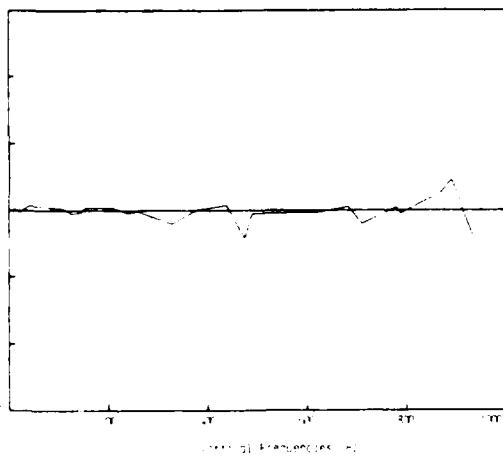


Fig. 7 Acoustics-coupled vorticity instability growth constants (α_H) versus vorticity frequencies, $\omega_N=2553$ Hz, $Re=10^3$, $\theta=20^\circ$, laminar flow

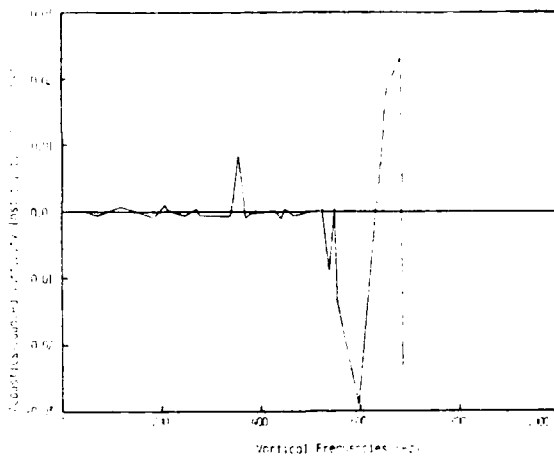


Fig. 9 Acoustics-coupled vorticity instability growth constants (α_H) versus vorticity frequencies, $\omega_N=2553$ Hz, $Re=10^3$, $\theta=34^\circ$, laminar flow

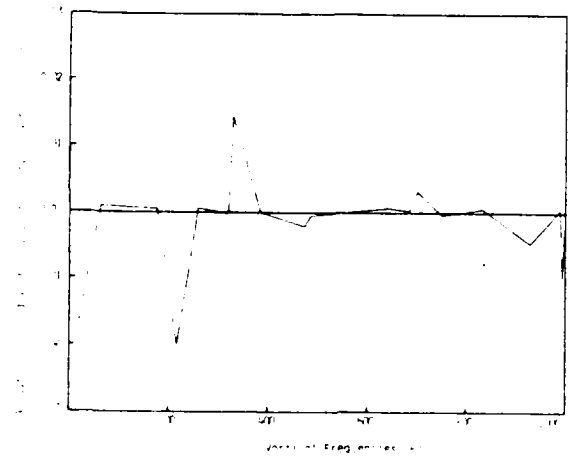


Fig. 8 Acoustics-coupled vorticity instability growth constants (α_H) versus vorticity frequencies, $\omega_N=2553$ Hz, $Re=10^3$, $\theta=20^\circ$, turbulent flow

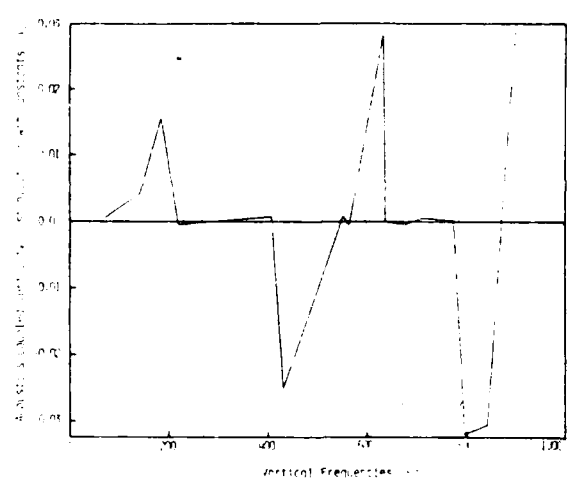


Fig. 10 Acoustics-coupled vorticity instability growth constants (α_H) versus vorticity frequencies, $\omega_N=2553$ Hz, $Re=10^3$, $\theta=34^\circ$, turbulent flow

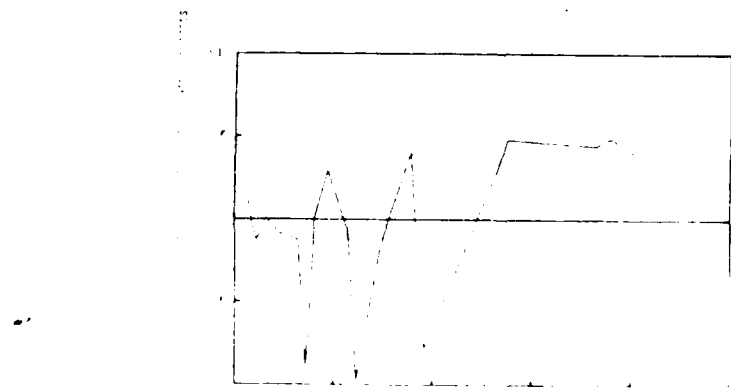


Fig. 11 Acoustics-coupled vorticity instability growth constants (α_H) versus vorticity frequencies, $\omega_N=34$ Hz, $Re=10^3$, $\theta=14^\circ$, turbulent flow

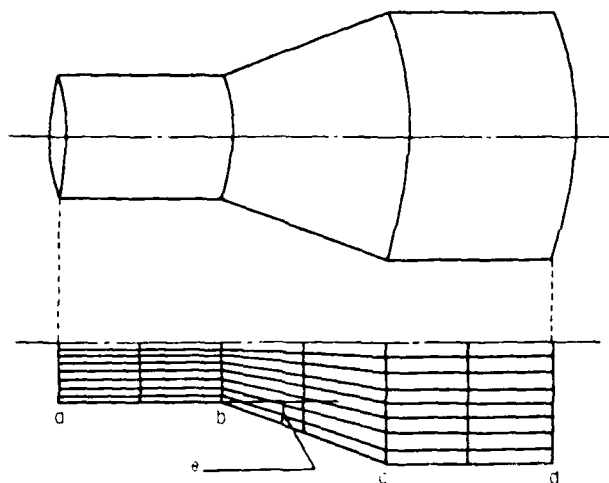


Fig. 1 Axisymmetric cylindrical geometry of a solid propellant rocket motor and finite element modeling with various transition angles: $\theta=14^\circ, 20^\circ, 34^\circ$ (48 linear isoparametric elements, 63 global nodes)

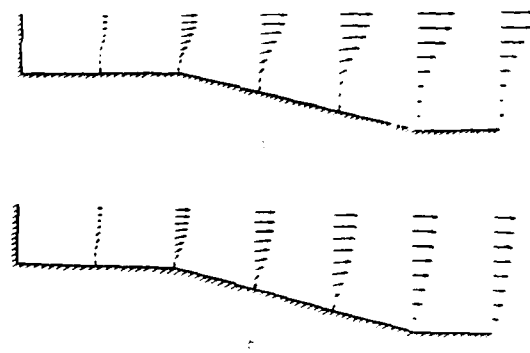


Fig. 2 Patterns of mean flow fields, (a) laminar flow, (b) turbulent flow, $Re=10^3$, $\theta=14^\circ$

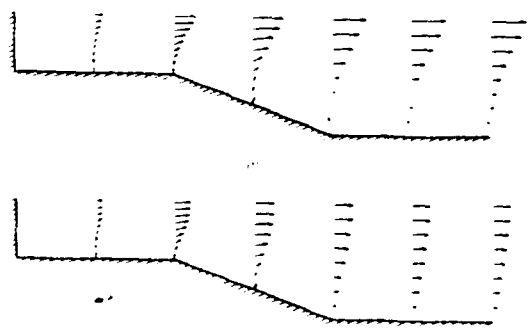


Fig. 3 Patterns of mean flow fields, (a) laminar flow, (b) turbulent flow, $Re=10^3$, $\theta=20^\circ$

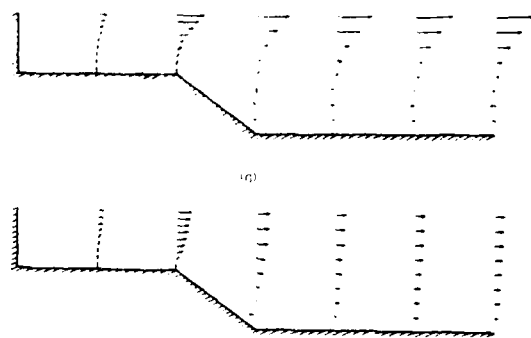


Fig. 4 Patterns of mean flow fields, (a) laminar flow, (b) turbulent flow, $Re=10^3$, $\theta=34^\circ$

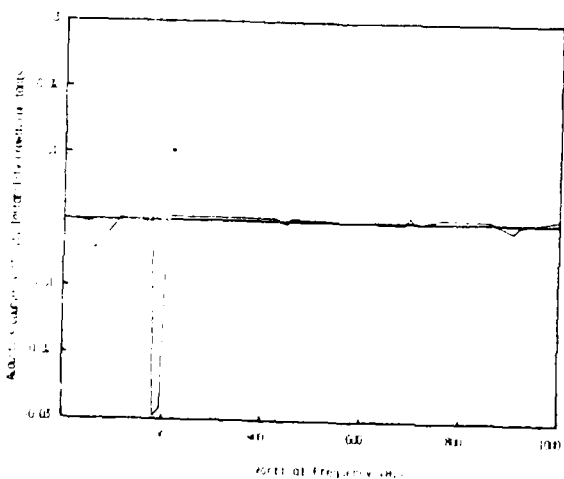


Fig. 5 Acoustics-coupled vorticity instability growth constants (α_H) versus vertical frequencies, $\omega_N=2553$ Hz, $Re=10^3$, $\theta=14^\circ$, laminar flow

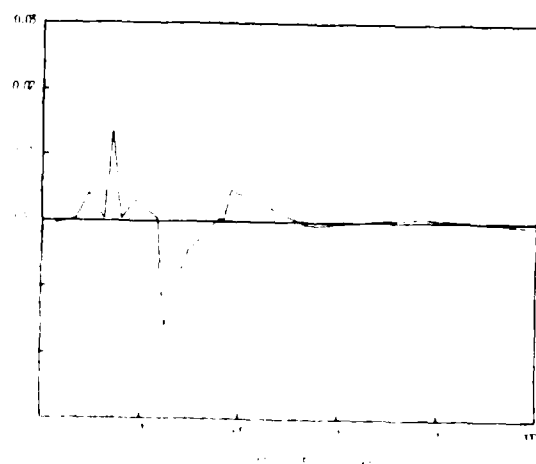


Fig. 6 Acoustics-coupled vorticity instability growth constants (α_H) versus vertical frequencies, $\omega_N=2553$ Hz, $Re=10^3$, $\theta=14^\circ$, turbulent flow

7. Culick, F.E.C. and Magiawala, K., "Excitation of Acoustic Modes in a Chamber by Vortex Shedding", Journal of Sound and Vibration, Vol. 64, No. 3, 1979.
8. Flandro, G.A., "Influence of Vortex Shedding on Acoustic Instability in Solid Propellant Rockets", 16th JANNAF Combustion Meeting, Sept., 1979.
9. Brown, R.S. et. al, "Vortex Shedding Studies", AFRPL TR 80-13, April, 1980.
10. Brown, R.S. et. al, "Vortex Shedding as an Additional Source of Acoustic Energy in Segmented Solid Propellant Rocket Motors", AIAA paper No. 80-1092, AIAA/SAE/ASME 16th Joint Propulsion Conference, June, 1980.
11. Michalke, A., "On the Inviscid Instability of the Hyperbolic-tangent Velocity Profile", Journal of Fluid Mechanics, Vol. 19, 1964, pp. 543-556.
12. Martin, W.W., Naudascher, E. and Padmanabhan, M., "Fluid Dynamic Excitation Involving Flow Instability", Proc. ASCE, Vol. 101, 1975.
13. Cumpsty, N.A. and Whitehead, D.S., "The Excitation of Acoustic Resonances by Vortex Shedding", Journal of Sound and Vibration, Vol. 18, No. 3, 1971.
14. Yates, J.E., Interaction with and Production of Sound by Vortex Flows", AIAA Paper No. 77-1352, AIAA 16th Aerospace Conference, 1977.
15. Rockwell, D. and Knisely, C., "The Organized Nature of Flow Impingement Upon a Corner", Journal of Fluid Mechanics, Vol. 93, Pt. 3, 1979.
16. Rockwell, D. and Knisely, C., "Vortex - Edge Interaction: Mechanisms for Generating Low Frequency Components", Phys. Fluids, Vol. 23, 1980.
17. Michalke, A., "Vortex Formation in a Free Boundary Layer According to Stability Theory", Journal of Fluid Mechanics, Vol. 22, Pt. 2, 1965.
18. Michalke, A., "On Spatially Growing Disurbances in an Inviscid Shear Layer", Journal of Fluid Mechanics, Vol. 25, Pt. 4, 1966, pp. 521-554.
19. Freymuth, P., "On Transition in a Separated Laminar Boundary Layer", Journal of Fluid Mechanics, Vol. 25, Pt. 4, 1966, pp. 683-704.
20. Chung, T.J., Hackett, R.M. and Kim, J.Y., "A New Approach to Combustion Analysis for Solid Propellant Rocket Motors", 19th JANNAF Combustion Meeting, Oct. 4-7, 1982, Greenbelt, M.D.
21. Chung, T.J., Hackett, R.M., Chan, S.C., Moon, K.J. and Sohn, J.L., "Three-Dimensional Vorticity-Pressure Interactions in Combustion Instability Analysis", 20th JANNAF Combustion Meeting, Monterey, CA, Oct. 16-20, 1983.
22. Chung, T.J. and Chan, S.C., "Particle Damping Effects on Combustion Instability", 22nd AIAA Aerospace Science Meeting, Reno, Nevada, Jan. 9-12, 1984.
23. Morse and Feshbach, "Methods of Theoretical Physics, Part I and II", McGraw-Hill, 1953.
24. Bradshaw, Cebeci, and Whitelaw, "Engineering Calculation Methods for Turbulent Flow", Academic Press, 1981.
25. Chung, T.J., "Finite Element Analysis in Fluid Dynamics", McGraw-Hill, 1978.
26. Li, Y.S. and Kot, S.C., "One-Dimensional Finite Element Method in Hydrodynamic Stability", International Journal for Numerical Methods in Engineering, Vol. 17, 1981, pp. 853-870.
27. Saraph, V.A., et. al, "Stability of Parallel Flows by the Finite Element Method", International Journal for Numerical Methods in Engineering, Vol. 14, 1979, pp. 1257-1270.
28. Orszag, S.A., "Accurate Solution of the Orr-Sommerfeld Stability Equation", Journal of Fluid Mechanics, Vol. 50, 1971, pp. 689-703.
29. Schlitzching, "Boundary Layer Theory", McGraw-Hill, 1960.
30. Taylor, C., "A Numerical Analysis of Turbulent Flow in Pipes", Computers and Fluids, Vol. 5, 1977, pp. 191-204.

Acoustic Frequency ω_N (Hz)		Surface Combustion (A)	Surface Convection (B)	Surface Viscous Damping (C)	Combustion into Domain (D)	Convection into Domain (E)	Viscous Momentum (F)	Dissipative Energy (G)	SUM	TOTAL $\alpha = \alpha_A + \alpha_H$
34	ω_A	15.458	4.176	0.0	1.842	-12.481	-0.3×10^{-4}	—	8.996	9.0153
	ω_H	—	0.0	0.0	—	0.019	0.0	0.0	0.0193	
476	ω_A	-34.255	-15.667	0.0	25.965	21.688	-0.005	—	-2.225	-2.1766
	ω_H	—	0.0	0.0	—	0.048	0.5×10^{-4}	-0.8×10^{-5}	0.0484	

Table 1. Contributions of various terms of stability integrals based on turbulent mean flow with ω_N (the vortical frequency) = 24 Hz, $Re=10^3$, $\theta=14^\circ$.

to the gain of energy, increasing with frequency. It is interesting to note that the trend of convection into domain (E) is opposite from the behavior of the surface convection. Note that energy is lost due to convection into the domain at a low frequency, but it gains at a higher frequency, contrary to the case of surface convection. This trend appears to be the result of the turbulent mean flow field.

Acoustics-coupled vorticity instability growth constants (α_H) versus vortical frequencies for the laminar flow, with $\omega_N = 2553$ Hz, $Re=10^3$, $\theta=14^\circ$, are shown in Fig. 5. In view of negligible positive growth constants, it is concluded that the system does not appear to be unstable. If turbulent flow is considered, however, several unstable motions at low frequencies are observed (Fig. 6). As the transition angle increases to $\theta=20^\circ$, the system gradually turns to instability at higher frequencies for laminar flow (Fig. 7). Such instability appears to occur at a lower frequency if turbulent flow is considered (Fig. 8). These trends are more pronounced as the transition angle is increased to $\theta=34^\circ$. To compare these observations with the case of a low acoustic frequency combination, the result of $\omega_N = 34$ Hz is investigated (Fig. 11). It is clear that, for a small transition angle ($\theta=14^\circ$), positive growth constants increase in magnitude significantly, not only at low frequencies, but also at high frequencies in contrast to the case of high acoustic frequency, $\omega_N = 2553$ Hz, as shown in Fig. 6.

The foregoing discussions on acoustics-coupled vortical instability lead us to a critical point of re-examination of the present theory. It is asserted that there exists a combination of any acoustic frequency with any other vortical frequency which may produce a certain state of stable or unstable motion. It is possible that not all combinations of acoustic and vortical frequencies theoretically postulated may be excited. In fact, only a limited number of combinations would be considered significant in practice. To determine whether any of the combinations of acoustic and vortical frequencies are excited, one may resort to the plots of both acoustic and vortical modes of all possible combinations, the process of which can easily be automated by means of computer graphics. Such an effort is currently under progress. As a result of this analysis, it is possible to construct stability boundaries similar to those via solutions of the Orr-Sommerfeld equation. It is seen that for $\omega_N = 2553$ Hz, $\theta=14^\circ$, the stability boundaries for acoustic-vorticity interactions with various vortical frequencies versus Reynolds numbers exhibit multiple islands as shown in Fig. 12 for the laminar flow. If turbulent flow is considered, however, the stability boundaries expand significantly in size, and move toward lower vortical frequencies. It is shown that the critical Reynolds number appears to be around 400-500. The most interesting aspect of the multiple-island stability boundaries is that large bay areas, which indicate stable regions, exist for certain combinations of vortical frequencies and Reynolds numbers. The trends observed herein are based on the limited number of data reductions. It is anticipated that more conclusive observations will be made available, pending additional computer graphics data reductions.

6. Conclusions

There are several major findings in this work. They are summarized as follows:

- (1) A consistent derivation of stability integrals for the growth constants associated with acoustic and vortical oscillations leads to various terms which have appeared for the first time. As a special case, the flow turning term arises as a consequence of integrations by parts twice of the convective terms.
- (2) The K- ϵ turbulence model appears to provide reasonable flow fields consistent with the transition angles of a circular cross-section, which are used in the calculation of growth constants.
- (3) The convection into domain at a low frequency leads to the loss of energy, a trend reversed at a higher frequency resulting in the gain of energy. This phenomenon is contrary to the case of surface convection, which is considered to be the effect of the turbulent mean flow field.
- (4) Unstable motions at low frequencies appear to be the result of turbulent flow, increasing in magnitude for larger transition angles.
- (5) There exists a combination of any acoustic frequency with any other vortical frequency which may produce a certain state of stable or unstable motion. Excitations of such frequencies may not be assured for all combinations.
- (6) Stability boundaries similar to those as calculated by the Orr-Sommerfeld equation are constructed for a given acoustic frequency, resulting in multiple islands.
- (7) The effect of turbulent flow on stability boundaries is to expand their sizes and to move toward lower vortical frequencies, with large bay areas indicating stable regions for certain combinations of vortical frequencies and Reynolds numbers.

References

1. Crocco, L. and Chen, S.I., "Theory of Combustion Instability in Liquid Propellant Rocket Motors", AGARDograph No. 8, Butterworth Scientific Publication, London, 1956.
2. Cantrell, R.H. and Hart, R., "Interaction Between Sound and Flow in Acoustic Cavities: Mass, Momentum, and Energy Considerations", Journal of the Acoustical Society of America, Vol. 36, April, 1964, pp. 697-706.
3. Culick, F.E.C., "The Stability of One-Dimensional Motions in a Rocket Motor", Comb. Sci. and Tech., Vol. 7, 1973, pp. 165-175.
4. Culick, F.E.C., "Stability of Three-Dimensional Motions in a Combustion Chamber", Comb. Sci. and Tech., Vol. 10, 1975, pp. 109-124.
5. Flandro, G.A. and Jacobs, H.P., "Vortex Generated Sound in Cavities", Progress in Aeronautics and Astronautics, Vol. 37, AIAA, 1975, pp. 521-533.
6. Flandro, G.A., "Stability Prediction for Solid Propellant Rocket Motors with High Speed Mean Flow", AFRPL-TR-79-98, 1980.

Similarly, for the K- α system, we have

$$\begin{bmatrix} \frac{\partial S_\alpha}{\partial K_B} & \frac{\partial S_\alpha}{\partial \epsilon_B} \\ \frac{\partial T_\alpha}{\partial K_B} & \frac{\partial T_\alpha}{\partial \epsilon_B} \end{bmatrix} \begin{bmatrix} (n) \\ (n+1) \end{bmatrix} = - \begin{bmatrix} S_\alpha \\ T_\alpha \end{bmatrix} \quad (71)$$

where

$$\frac{\partial S_\alpha}{\partial K_B} = \int_{\Omega} (\phi_\alpha \phi_B, i \phi_Y \bar{u}_Y, i + \frac{1}{Re_t \sigma_k} \phi_\alpha, j \phi_B, j) d\Omega \quad (72)$$

$$\frac{\partial S_\alpha}{\partial \epsilon_B} = \int_{\Omega} \phi_\alpha \phi_B d\Omega \quad (73)$$

$$\begin{aligned} \frac{\partial T_\alpha}{\partial K_B} = & \int_{\Omega} \{ \phi_\alpha \phi_B \phi_Y, j \phi_Y \bar{u}_n \bar{u}_j \\ & + \frac{1}{Re_t \sigma_\epsilon} (\phi_\alpha, j \phi_B + \phi_\alpha \phi_B, j) \phi_Y, j \epsilon_Y \} d\Omega \quad (74) \end{aligned}$$

$$\begin{aligned} \frac{\partial T_\alpha}{\partial \epsilon_B} = & \int_{\Omega} \{ \phi_\alpha \phi_B K \phi_B, j \phi_n \bar{u}_n \\ & + \frac{1}{Re_t \sigma_\epsilon} (\phi_\alpha, j \phi_K + \phi_\alpha \phi_K, j) \phi_B, j \\ & - \frac{1}{Re_t} \phi_\alpha \phi_B \phi_Y, j \bar{u}_i (\phi_n, j \bar{u}_n + \phi_n, i \bar{u}_n) \\ & + 2C_{\epsilon_2} \phi_\alpha \phi_B \phi_Y \epsilon_Y \} d\Omega \quad (75) \end{aligned}$$

and

$$\begin{aligned} S_\alpha = & \int_{\Omega} \{ \phi_\alpha \phi_B, j K \phi_B \bar{u}_Y, j + \frac{1}{Re_t \sigma_k} \phi_\alpha, j \phi_B, j K_B \\ & - \frac{1}{Re_t} \phi_\alpha \phi_B, j \bar{u}_B, j (\phi_Y, j \bar{u}_Y + \phi_Y, i \bar{u}_Y) \\ & + \phi_\alpha \phi_B \epsilon_B \} d\Omega - \int_{\Gamma} \frac{1}{Re_t \sigma_k} K, j \bar{u}_\alpha d\Gamma \quad (76) \end{aligned}$$

$$\begin{aligned} T_\alpha = & \int_{\Omega} \{ \phi_\alpha \phi_B K \phi_B \phi_Y, j \phi_n \bar{u}_n \\ & + \frac{1}{Re_t \sigma_\epsilon} (\phi_\alpha, j \phi_B K_B + \phi_\alpha \phi_B, j K_B) \phi_Y, j \epsilon_Y \\ & + C_{\epsilon_1} \phi_\alpha \phi_B \phi_Y \epsilon_Y \} d\Omega - \int_{\Gamma} \frac{1}{Re_t \sigma_\epsilon} \epsilon, j K \bar{u}_\alpha d\Gamma \quad (77) \end{aligned}$$

Simultaneous iterative solutions of Eqs. (71) provide the turbulent mean flow field. Together with the eigenvalue analyses for the acoustic field of Eq. (53) and the oscillatory vortical field given by Eq. (58), the turbulent mean flow calculations will then provide necessary information for the calculation of growth constants by means of Eqs. (33-35). The stability integrals as dictated by Eqs. (34-35) can be performed ideally by the Gaussian quadrature approximations [25].

5. Numerical Applications

To verify the validity of the theory and the

formulations presented in the previous sections, a typical solid propellant rocket motor with an axisymmetric cylindrical geometry has been analyzed. As shown in Fig. 1, 48 linear isoparametric elements with 63 global nodes are chosen to model the cavity geometry. Transition angles for the cross-section of the motor are varied $\theta=14^\circ, 20^\circ, 34^\circ$.

Various constants used in this analysis include the following:

Admittance, $AM = 10.0$ applied normal to the burning surface for the region designated by a through c (Fig. 1)

Empirical constants in turbulent mean flow

$$C_\mu = 0.09$$

$$\sigma_k = 1.0$$

$$\sigma_\epsilon = 1.208$$

$$C_{\epsilon_1} = 1.8$$

$$C_{F_2} = 0.6$$

Reynolds number, $Re = 10^3, 10^4, 10^5$

The results of mean flow calculations are shown in Figs. 2-4. In general, turbulent velocity profiles are steeper in the vicinity of the wall, and flatter in the core region of the combustion chamber than laminar velocity profiles. These variations are caused by the shear stresses which are increased by the turbulent effects [29], a similar trend as the turbulent pipe flow [30]. However, it should be noted that the recirculation, which would occur near downstream, is greatly suppressed since the admittance is applied normal to the burning surface, contrary to the usual entrance boundary condition of a pipe flow in which the boundary velocity is applied parallel to the axis. Separation and recirculation flows appear in both the laminar and the turbulent cases as the transition angles are increased. But, in a turbulent flow, they appear only at a relatively large transition angle since an increase of shear stresses with turbulence near the wall overcomes the effect of adverse pressure gradients.

Typical results for the growth constants, based on the turbulent mean flow, are shown in table 1, listing contributions of various terms in the stability integrals for the acoustic frequencies ($\omega_N = 34$ Hz, 476 Hz) in combination with the vortical frequency $\omega_v = 24$ Hz for Reynolds number $Re=10^3$, and transition angle $\theta=14^\circ$. Note that the so-called pressure coupling and velocity coupling defined as the surface combustion, designated as (A), provide a significant source of acoustic instability ($\alpha_A = 15.458$) for $\omega_N = 34$ Hz, whereas

for a higher acoustic frequency ($\omega_N = 476$ Hz), the acoustic growth constant assumes $\alpha_A = -34.255$, an indication of strong stability. The flow turning effect which is included in the surface convection, designated as (B), exhibits a similar trend as the surface combustion, but less in magnitude. For the Reynolds number and the transition angle investigated ($Re=10^3, \theta=14^\circ$), the effect of viscosity is negligible as indicated by (C), (F), and (G). However, it will be found in the later analysis that there is a significant contribution from the viscous terms through the mechanism of a vorticity generation in creating the Reynolds number-dependent stability boundaries. The combustion into the domain, as identified by (D), leads

tions 2 and 3.

4. Finite Element Analysis

The use of finite elements in fluid mechanics problems has increased significantly in recent years [25]. Especially, finite elements offer greater flexibilities for the complex geometry such as combustion chambers in the solid propellant rocket motors. In this paper, finite elements are used in three parts, i.e., the eigenvalue analysis in the classical acoustics and the oscillatory vortical field, calculations of mean velocity fields, and stability integrals.

First of all, we return to a classical acoustic problem characterized by Eqs. (24-25). Using Galerkin finite elements, Eq. (24) leads to

$$\int_{\Omega} (\rho_{N,ii} + k_N^2 \rho_N) \phi_{\alpha} d\Omega = 0 \quad (53)$$

where ϕ_{α} is the test function which is set equal to the trial function such that

$$\hat{\rho}_N(x_i) = \phi_{\alpha}(x_i) \hat{\rho}_{N\alpha} \quad (54)$$

Eq. (53) can be solved by the finite element eigenvalue equation of the form

$$|A_{\alpha\beta} - k_N^2 B_{\alpha\beta}| = 0 \quad (55)$$

where k_N is the wave number from which the acoustic frequency ω_N may be determined,

$$A_{\alpha\beta} = \int_{\Omega} \phi_{\alpha,i} \phi_{\beta,i} d\Omega \quad (56)$$

$$B_{\alpha\beta} = \int_{\Omega} \phi_{\alpha} \phi_{\beta} d\Omega \quad (57)$$

Similarly, the vortical fluctuation Eq. (51) is cast in the form

$$|A_{\alpha\beta}^{ik} + B_{\alpha\beta}^{ik} - k_c^{ik} C_{\alpha\beta}^{ik}| = 0 \quad (58)$$

where \hat{k} denotes the vortical wave number from which the vortical frequency $\hat{\omega}_N$ may be calculated.

$$A_{\alpha\beta}^{ik} = i \begin{bmatrix} A_{\alpha\beta,11}^{ik} & A_{\alpha\beta,12}^{ik} \\ A_{\alpha\beta,21}^{ik} & A_{\alpha\beta,22}^{ik} \end{bmatrix} \quad (59)$$

where

$$A_{\alpha\beta,11}^{ik} = \int_{\Omega} (\phi_{\alpha,i} \phi_{\beta,j} \bar{u}_j \bar{u}_i + \phi_{\alpha,i} \phi_{\beta,j} \bar{u}_i \bar{u}_j) d\Omega$$

$$A_{\alpha\beta,12}^{ik} = \int_{\Omega} \phi_{\alpha,i} \phi_{\beta,j} \bar{u}_j d\Omega$$

$$A_{\alpha\beta,21}^{ik} = \int_{\Omega} \phi_{\alpha,i} \phi_{\beta,j} \bar{u}_i d\Omega$$

$$A_{\alpha\beta,22}^{ik} = \int_{\Omega} (\phi_{\alpha,i} \phi_{\beta,j} \bar{u}_i \bar{u}_j + \phi_{\alpha,i} \phi_{\beta,j} \bar{u}_j \bar{u}_i) d\Omega$$

$$B_{\alpha\beta}^{ik} = \int_{\Omega} \phi_{\alpha,i} \phi_{\beta,j} \bar{u}_i \bar{u}_j d\Omega \quad (60)$$

$$C_{\alpha\beta}^{ik} = \int_{\Omega} \phi_{\alpha} \phi_{\beta} \delta_{ik} d\Omega \quad (61)$$

As a result, frequencies of normal acoustic modes and vortical oscillations can be obtained by taking the real parts of the eigenvalues of Eqs. (55,58), respectively. The vorticity growth constants can be obtained by taking the imaginary parts of the eigenvalues of Eq. (58) [26-29]. However, the imaginary parts of the eigenvalues of Eq. (55) are absent because the acoustic growth constants do not exist in the normal modes.

The mean flow calculations are performed under the assumption of a steady state, isothermal, incompressible flow. It follows, then, that the governing equations of the mean flow are simplified as follows:

$$\tilde{u}_{i,i} = 0 \quad (62)$$

$$\tilde{u}_{i,j} \tilde{u}_j + \frac{1}{\gamma} \tilde{p}_{,i} - \frac{1}{Re_{eff}} \tilde{u}_{i,j,j} = 0 \quad (63)$$

where

$$\frac{1}{Re_{eff}} = \frac{1}{Re} + \frac{1}{Re_t} \quad (64)$$

With an assumption of incompressible flow, the K- ϵ equations can be simplified as follows:

$$\tilde{u}_{i,k,i} - \left(\frac{1}{Re_t} \sigma_k \right)_{,j} - \frac{1}{Re_t} (\tilde{u}_{i,j} + \tilde{u}_{j,i}) \tilde{u}_{i,j} + \epsilon = 0 \quad (65)$$

$$\tilde{u}_{i,\epsilon,i} - \left(\frac{1}{Re_t} \sigma_{\epsilon} \right)_{,j} - \frac{C_{\epsilon_1}}{Re_t} \epsilon (\tilde{u}_{i,j} + \tilde{u}_{j,i}) \tilde{u}_{i,j} - C_{\epsilon_2} \frac{\epsilon^2}{K} = 0 \quad (66)$$

To solve these non-linear equations by Galerkin finite elements, the Newton-Raphson method is used. In order to reduce computational efforts, the Jacobian matrices for the flow field and the K- ϵ system are separated, which will then be updated iteratively between the two Jacobian matrices. The Newton-Raphson scheme for the velocity field is given by

$$J_{pq}^{(n)} \Delta x_q^{(n+1)} = -f_p^{(n)} \quad (67)$$

where

$$x_q^{(n+1)} = x_q^{(n)} + \Delta x_q^{(n+1)} \quad (68)$$

with

$$J_{pq}^{(n)} = \int_{\Omega} (\phi_{\alpha,i} \phi_{\beta,j} \delta_{ik} \bar{u}_j + \phi_{\alpha,i} \phi_{\beta,j} \bar{u}_i \bar{u}_j) d\Omega + \frac{\lambda}{\gamma} \phi_{i,i} \delta_{ik} + \frac{1}{Re_{eff}} \phi_{i,j} \delta_{ik} \tilde{u}_{j,j} \quad (69)$$

$$f_p^{(n)} = \int_{\Omega} (\phi_{\alpha,i} \phi_{\beta,j} \bar{u}_i \bar{u}_j + \frac{\lambda}{\gamma} \phi_{i,i} \phi_{\beta,j} \bar{u}_j) d\Omega + \int_{\Omega} \left(\frac{\lambda}{\gamma} \bar{u}_{i,j} \bar{u}_{i,j} \right) d\Omega + \frac{1}{Re_{eff}} \phi_{i,j} \phi_{\beta,j} \tilde{u}_{i,i} + \frac{1}{Re_{eff}} u_{i,j} \phi_{\beta,j} \tilde{u}_{i,i} \quad (70)$$

$$k_N = a\bar{k}_N, P = \bar{P}/P_0, u = \bar{u}/a, a = (\gamma P_0/\bar{P})^{1/2}$$

Substituting these relations and Eq. (31) to Eq. (34), collecting the first two terms of (A) and the flow turning term, and rewriting in the same form as Eq. (27), we obtain

$$(k^2 - k_N^2)E_N^2 = i\bar{a}k_N \int_T (\hat{u}^* \hat{P}_N + \frac{N}{\bar{P}a^2} \bar{u}) \cdot \bar{n} d\Gamma + i \frac{1}{\bar{P}a k_N} \int_T (\nabla \hat{P}_N)^2 \bar{P} \bar{u} \cdot \bar{n} d\Gamma \quad (36)$$

It is seen that $\bar{P} \bar{u} \cdot \bar{n}$ is equivalent to $\bar{M}_b \delta_{\parallel}$ in terms of the notations used in [4]. Notice that Eq. (36) above is the same as Eq. (4.14) in [4] neglecting the particle distribution of the two phase flow.

3. Turbulent Mean Flow And Fluctuation Vorticities

A glance at Eq. (33) with details given by Eqs. (34-35) indicates that the flow field, including the mean velocity and the vorticity together with the vortical component of the fluctuation velocity, as well as the acoustic pressure modes, must be calculated. To this end, we include turbulent effects on the mean flow field, but at this time, shock waves are excluded from consideration. Turbulent modelling for solid propellant rocket motors has been the subject of controversy particularly due to complex burning surface phenomena. Pending development of an adequate model in the future, we examine here the K- ϵ model for a computational purpose. Thus, the Reynolds decomposition becomes

$$u_i(x_j, t) = \bar{u}_i(x_j) + u_i^*(x_j, t) \quad (37)$$

Then, the time-averaged velocity is defined as

$$\bar{u}_i = \bar{p}u_i/\bar{P} \quad (38)$$

and

$$\bar{(p}u_i)^* = 0 \quad (39)$$

It follows that

$$\bar{p}u_i \bar{u}_j = \bar{p}u_i \bar{u}_j + \bar{(p}u_i)^* \bar{u}_j^* \quad (40)$$

where the bars, tildes and primes denote time-averaged, mean, and fluctuating values, respectively. Eqs. (37-40) refer to the time-averaged and fluctuating components of the scalar fields, P and T.

Substituting Eqs. (37-40) into Eqs. (1-4), the time-averaged governing equations are written as follows:

$$\frac{\bar{P}}{it} + (\bar{p}u_i)_{,i} = 0 \quad (41)$$

$$\frac{i}{it} (\bar{p}u_i) + [\bar{p}u_i \bar{u}_j + \bar{(p}u_i)^* \bar{u}_j^*]_{,j} + \frac{1}{\gamma} \bar{P}_{,i} - \frac{1}{Re} (\bar{u}_{i,jj} + \frac{1}{3} \bar{u}_{j,ji}) = 0 \quad (42)$$

$$\frac{2}{it} (\bar{T}) + [\bar{p}u_i \bar{T} + \bar{(p}u_i)^* \bar{T}^*]_{,i} - \frac{\gamma-1}{\gamma} (\bar{u}_i \bar{P}_{,i} + \bar{u}_i^* \bar{P}_{,i}^*) + \frac{\gamma-1}{Re} (\frac{2}{3} \bar{u}_{i,i} \bar{u}_{j,j} - \bar{u}_{i,j} \bar{u}_{j,i} - \bar{u}_{i,j} \bar{u}_{i,j})$$

$$+ \frac{2}{3} \bar{u}_{i,i} \bar{u}_{j,j} - \bar{u}_{i,j} \bar{u}_{j,i} - \bar{u}_{i,j} \bar{u}_{i,j} = 0 \quad (43)$$

$$\bar{P} = \bar{p} \bar{T} \quad (44)$$

In terms of the eddy viscosity hypothesis [30], the Reynolds stress $\bar{(p}u_i)^* \bar{u}_j$ can be expressed as

$$- \bar{(p}u_i)^* \bar{u}_j = \frac{1}{Re_t} \bar{u}_{i,j} \quad (45)$$

where

$$Re_t = P_0 a L / \mu_t \quad (46)$$

with μ_t being the eddy viscosity. The eddy viscosity can be expressed as a function of turbulent kinetic energy K and energy dissipation ϵ by the Prandtl-Kolmogorov law

$$\frac{1}{Re_t} = C_{\mu} D \frac{K^2}{\epsilon} \quad (47)$$

where C_{μ} is the empirical constant.

The governing equations for K and ϵ are derived from the momentum equation [24] as

$$\rho \frac{\partial K}{\partial t} + \bar{p} \bar{u}_i K_{,i} - (\frac{1}{Re_t \sigma_k} K)_{,j} - \frac{1}{Re_t} (\bar{u}_{i,j} + \bar{u}_{j,i}) \bar{u}_{i,j} + \rho \epsilon = 0 \quad (48)$$

$$\rho \frac{\partial \epsilon}{\partial t} + \bar{p} \bar{u}_i \epsilon_{,i} - (\frac{1}{Re_t \sigma_{\epsilon}} \epsilon)_{,j} - \frac{C_{\epsilon_1}}{Re_t} \frac{\epsilon}{K} (\bar{u}_{i,j} + \bar{u}_{j,i}) \bar{u}_{i,j} + C_{\epsilon_2} \rho \frac{\epsilon^2}{K} = 0 \quad (49)$$

in which the following non-dimensional quantities are used:

$$K = \bar{K}/a^2, \epsilon = \bar{\epsilon} L/a^3, Re_t = P_0 a L / \mu_t$$

Furthermore, σ_k and σ_{ϵ} are the effective Prandtl-Schmidt numbers, and C_{ϵ_1} and C_{ϵ_2} are the empirical constants.

In addition to the turbulent mean flow, we require that the vortical component of the fluctuation velocity and the fluctuation vorticity be calculated. In this regard, we set $u_i = \bar{u}_i + u_i^*$, $P=1$, and $\rho=1$ to obtain the first order perturbation momentum equation in the form

$$\frac{\partial u_i^*}{\partial t} + u_i^* \bar{u}_j + \bar{u}_i \bar{u}_j^* - \frac{1}{Re} (u_{i,jj}^* + \frac{1}{3} u_{j,ji}^*) = 0 \quad (50)$$

It follows from Eq. (17) and Eq. (50) that

$$i(\bar{u}_{i,j} \bar{u}_j + \bar{u}_{i,j} \bar{u}_j^* - \frac{1}{Re} (u_{i,jj}^* + \frac{1}{3} u_{j,ji}^*)) - Ku_i^* = 0 \quad (51)$$

The fluctuation vorticity is then calculated from

$$v_i^* = \epsilon_{ijk} K u_{k,j} \quad (52)$$

in which the vortical component of the fluctuation velocity $u_{k,j}^*$ is obtained as a consequence of Eq. (51).

In the sequel, we discuss finite element solutions to all of the equations presented in Sec-

constant α by equating the imaginary parts between Eqs. (27) and (29),

$$\begin{aligned}
 \alpha &= -\frac{1}{2E_N^2} \left[\int_{\Gamma} \{ Y \hat{u}_i^{(R)} \hat{p}_N n_i + (\gamma+1) \bar{u}_i \hat{p}_N^2 n_i \} \right. \\
 &\quad \left. + \frac{Y}{k_N} [\bar{u}_i (\hat{u}_j^* + \hat{u}_j^{(I)})^{(I)} + (\hat{u}_i^* + \hat{u}_i^{(I)})^{(I)} \bar{u}_j] \hat{p}_N n_j \right] \\
 &\quad - \frac{Y}{k_N \text{Re}} [(\hat{u}_i^* + \hat{u}_i^{(I)})^{(I)}] \hat{p}_N n_j \\
 &\quad + \frac{1}{3} (\hat{u}_j^* + \hat{u}_j^{(I)})^{(I)} \hat{p}_N n_i \} d\Gamma \\
 &\quad + \int_{\Omega} \{ -\bar{u}_i n_j \hat{p}_N^2 - (2\gamma+1) \bar{u}_i \hat{p}_N \hat{p}_N n_j \} \\
 &\quad - \frac{Y}{k_N} [\bar{u}_i (\hat{u}_j^* + \hat{u}_j^{(I)})^{(I)} + (\hat{u}_i^* + \hat{u}_i^{(I)})^{(I)} \bar{u}_j] \hat{p}_N n_i \\
 &\quad - \frac{Y}{k_N} [\bar{u}_i (\hat{u}_j^* + \hat{u}_j^{(I)})^{(I)} + (\hat{u}_i^* + \hat{u}_i^{(I)})^{(I)} \bar{u}_j] \hat{p}_N n_j \\
 &\quad + \frac{Y}{k_N \text{Re}} [(\hat{u}_i^* + \hat{u}_i^{(I)})^{(I)}] \hat{p}_N n_j + \frac{1}{3} (\hat{u}_j^* + \hat{u}_j^{(I)}) \hat{p}_N n_i \\
 &\quad + \frac{2Y(\gamma-1)}{\text{Re}} [\frac{2}{3} \bar{u}_i n_i (\hat{u}_j^* + \hat{u}_j^{(I)})^{(R)} \\
 &\quad - \bar{u}_i n_j (\hat{u}_j^* + \hat{u}_j^{(I)})^{(R)} - \bar{u}_j n_i (\hat{u}_j^* + \hat{u}_j^{(I)})^{(R)}] \hat{p}_N \} d\Omega \quad (30)
 \end{aligned}$$

where the superscripts (R) and (I) refer to the real and the imaginary parts, respectively.

The normal velocity at the surface can be expressed in terms of the admittance, $A = A^{(R)} + iA^{(I)}$, and the mean flow Mach number \bar{M} such that

$$\hat{u}_i n_i = (\hat{u}_i^{(R)} + i\hat{u}_i^{(I)}) n_i = \bar{M} \hat{p}_N / Y \quad (31)$$

whereas the acoustic fluctuation velocity in the domain is given by

$$\hat{u}_i^* = \frac{i}{k_N Y} \hat{p}_{N,i} \quad (32)$$

For the purpose of investigating the coupling mechanism of acoustic and hydrodynamic instabilities, it is convenient to separate Eq. (30) into two parts:

$$\alpha = \alpha_A + \alpha_H \quad (33)$$

where α_A and α_H refer to the acoustic and the hydrodynamic contributions, respectively.

$$\begin{aligned}
 \alpha_A &= -\frac{1}{2E_N^2} \left[-A_b^{(R)} \bar{M}_b \int_{\Gamma_b} \hat{p}_N^2 d\Gamma_b \right. \\
 &\quad \left. + A_n^{(R)} \bar{M}_n \int_{\Gamma_n} \hat{p}_N^2 d\Gamma_n - (\gamma+1) \int_{\Gamma} \bar{u}_i \hat{p}_N^2 n_i d\Gamma \right] \\
 &\quad + \frac{1}{k_N^2} \int_{\Gamma} (\bar{u}_j \hat{p}_{N,i} \hat{p}_{N,i} n_j + \bar{u}_i \hat{p}_{N,i} \hat{p}_{N,j} n_j) d\Gamma \\
 &\quad - \frac{1}{k_N^2 \text{Re}} \int_{\Gamma} (\hat{p}_{N,i} \hat{p}_{N,i} n_j + \frac{1}{3} \hat{p}_{N,jj} \hat{p}_{N,i} n_i) d\Gamma \\
 &\quad + \int_{\Omega} \{ -\bar{u}_i \hat{p}_N^2 - (2\gamma+1) \bar{u}_i \hat{p}_N \hat{p}_N n_i \} \\
 &\quad - \frac{1}{k_N^2} (\bar{u}_i \hat{p}_{N,jj} \hat{p}_{N,i} + \hat{u}_j \hat{p}_{N,i} \hat{p}_{N,i} + \bar{u}_i \hat{p}_{N,j} \hat{p}_{N,i}) \\
 &\quad + \bar{u}_j \hat{p}_{N,i} \hat{p}_{N,i} \\
 &\quad + \frac{1}{k_N^2 \text{Re}} (\hat{p}_{N,i} \hat{p}_{N,i} + \frac{1}{3} \hat{p}_{N,ii} \hat{p}_{N,jj}) \} d\Omega \quad (34) \\
 &\quad + \frac{1}{k_N^2} \left[\int_{\Gamma} \{ \frac{Y}{k_N} (\bar{u}_j \hat{u}_i^* + \hat{u}_j^* \bar{u}_i) \hat{p}_{N,i} n_j \} \right. \\
 &\quad - \frac{Y}{k_N \text{Re}} [(\hat{u}_i^* n_j) p_{N,i} n_j + \frac{1}{3} \hat{u}_j^* n_j p_{N,i} n_i] \} d\Gamma \\
 &\quad + \int_{\Omega} \{ -\frac{Y}{k_N} (\bar{u}_i \hat{u}_j^* \hat{p}_{N,i} + \bar{u}_j \hat{u}_i^* \hat{p}_{N,i}) \\
 &\quad + \bar{u}_i \hat{u}_j^* \hat{p}_{N,i} + \bar{u}_j \hat{u}_i^* \hat{p}_{N,i} \} \\
 &\quad + \frac{Y}{k_N \text{Re}} (\hat{u}_i^* \hat{p}_{N,i} + \frac{1}{3} \hat{u}_j^* \hat{p}_{N,ii}) \\
 &\quad + \frac{2Y(\gamma-1)}{\text{Re}} (\frac{2}{3} \bar{u}_i n_i \hat{u}_j^* - \bar{u}_i n_j \hat{u}_j^*) \hat{p}_N \} \\
 &\quad - \bar{u}_j n_i \hat{u}_j^* \hat{p}_N \} d\Omega \quad (35)
 \end{aligned}$$

Note that the first term of the boundary integrals, designated as (8)

$$-\frac{1}{2E_N^2} \int_{\Gamma} \frac{1}{k_N} \bar{u}_j \hat{p}_{N,i} \hat{p}_{N,i} n_j d\Gamma$$

is seen to be identical to the three-dimensional equivalent of the one-dimensional flow turning term which appeared in Culick [3], but which did not arise in due course of mathematical derivations for the three-dimensional case [Culick, 4]. To reconstruct the present results in terms of the same dimensions and notations as in [4], we set

$$-\bar{u}_{j,i}(\bar{u}_j^* + \bar{u}_j'),_i \quad (12)$$

The boundary condition can be obtained from the momentum equation by constructing a dot product with the normal vector,

$$-\hat{p}_{N,i}n_i = f \quad (13)$$

where

$$f = \gamma \left[\frac{\partial \bar{u}_i}{\partial t} + \bar{u}_{i,j}(\bar{u}_j^* + \bar{u}_j') + (\bar{u}_{i,j}^* + \bar{u}_{i,j}')\bar{u}_j \right. \\ \left. - \frac{1}{Re} [(\bar{u}_i^* + \bar{u}_i'),_{jj} + \frac{1}{3}(\bar{u}_j^* + \bar{u}_j'),_{ji}]n_i \right] \quad (14)$$

The oscillatory motions in both the acoustic and the vortical fields are modeled by

$$p' = \hat{p}e^{ikt} \quad (15)$$

$$u'_i = \hat{u}_i e^{ikt}, \quad u_i^* = \hat{u}_i^* e^{ikt} \quad (16)$$

$$\xi_i^* = \hat{\xi}_i^* e^{ikt} \quad (17)$$

where k is the complex dimensionless frequency given by

$$k = \omega - i\alpha \quad (18)$$

Here, the imaginary part α is known as the growth rate.

Substituting Eqs. (15-18) into the wave equation, we arrive at the nonhomogeneous Helmholtz equation,

$$\hat{p}_{,ii} + k^2 \hat{p} = \hat{h} \quad (19)$$

and the boundary condition,

$$-\hat{p}_{,i}n_i = \hat{f} \quad (20)$$

The nonhomogeneous terms \hat{h} and \hat{f} are given by

$$\hat{h} = i\bar{u}_i \hat{p}_{,i} + i\gamma \bar{u}_{i,i} \hat{p} - \gamma [\bar{u}_{i,j}(\hat{u}_j^* + \hat{u}_j')] \\ + (\hat{u}_{i,j}^* + \hat{u}_{i,j}')\bar{u}_j, _i + \frac{\gamma}{Re} [(\hat{u}_i^* + \hat{u}_i'),_{jjj}] \\ + \frac{1}{3}(\hat{u}_j^* + \hat{u}_j'),_{jii}] + \frac{2ik\gamma(\gamma-1)}{Re} \\ [\frac{2}{3}\bar{u}_{i,i}(\hat{u}_j^* + \hat{u}_j'),_j - \bar{u}_{i,j}(\hat{u}_j^* + \hat{u}_j'),_i \\ - \bar{u}_{j,i}(\hat{u}_j^* + \hat{u}_j'),_i] \quad (21)$$

and

$$\hat{f} = \gamma \{ i\bar{u}_i' + \bar{u}_{i,j}(\hat{u}_j^* + \hat{u}_j') + (\hat{u}_{i,j}^* + \hat{u}_{i,j}')\bar{u}_j \\ - \frac{1}{Re} [(\hat{u}_i^* + \hat{u}_i'),_{jj} + \frac{1}{3}(\hat{u}_j^* + \hat{u}_j'),_{ji}]n_i \} \quad (22)$$

Making use of the Green's function integral (23), it can be shown that

$$(k^2 - k_N^2)E_N^2 = \int_{\Omega} \hat{h} \hat{p}_N d\Omega + \int_{\Gamma} \hat{f} \hat{p}_N d\Gamma \quad (23)$$

where the unperturbed mode shape \hat{p}_N and its frequency k_N are determined from the classical acoustic problem:

$$\hat{p}_{N,ii} + k^2 \hat{p}_N = 0 \quad (24)$$

$$\hat{p}_{N,i}n_i = 0 \quad (25)$$

and E_N is given by

$$E_N^2 = \int_{\Omega} \hat{p}_N^2 d\Omega \quad (26)$$

At this point, an important remark is in order. A close examination of Eq. (23) reveals that the domain integral on the right hand side of Eq. (23) contains the terms from the momentum equation which were differentiated once. Thus, these terms must be integrated by parts to produce an acoustic boundary condition. The resulting domain integral represents the functional space equivalent to the mean flow characterized by the Navier-Stokes system. This implies that an additional integration by parts must be carried out such that the familiar Neumann boundary conditions may be brought to the surface. The boundary integrals arrived at in this manner account for the stress and/or the pressure boundary conditions by means of velocity gradients. Such Neumann boundary conditions stem from the convective and viscous terms.

In view of these requirements, the resulting expression upon integration by parts twice of Eq. (23) takes the form

$$(k^2 - k_N^2)E_N^2 = i\gamma k_N \int_{\Gamma} \hat{u}_i \hat{p}_N n_i d\Gamma + ik_N(\gamma+1) \\ \int_{\Gamma} \bar{u}_i \hat{p}_N^2 n_i d\Gamma - ik_N \int_{\Omega} \bar{u}_{i,i} \hat{p}_N^2 d\Omega - ik_N(2\gamma+1) \\ \int_{\Omega} \bar{u}_i \hat{p}_N \hat{p}_{N,i} d\Omega + \gamma \int_{\Gamma} [\bar{u}_i (\hat{u}_j^* + \hat{u}_j') + (\hat{u}_i^* + \hat{u}_i')\bar{u}_j] \\ \hat{p}_{N,i} n_j d\Gamma - \gamma \int_{\Omega} [(\bar{u}_i (\hat{u}_j^* + \hat{u}_j'),_j + (\hat{u}_i^* + \hat{u}_i')\bar{u}_j,j) \\ \hat{p}_{N,i} n_j d\Gamma + (\bar{u}_i (\hat{u}_j^* + \hat{u}_j') + (\hat{u}_i^* + \hat{u}_i')\bar{u}_j) \hat{p}_{N,i} d\Omega \\ - \frac{\gamma}{Re} \int_{\Gamma} [(\hat{u}_i^* + \hat{u}_i'),_j \hat{p}_{N,i} n_j + \frac{1}{3}(\hat{u}_j^* + \hat{u}_j'),_j] \\ \hat{p}_{N,i} n_i d\Gamma + \frac{\gamma}{Re} \int_{\Omega} [(\hat{u}_i^* + \hat{u}_i'),_j \hat{p}_{N,i} j] \\ + \frac{1}{3}(\hat{u}_j^* + \hat{u}_j'),_j \hat{p}_{N,ii} d\Omega + \frac{2ik_N\gamma(\gamma-1)}{Re} \\ \int_{\Omega} [\frac{2}{3}\bar{u}_{i,i}(\hat{u}_j^* + \hat{u}_j'),_j - \bar{u}_{i,j}(\hat{u}_j^* + \hat{u}_j'),_i \\ - \bar{u}_{j,i}(\hat{u}_j^* + \hat{u}_j'),_i] \hat{p}_N d\Omega \quad (27)$$

Squaring both sides of Eq. (18) and noting that

$$\omega \approx \omega_N \approx k_N \quad (28)$$

for $\alpha \approx 0$, we obtain

$$k^2 - k_N^2 = -i2\gamma k_N + \gamma^2 \quad (29)$$

Since $\gamma^2 \ll |2\gamma k_N|$ from the condition set by Eq. (28), it is now possible to solve for the growth

stability can be significant [7-13]. Although it can be argued that the hydrodynamic instability may not occur in high Reynolds numbers, the turbulent shear layer instabilities have been found to be affected by various combinations of Strouhal numbers and Reynolds numbers. The acoustic field may interact with vortex motions known as the "feedback" resulting in the vortex generated sound [14]. Some studies [15,16] indicate that the vortices may undergo "clipping", a phenomenon corresponding to the vortex disruption. It is also possible that lateral periodic motion of the vortex street known as "jitters" may lead to partial or complete escape of the vortices [15,16]. Whether these conditions prevail in large rocket motors in which flow separations at interface restrictors or inhibitors are likely to produce vortex motion must be clarified. No simple models such as hyperbolic tangent velocity profile for the shear layer [11,17] and temporal or spatial growth theories [18,19] appear to be adequate for the interactions of acoustic and vortical oscillations in a rocket chamber.

In the previous papers [20-22], finite element applications to the combustion instability analysis were discussed. Although a rigorous mathematical formulation of the stability integral was presented, the mean flow calculations did not include turbulent flows. Since the turbulent flow field is involved in shear boundary layers and vortex motions, it is intended that this subject be considered in the mean flow calculations and subsequently in the stability integral. Shock waves will not be included in the present paper.

The numerical results for certain combinations of acoustic and vortical frequencies indicate that stability boundaries for acoustics-coupled hydrodynamic oscillations are somewhat similar to the classical hydrodynamic stability boundaries, but they occur in the form of multiple islands. The turbulent flow field appears to contribute toward instability, and this trend increases with larger transition angles of the rocket motor cross-section.

In what follows, pertinent governing equations are presented, from which the expression for the growth constant coupling the acoustic and hydrodynamic oscillations is derived in section 2. Subsequently, the K-ε turbulence model and calculations of the vortical component of fluctuation velocities and the fluctuation vorticity are described in section 3. It is also shown in section 4 that the finite element is one of the most expeditious methods of calculation. Numerical results via finite elements are then displayed and pertinent discussions and conclusions are presented in sections 5 and 6, respectively.

2. Vorticity-Coupled Acoustic Instability Integral

The basic governing equations for compressible viscous flow without particle distributions are represented as follows:

Continuity

$$\frac{\partial \rho}{\partial t} + (\rho u_i)_{,i} = 0 \quad (1)$$

Momentum

$$\frac{\partial}{\partial t} (\rho u_i) + (\rho u_i u_j)_{,j} + \frac{1}{\gamma} p_{,i}$$

$$- \frac{1}{Re} (u_{i,jj} + \frac{1}{3} u_{j,ji}) = 0 \quad (2)$$

Energy

$$\begin{aligned} \frac{\partial}{\partial t} (\rho T) - \frac{\gamma-1}{\gamma} \frac{\partial p}{\partial t} + (\rho u_i T)_{,i} - \frac{\gamma-1}{\gamma} u_i p_{,i} \\ + \frac{\gamma-1}{Re} \left(\frac{2}{3} u_{i,i} u_{j,j} - u_{i,j} u_{j,i} - u_{i,j} u_{i,j} \right) = 0 \end{aligned} \quad (3)$$

State

$$p = \rho T \quad (4)$$

where the commas denote partial derivatives, the repeated indices imply summing. The following non-dimensional quantities are used in the above equations:

$$\begin{aligned} u_i = \bar{u}_i/a, \quad a = (\gamma p_0 / \rho_0)^{1/2}, \quad p = \bar{p}/p_0 \\ T = c_p (\gamma-1) \bar{T} / a^2, \quad x_i = \bar{x}_i / L, \quad t = \bar{a} \bar{t} / L \\ Re = \rho_0 a L / u, \quad \rho = \bar{\rho}/\rho_0 \end{aligned}$$

where the double bars denote dimensional quantities.

Interactions between acoustic and vortical oscillations can be introduced by superimposing the acoustic component upon the vortical component of the perturbed velocity in the form

$$u_i = \bar{u}_i + \epsilon (u'_i + u''_i) \quad (5)$$

where the bars, primes, and asterisks indicate the mean flow, the acoustic and vortical oscillations, respectively; and ϵ represents the perturbation parameter. On the other hand, the pressure and the density are given by

$$p = 1 + \epsilon p' \quad (6)$$

$$\rho = 1 + \epsilon \rho' \quad (7)$$

And, the vorticity field is given by

$$\xi_i = \bar{\xi}_i + \epsilon \xi''_i \quad (8)$$

$$\bar{\xi}_i = \epsilon_{ijk} \bar{u}_k,j \quad (9)$$

$$\xi''_i = \epsilon_{ijk} u''_k,j \quad (10)$$

where ϵ_{ijk} is the permutation symbol. In view of Eqs. (1-10), it can be shown that the nonhomogeneous wave equation takes the following form:

$$p'_{,ii} - \frac{\gamma^2 p''}{\partial t^2} = h \quad (11)$$

where

$$h = \bar{u}_i \frac{\partial p'}{\partial t} + \gamma \frac{\partial p'}{\partial t} \bar{u}_{i,i} - \gamma (\bar{u}_{i,j} (u'_j + u''_j)_{,ji}$$

$$+ (u'_{i,j} + u''_{i,j}) \bar{u}_j,j_{,i} + \frac{\gamma}{Re} [(u''_{i,i} + u'_{i,i})_{,jji}$$

$$+ \frac{1}{3} (u'_{j,j} + u''_{j,j})_{,jji}] + \frac{2\gamma(\gamma-1)}{Re} \frac{\partial}{\partial t}$$

$$[\frac{2}{3} \bar{\xi}_{i,i} (u'_j + u''_j)_{,j} - \bar{u}_{i,j} (u''_j + u'_{j,j})_{,i}]$$

APPENDIX 1

INTEGRATIONS OF UNSTEADY ACOUSTIC AND VORTICAL OSCILLATIONS IN AXISYMMETRIC CYLINDRICAL CAVITY

T.J. Chung* and J.L. Sohn**
 Department of Mechanical Engineering
 The University of Alabama in Huntsville
 Huntsville, Alabama

Abstract

A physical phenomenon of interactions between the acoustic and vortical oscillations is examined herein. This subject is important in rocket motor chambers when the vorticity field is coupled with acoustic pressure oscillations. In the past, the acoustic combustion instability was studied independently of the hydrodynamic instability induced by vortex motions and turbulent shear boundary layers. However, it is quite conceivable that these two distinctly different oscillations are coupled and interact together in the flow field of a solid propellant rocket motor. The present paper introduces an analytical approach to resolving the seemingly complex phenomena of mutual interactions between the acoustic and vortical oscillatory motions. Toward this end, governing equations for all variables are constructed, and finite elements are applied to solve the governing equations. Combustion instability integrals including the mean flow field, perturbed acoustic oscillations, and oscillatory velocities and vortices are also derived and calculated by finite elements. From the growth constants for acoustic and hydrodynamic contributions, stability boundaries are determined in terms of Reynolds numbers. The numerical results indicate that an overall instability phenomenon results from certain combinations of acoustic and vortical frequencies. It is also found that stability boundaries for acoustics-coupled hydrodynamic oscillations are somewhat similar to the classical hydrodynamic stability boundaries, but they occur in the form of multiple islands. The turbulent flow field appears to contribute toward instability and this trend increases with larger transition angles of the rocket motor cross-section.

Nomenclature

A	admittance at the burning surface
a	sonic velocity ($\gamma P_0 / \rho_0$)
c _P	specific heat at constant pressure
L	length of the combustion chamber
k	complex wave number ($\omega - i\alpha$)
K	turbulence kinetic energy
M	Mach number
P	pressure
Re	Reynolds number ($\rho_0 a L / \mu$)
T	temperature
t	time
u _i	velocities
x _i	spatial coordinates

*Professor

**Graduate Research Assistant

This research was supported by AFOSR 83-0084 with Dr. Leonard Caveny as technical monitor.

α	growth constant
ϵ	turbulent energy dissipation, perturbation parameter
ϵ_{ijk}	permutation symbol
σ	effective Prandtl-Schmidt number
Φ_a	finite element interpolation function
ξ_i	vorticities
ρ	density
γ	specific heat ratio
μ	viscosity
Γ	boundary
Ω	domain

Subscripts and Superscripts

$\acute{}$	acoustic fluctuation
\ast	vortical fluctuation
t	turbulence
N	normal mode
A	acoustic field
H	hydrodynamic field

I. Introduction

The flow field, such as occurs in solid propellant rocket motors, offers a fertile ground for fundamental research in fluid mechanics and heat transfer. Combustion induces not only the mean flow field, but also acoustic pressure oscillations and possibly vortex fluctuations together with turbulent shear boundary layers. Furthermore, shock waves are commonplace in most instances. Obviously, a most rigorous analysis taking into account all of these phenomena would be difficult, if not impossible. However, with the advent of the electronic computer and the modern technology of numerical methods, it has become feasible to resolve hitherto unsolved problems.

Despite difficulties in analytical and numerical solutions to the complex physical phenomena in a rocket motor chamber, many researchers have contributed to the advancement of analysis and design of successful rocket motors. A large body of literature exists relative to this subject, the study of which has been pioneered by Crocco [1], Cantrell and Hart [2], Culick [3,4], and others. Flandro and Jacobs [5], among others, have noted that vortex shedding may lead to an instability in solid propellant rocket motors. It is quite possible that high speed mean flows also affect the stability [6] significantly.

The basic mathematical formulations of combustion instability were contributed by Culick [3,4]. Recently, it has been observed in both full-scale firings and cold flow simulations that interactions of acoustic and hydrodynamical (vortical) in-

16. Flandro, G.A., "Nonlinear Time-Dependent Combustion of a Solid Rocket Propellant", 19th JANNAF Combustion Meeting, Greenbelt, MD, Oct., 1982.
17. Chung, T.J. and Kim, P.K., "Finite Element Approach to Response Function Calculations for Solid Propellant Rocket Motors", AIAA Paper 84-1433, AIAA/SAE/ASME 20th Joint Propulsion Conf., June 11-13, 1984.
18. Cohen, N.S. and Strand, L.D., "Non-Steady Combustion of Composite Solid Propellants", JPL D-1602, May 1984.
19. Chung, T.J. and Kim, P.K., "Unsteady Response of Burning Surface in Solid Propellant Combustion", AIAA paper 85-0234, 1985.

turbation compared to the first order. Further details are presented in Reference [18] or Appendix 3.

4.2 References

1. Culick, F.E.C., "A Review of Calculations for Unsteady Burning of a Solid Propellant", AIAA J., Vol. 7, No. 12, Dec. 1968, pp. 2241-2255.
2. Grad, H., "Resonanic Burning in Rocket Motors", Commun. in Pure Appl. Math. 2, Mar. 1949, pp. 79-102.
3. Hart, R.W. and McClure, F.T., "Combustion Instability: Acoustic Interaction with a Burning Propellant Surface", J. Chem. Phys., 30, Sept. 1959, pp. 1501-1514.
4. Cheng, Sin-I, "Unstable Combustion in Solid Propellant Rocket Motors", in 8th Symposium on Combustion, Williams and Wilkins, 1962, pp. 81-96.
5. Denison, M.R. and Baum, E., "A Simplified Model of Unstable Burning on Solid Propellants", ARS J. 31, Aug. 1961, pp. 1112-1122.
6. Beckstead, M.W. and Price, E.W., "Non-acoustic Combustion Instability", AIAA J., Vol. 5, No. 11, Nov. 1967, pp. 1989-1996.
7. Williams, F.A., "Response of a Burning Solid to Small Amplitude Pressure Oscillations", J. of Applied Phys., Vol. 33, No. , 1962, p. 3153.
8. Cohen, N.S., "Response Function Theories that Account for Size Distribution Effects - A Review", AIAA J., Vol. 19, No. 7, July 1981, pp. 907-912.
9. Williams, F.A. and Lengelle, G., "Simplified Model for Effect of Solid Heterogeneity on Oscillatory Combustion", Astronautica Acta, Vol. 14, Jan. 1968, pp. 97-118.
10. Law, C.K. and Williams, F.A., "A Theory for the Influence of Solid Heterogeneity on L* Instability", Combustion Science and Technology, Vol. 6, Feb. 1973, pp. 335-345.
11. Beckstead, M.W., Derr, R.L. and Price, C.F., "A Model of Solid Propellant Combustion Based on Multiple Flames", AIAA J., Vol. 8, Dec. 1970, pp. 2200-2207.
12. Condon, J.A., Osborn, J.R. and Glick, R.L., "Statistical Analyses of Polydisperse, Heterogeneous Propellant Combustion: Non-Steady-State", 13th JANNAF Combustion Meeting, CPIA publication 281, Vol. 2, 1976, pp. 209-223.
13. Beckstead, M.W., "Combustion Calculations for Composite Solid Propellants", 13th JANNAF Combustion Meeting, CPIA publication 281, Vol. 2, 1976, pp. 299-312.
14. Cohen, N.S. and Bower, J.M., "Combustion Response Modeling for Composite Solid Propellants", AFRPL-TR-78-39, Jet Propulsion Laboratory, Pasadena, CA, June 1978.
15. T'ien, J.S., "Oscillatory Burning of Solid Propellants Including Gas Phase Time Lag", Combustion Science and Technology, Vol. 5, 1972.

SECTION 4

UNSTEADY RESPONSE OF BURNING SURFACE IN
SOLID PROPELLANT COMBUSTION

4.1 Summary

The response function as related to the combustion of solid propellants has been studied by numerous investigators. Some of the review articles include Culick [1] on homogeneous propellants [2-6] and Cohen [8] on heterogeneous propellants [9-14]. Both of them are limited to one-dimensional and quasi-steady situations. In recent years, some works toward non-steady problems have been attempted [15-17]. The majority of the discussions of response functions in the literature are concerned with pressure-coupling usually applicable in the linear stability. Computations of the response function for velocity-coupling important in a nonlinear process, however, remain in a state of infancy, although some initial attempts toward this subject have been made [16, 18].

As noted by Flandro [16], the velocity-coupling may be accommodated by second order perturbations of multi-dimensional gas/solid governing equations. This approach deviates drastically from the one-dimensional analysis which has been adopted for nearly three decades. With modern computers and various tools of numerical analysis available, however, it seems possible to relax many undesirable restrictions. Observations indicate that combustion oscillations are time-dependent and often nonlinear as influenced by turbulent flowfields, which may lead to erosive burning and unstable oscillations. Unfortunately, however, a computational tool for the most exact analysis of complicated physical phenomena such as these, even if developed, will not fit into the currently available computer. Thus, naturally, some approximations and simplifications must still be introduced to any theoretical formulations conducive to numerical analysis.

With this in mind, some additional materials and reassessments concerning the multi-dimensional calculations of combustion response functions are presented herein as an extension to the previous paper [17]. The influence of heterogeneity, surface roughness, particulate matter, or turbulence will not be considered at this time. We include the effect of radiation, adopt a simple, premixed, single-step laminar flame, expand the solid-gas governing equations into first and second order perturbations, and finally perform eigenvalue analyses. Complicated boundary conditions at the solid-gas interface and flame edges are imposed ideally by means of Lagrange multipliers together with finite elements. Calculations are carried out for various incident angles of impressed pressure waves at the flame edge boundaries [16].

Computed results show that the natural frequencies are clustered around low frequency range ($\omega < 10$). Spatial distributions of field variables corresponding to the computed frequencies indicate that the oscillatory behavior is pronounced at upstream and gradually diminishes toward downstream. Response functions oscillate in the axial direction with peaks occurring at the midstream, but diminishing toward flame edges for both first and second order perturbations. It is also shown that two-dimensional response functions are multi-peaked and may become negative as energy sinks. Finally, it is seen that the effect of radiation is more pronounced in the second order per-

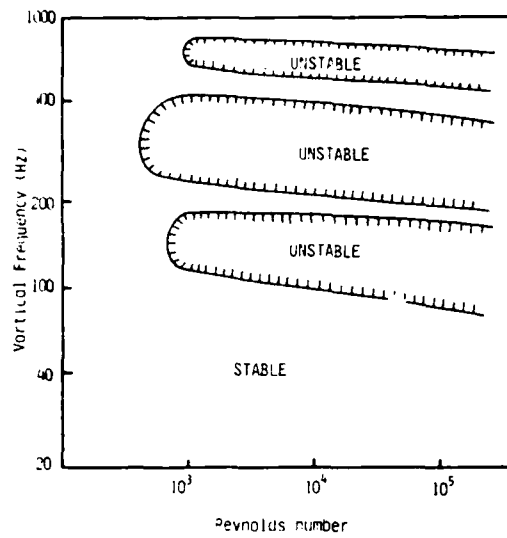


Fig. 12 Stability boundaries for acoustics-vorticity interactions with various vortical frequencies versus Reynolds numbers, $\theta=14^\circ$, $\omega_N=2553$ Hz, laminar flow

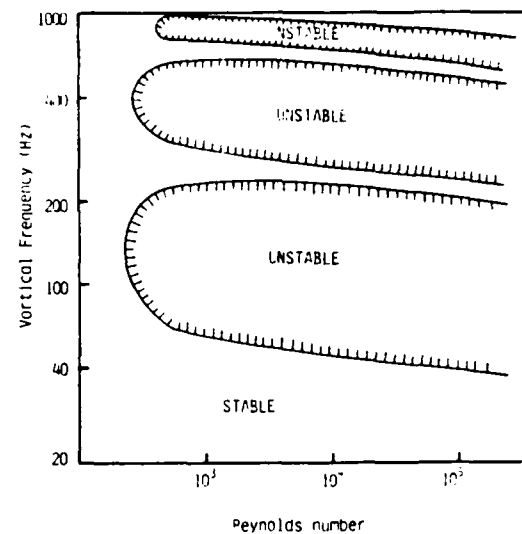


Fig. 13 Stability boundaries for acoustics-vorticity interactions with various vortical frequencies versus Reynolds numbers, $\theta=14^\circ$, $\omega_N=2553$ Hz, turbulent flow

APPENDIX 2

PARTICLE DAMPING EFFECTS
ON COMBUSTION INSTABILITY

T. J. Chung* and S. C. Chan**
 Department of Mechanical Engineering
 The University of Alabama in Huntsville
 Huntsville, AL 35899

Abstract

The paper discusses the formulation and solution strategies to analyze combustion instability due to aluminum particle distributions in the solid propellant rocket motor chambers. Specifically, the finite element method is utilized in order to accommodate complicated geometries and boundary conditions. To demonstrate the validity, one dimensional results are first compared with those of analytical solutions. A similar process is then extended to handle two-dimensional problems.

Nomenclature

a	speed of sound
C	specific heat of particle
C_p, C_v	specific heat of gas at constant pressure, volume
\bar{C}_p, \bar{C}_v	specific heat of mixture at constant pressure, volume
d	particle diameter
e	total energy of gas
e_p	total energy of particle
F_p	drag force
k	wave number
n	vector normal to surface
p	mean pressure
p'	acoustic pressure
Pr	Prandtl number
R	gas constant
T	temperature of gas
T_p	temperature of particle
r	radial coordinate
u	gas velocity
u_p	particle velocity
w_p	particle mass rate of flow
z	axial coordinate
α	growth rate
β	ratio of particle density to gas density
γ	specific heat ratio of gas
γ'	specific heat ratio of mixture
ρ	total density
ρ_g, ρ_p	density of gas, particle
θ	tangential coordinate
ζ	ratio R/C_v
ω	frequency
κ	thermal conductivity
μ	viscosity constant
ϕ	finite element interpolation function
ξ	vorticity vector
τ_d	dynamic relaxation time
τ_t	thermal relaxation time

1. Introduction

The study of acoustic energy losses due to aluminum particles in the solid propellant rocket motor combustion chamber has been carried out by a number of investigators. Epstein and Charhart [1] studied the absorption of sound in suspensions of non-interacting inert spherical particles and uniform temperatures. The validity of this investigation was subsequently substantiated by other researchers [2-4]. In a rocket motor, the particles are neither spherical nor inert and subjected to nonuniform temperature distributions [5].

Despite the extensive research on the subject of acoustic energy dissipation due to particle damping in the rocket motor [5-10], calculations of the stability integral arising from particle damping are limited to simple one-dimensional cases.

Thus, the purpose of the present study is to demonstrate the feasibility of mathematical formulations and numerical calculations via finite elements. Furthermore, interactions of particle damping with fluid viscosity and heat transfer are included. It is shown that additional boundary and domain terms arise from integrating by parts "twice" of the Green function stability integral containing the momentum equation. A simple example problem is solved for comparison with the analytical solution.

2. Governing Equations

Conservation laws for the mass, momentum, and energy in the two-phase flow of the gas/particle mixture are written as follows [5]:

Continuity (gas)

$$\frac{\partial \rho_g}{\partial t} + \nabla \cdot (\rho_g u) = w_p \quad (1)$$

Continuity (particle)

$$\frac{\partial \rho_p}{\partial t} + \nabla \cdot (\rho_p u_p) = -w_p \quad (2)$$

Momentum

$$\frac{\partial}{\partial t} (\rho_g u + \rho_p u_p) + \frac{\partial}{\partial x_j} (\rho_g u_i u_j + \rho_p u_i u_p_j)_{i,j} + \nabla p = S \quad (3)$$

Energy

$$\frac{\partial}{\partial t} (\rho_g e + \rho_p e_p) + \nabla \cdot (\rho_g e u + \rho_p e_p u_p) + \nabla \cdot (u_p) = Q + \Phi \quad (4)$$

*Professor of Mechanical Engineering

**Graduate Student

This research was supported by the Air Force Office of Scientific Research.

where w_p is the particle mass rate of flow and

$$\underline{S} = \mu [\nabla^2 \underline{u} + \frac{1}{3} \nabla \cdot (\nabla \cdot \underline{u})] \quad (5)$$

$$\underline{Q} = \nabla \cdot \underline{q}^{(C)} + \nabla \cdot \underline{q}^{(R)} \quad (6)$$

$$\phi = \mu \left[\frac{2}{3} (\nabla \cdot \underline{u})^2 - \frac{\partial \underline{u}_i}{\partial x_j} \frac{\partial \underline{u}_j}{\partial x_i} - \frac{\partial \underline{u}_i}{\partial x_j} \frac{\partial \underline{u}_j}{\partial x_i} \right] \quad (7)$$

with $\underline{q}^{(C)}$ and $\underline{q}^{(R)}$ being the conduction heat flux and radiation heat flux, respectively.

Combining (1), (2) and (3), we obtain

$$\rho_g \frac{\partial \underline{u}}{\partial t} + \rho_g (\underline{u} \cdot \nabla) \underline{u} + \nabla p = \underline{F}_p + \underline{g} + \underline{S} \quad (8)$$

where

$$\underline{F}_p = -\rho_p \left[\frac{\partial \underline{u}_p}{\partial t} + (\underline{u}_p \cdot \nabla) \underline{u}_p \right] \quad (9)$$

$$\underline{g} = (\underline{u}_p - \underline{u}) w_p \quad (10)$$

Combining (1), (2), and (4) leads to

$$\begin{aligned} \rho_g C_v \frac{\partial T}{\partial t} + \rho_g C_v (\underline{u} \cdot \nabla) T + p \nabla \cdot \underline{u} &= \underline{Q} + \phi + \underline{Q}_p \\ - \underline{u} \cdot \underline{S} + (\underline{e}_p - \underline{e}) w_p + (\underline{u}_p - \underline{u}) \underline{F}_p + \underline{u} \cdot \underline{g} & \end{aligned} \quad (11)$$

where

$$\underline{Q}_p = -\rho_p C \left[\frac{\partial T_p}{\partial t} + (\underline{u}_p \cdot \nabla) T_p \right] \quad (12)$$

Now let us denote that

$$\underline{u}_p = \underline{u} + \underline{s} \underline{u}_p \quad (13)$$

$$T_p = T + \zeta T_p \quad (14)$$

In view of (13) we rewrite (9) in the form

$$\underline{F}_p = -\rho_p \left[\frac{\partial \underline{u}}{\partial t} + (\underline{u} \cdot \nabla) \underline{u}_p + \delta \underline{F}_p \right] \quad (15)$$

where

$$\delta \underline{F}_p = -\rho_p \left[\frac{\partial \underline{s} \underline{u}_p}{\partial t} + (\underline{u} \cdot \nabla) \underline{s} \underline{u}_p + (\underline{s} \underline{u}_p \cdot \nabla) \underline{u} \right] \quad (16)$$

Substituting (15) into (8) yields

$$\rho \frac{\partial \underline{u}}{\partial t} + \rho (\underline{u} \cdot \nabla) \underline{u} + \nabla p = \underline{H} + \underline{S} \quad (17)$$

where

$$\rho = \rho_g + \rho_p = \rho_g (1 + \beta), \quad \beta = \rho_p / \rho_g$$

$$\underline{H} = \underline{F}_p + \underline{g}$$

Similarly

$$\underline{Q}_p = -\rho_p C \left[\frac{\partial T}{\partial t} + (\underline{u} \cdot \nabla) T \right] + \underline{Q}_p \quad (18)$$

where

$$\underline{Q}_p = -\rho_p C \left[\frac{\partial \delta T_p}{\partial t} + (\underline{u} \cdot \nabla) \delta T_p + (\delta \underline{u}_p \cdot \nabla) T \right] \quad (19)$$

with C being the specific heat of the particle. Substituting (18) into (11) gives

$$\begin{aligned} \rho_g (C_v + \beta C) \frac{\partial T}{\partial t} + \rho_g (C_v + \beta C) (\underline{u} \cdot \nabla) T + p \nabla \cdot \underline{u} \\ = \underline{Q} + \phi + \underline{Y} \end{aligned} \quad (20)$$

where C_v is the specific heat of gas at constant volume and

$$\begin{aligned} \underline{Y} = \underline{Q}_p + (\underline{e}_p - \underline{e}) w_p + (\underline{u}_p - \underline{u}) \underline{F}_p - \underline{u} \cdot \underline{g} \\ - \underline{u} \cdot \underline{S} \end{aligned} \quad (21)$$

To obtain the wave equation we make use of the perfect gas law

$$p = \rho_g R T \quad (22)$$

which is substituted into (20). We then differentiate (20) with respect to time and substitute from the spatial derivative of (17). Denote the specific heats of the mixture at constant volume and constant pressure, respectively, as

$$\bar{C}_v = \frac{C_v + \beta C}{1 + \beta}, \quad \bar{C}_p = \frac{C_p + \beta C}{1 + \beta}$$

it then follows that the gas constant for the mixture takes the form

$$\bar{R} = \bar{C}_p - \bar{C}_v = \frac{R}{1 + \beta}$$

Substituting (22) and (1) into (20) yields

$$\frac{\partial p}{\partial t} + (1 + \zeta) p \nabla \cdot \underline{u} + (\underline{u} \cdot \nabla) p = \zeta (\underline{Q} + \phi + \underline{Z}) \quad (23)$$

$$\text{where } \zeta = \bar{R} / \bar{C}_v$$

$$\underline{Z} = \underline{Y} + (1 + \beta) \bar{C}_v \underline{T}_p$$

Now the time derivative of (23) and spatial derivative of (17) are written, respectively, as follows:

$$\begin{aligned} \frac{\partial^2 p}{\partial t^2} + (1 + \zeta) \left[\frac{\partial p}{\partial t} \nabla \cdot \underline{u} + p \frac{\partial}{\partial t} (\nabla \cdot \underline{u}) \right] \\ + \frac{\partial}{\partial t} (\underline{u} \cdot \nabla) p = \zeta \frac{\partial}{\partial t} (\underline{Q} + \phi + \underline{Z}) \end{aligned} \quad (24)$$

$$\begin{aligned} \rho \frac{\partial}{\partial t} (\underline{u} \cdot \underline{u}) + \rho (\underline{u} \cdot \nabla) \underline{u} + \nabla^2 p \\ = \nabla \cdot \underline{H} + \nabla \cdot \underline{S} + \underline{B} \end{aligned} \quad (25)$$

where

$$\underline{B} = \frac{1}{\rho} (\underline{u} \cdot \underline{u}) + (- \underline{F}_p + \underline{H} + \underline{S})$$

Substituting (25) into (24) gives

$$\begin{aligned} \frac{\partial^2 p}{\partial t^2} + \zeta \frac{\partial p}{\partial t} \nabla \cdot \bar{u} + \zeta \frac{p}{\rho} [-\rho \nabla \cdot (\bar{u} \cdot \nabla) \bar{u} - \nabla^2 p \\ + \nabla \cdot \bar{H} + \nabla \cdot \bar{S} + \bar{B}] + \frac{\partial}{\partial t} (\bar{u} \cdot \nabla) p = \zeta \frac{\partial}{\partial t} (Q + \bar{\phi} + Z) \quad (26) \end{aligned}$$

For linear stability, we introduce the perturbation expansion of $O(\epsilon)$ as follows:

$$\begin{aligned} \bar{u} &= \bar{\bar{u}} + \epsilon (\bar{u}' + \bar{u}^*) \\ p &= \bar{p} + \epsilon p' \\ \rho &= \bar{\rho} + \epsilon \rho' \\ e &= \bar{e} + \epsilon e' , \quad w_p = \bar{w}_p + \epsilon w_p' , \quad Q = \bar{Q} + \epsilon Q' \\ \bar{\phi} &= \bar{\bar{\phi}} + \epsilon (\bar{\phi}' + \bar{\phi}^*) , \quad Z = \bar{Z} + \epsilon Z' \\ \bar{H} &= \bar{\bar{H}} + \epsilon (\bar{H}' + \bar{H}^*) \\ \bar{S} &= \bar{\bar{S}} + \epsilon (\bar{S}' + \bar{S}^*) \end{aligned}$$

where the bar, asterisk, and prime denote the mean flow, acoustic fluctuation, and vortical fluctuation, respectively.

Now, collecting the terms of $O(\epsilon)$, we have

$$\nabla^2 p' - \frac{1}{\bar{a}^2} \frac{\partial^2 p'}{\partial t^2} = h \quad (27)$$

where

$$\begin{aligned} h = & - \bar{\rho} [\nabla^2 (\bar{u} \cdot \bar{u}') + \nabla^2 (\bar{u} \cdot \bar{u}^*) - \nabla \cdot (\bar{u} \times \bar{\xi}) \\ & + \bar{u}^* \times \bar{\xi} + \bar{u}' \times \bar{\xi}] + \frac{\bar{\gamma}}{\bar{a}^2} \frac{\partial p'}{\partial t} \nabla \cdot \bar{u} \\ & + \frac{1}{\bar{a}^2} \bar{u} \cdot \frac{\partial}{\partial t} (\nabla p) + \nabla \cdot \bar{H}' + \nabla \cdot \bar{S}' \\ & - \frac{\zeta}{\bar{a}^2} \frac{\partial}{\partial t} (Q' + \bar{\phi}' + Z') \quad (28) \end{aligned}$$

where

$$\bar{a}^2 = \bar{\gamma} \bar{R} T_0 = \bar{\gamma} \frac{p_0}{\bar{\rho}} = \frac{\bar{\gamma}}{(1+\beta)} \frac{p_0}{\bar{\rho} g} \quad (29)$$

$$Z' = (1+\beta) (e' \bar{w}_p + \bar{e}_p w') - \beta C \delta T \bar{w}_p + \delta Q_p' \quad (30)$$

The nonhomogeneous wave equation (27) is subject to the boundary condition of the form

$$\bar{n} \cdot \nabla p' = -f \quad (31)$$

where

$$\begin{aligned} f = & \bar{\rho} [\frac{\partial \bar{u}'}{\partial t} + \frac{\partial \bar{u}^*}{\partial t} + \nabla (\bar{u} \cdot \bar{u}') + \bar{u} \cdot \nabla \bar{u}^* \\ & - (\bar{u} \times \bar{\xi}^* + \bar{u}^* \times \bar{\xi} + \bar{u}' \times \bar{\xi})] \cdot \bar{n} - \bar{H}' \cdot \bar{n} - \bar{S}' \cdot \bar{n} \quad (32) \end{aligned}$$

To remove the time dependent terms, we introduce exponential oscillations of the form

$$p' = \hat{p} e^{i \bar{k} t} \quad (33a)$$

$$\bar{u}' = \bar{u} e^{i \bar{k} t} \quad (33b)$$

$$\bar{u}^* = \bar{u}^* e^{i \bar{k} t} \quad (33c)$$

and

$$(Q', \bar{\phi}', Z') = (\hat{Q}, \hat{\phi}, \hat{Z}) e^{i \bar{k} t} \quad (34)$$

where k is the wave number defined as

$$k = \frac{1}{\bar{a}} (\omega - i\alpha) \quad (35)$$

Substituting (33) into (27) and (31), respectively, we obtain

$$\nabla^2 \hat{p} + k^2 \hat{p} = \hat{h} \quad (36a)$$

$$\bar{n} \cdot \nabla \hat{p} = -\hat{f} \quad (36b)$$

The natural modes and frequencies corresponding to (36) are determined from

$$\nabla^2 \hat{p}_N + k^2 \hat{p}_N = 0 \quad (37a)$$

$$\bar{n} \cdot \nabla \hat{p}_N = 0 \quad (37b)$$

By means of the Green's function integral and using (35) - (37), it can be shown that

$$k^2 = k_N^2 + \frac{1}{E_N^2} \left(\int_{\Omega} \hat{h} \hat{p}_N d\Omega + \int_{\Gamma} \hat{f} \hat{p}_N d\Gamma \right) \quad (38)$$

where

$$E_N^2 = \int_{\Omega} \hat{p}_N^2 d\Omega \quad (39)$$

$$\begin{aligned} \hat{h} = & i \frac{k}{\bar{a}} (\bar{u} \cdot \nabla) \hat{p}_N + i \frac{k \bar{\gamma}}{\bar{a}} \hat{p}_N^2 \cdot \bar{u} \\ & - \bar{\rho} [\nabla^2 (\bar{u} \cdot \bar{u}') + \nabla^2 (\bar{u} \cdot \bar{u}^*) - \nabla \cdot (\bar{u} \bar{x}_2^* + \bar{u}^* \bar{x}_2) \\ & + \bar{u}^* \bar{x}_2^*] + \nabla \cdot \bar{S}' + \nabla \cdot \bar{H}' - i \frac{\zeta k}{\bar{a}} (Q' + \bar{\phi}' + Z') \quad (40) \end{aligned}$$

$$\begin{aligned} \hat{f} = & \bar{\rho} [i \bar{k} \hat{u} (\hat{u}' + \hat{u}^*) + (\bar{u} \cdot \bar{u}^* + \bar{u} \cdot \bar{u}) \\ & - (\bar{u} \bar{x}_2^* + \bar{u} \bar{x}_2 + \bar{u}^* \bar{x}_2)] \cdot \bar{n} - \bar{S}' \cdot \bar{n} - \bar{H}' \cdot \bar{n} \quad (41) \end{aligned}$$

From the definition given by (35) and (38) and equating the imaginary parts it follows that the growth rate α takes the form

$$\alpha = \alpha_p + \alpha_g \quad (42)$$

where α_p is the growth rate due to particle damping and α_g refers to the growth rate due to acoustic and vortical oscillations of the gas alone,

$$\begin{aligned} \alpha_p = & - \frac{1}{2E_N^2} \left[\frac{\bar{a}}{k_N} \int_{\Omega} ((\bar{H}' + \bar{S}')^{(1)} \cdot \nabla) \hat{p}_N d\Omega \right. \\ & \left. + \zeta \int_{\Omega} (\hat{Q}' + \hat{\phi}' + \hat{Z}')^{(R)} \hat{p}_N d\Omega \right] \quad (43) \end{aligned}$$

and

$$\begin{aligned} \alpha_g = & - \frac{1}{2E_N^2} \left[\frac{\bar{a}}{\bar{a}^2} \int_{\Gamma} ((\bar{u}' + \bar{u}^*)^{(R)} \hat{p}_N + \frac{\bar{u} \hat{p}_N^2}{\bar{a}^2}) \cdot \bar{n} d\Gamma \right. \\ & + \bar{\gamma} \int_{\Gamma} \hat{p}_N^2 \bar{u} \cdot \bar{n} d\Gamma + \frac{\bar{a}}{k_N} \int_{\Gamma} \bar{u} \cdot ((\bar{u}' + \bar{u}^*)^{(1)} \cdot \nabla) \hat{p}_N \cdot \bar{n} d\Gamma \\ & - (2\bar{\gamma} + 1) \int_{\Gamma} \hat{p}_N (\bar{u} \cdot \bar{n}) \hat{p}_N d\Gamma - \int_{\Gamma} \bar{u} \cdot \bar{u} \hat{p}_N^2 d\Gamma \\ & - \frac{\bar{a}}{k_N} \int_{\Gamma} \bar{u} \cdot ((\bar{u}' + \bar{u}^*)^{(1)} \cdot \bar{n}) \hat{p}_N d\Gamma \\ & \left. - \frac{\bar{a}}{k_N} \int_{\Gamma} ((\bar{u} \bar{x}_2^* + \bar{u}^* \bar{x}_2 + \bar{u}' \bar{x}_2)^{(1)} \cdot \bar{n}) \hat{p}_N d\Gamma \right] \quad (44) \end{aligned}$$

where (I) and (R) indicate imaginary and real parts, respectively.

Note that, in arriving at the stability integrals, it is necessary to perform integration by parts "twice" on all terms associated with the convection, viscous, and drag forces originated from the momentum equation as the wave equation was obtained by first differentiating the momentum equation. This will allow appropriate Neumann boundary conditions appearing on the boundary surfaces. A glance at (43) and (44), however, reveals that only the first integration by parts was performed on all terms other than the convective terms arising from the momentum equations. The remaining terms are yet to be integrated by parts "one more time" when their forms of derivatives are explicitly shown.

3. Evaluations of Particle Damping Stability Integral

3.1 Approximate Analytical Solution

We now return to (43) and examine (16) for perturbation quantities. The viscous drag forces are

$$\hat{H}' = \delta \hat{F}'_p + \hat{Q}' \quad (45)$$

where

$$\begin{aligned} \hat{F}'_p &= -\bar{\rho}_p [i\bar{a}k(\hat{u}' - \bar{u}') + (\bar{u}_p \cdot \nabla) \hat{u}'_p + (\hat{u}' \cdot \nabla) \bar{u}_p \\ &\quad - (\bar{u}' \cdot \nabla) \bar{u}' - (\hat{u}' \cdot \nabla) \bar{u}] \end{aligned} \quad (46)$$

$$\hat{Q}' = (\bar{u}_p - \bar{u}) \hat{u}'_p + (\hat{u}' - \bar{u}') \bar{u}_p \quad (47)$$

Similarly,

$$\hat{S}' = \mu [\nabla^2 \hat{u}' + \frac{1}{3} \nabla (\nabla \cdot \hat{u}')] \quad (48)$$

The linear viscous losses due to conduction heat transfer are contributed from \hat{Q}' ,

$$\hat{Q}' = \kappa \nabla^2 \hat{T}' \quad (49)$$

The heat transfer interaction energy \hat{T}' is given by

$$\hat{T}' = \hat{Y}' + \hat{Q}'_p \quad (50)$$

where

$$\begin{aligned} \hat{Y}' &= (1+\beta) (\hat{e}_p \bar{w}_p + \bar{e}_p \hat{w}'_p) - \beta C (\hat{T}'_p - \bar{T}') \bar{w}_p - \hat{S}' \cdot \bar{u} \\ &\quad - \bar{S}' \cdot \bar{u}' \end{aligned} \quad (51)$$

$$\begin{aligned} \hat{Q}'_p &= -\beta C_p [i\bar{a}k(\hat{T}'_p - \bar{T}') + (\bar{u}_p \cdot \nabla) \hat{T}'_p + (\hat{u}'_p \cdot \nabla) \bar{T}_p \\ &\quad - (\bar{u}' \cdot \nabla) \bar{T}' - (\hat{u}' \cdot \nabla) \bar{T}] \end{aligned} \quad (52)$$

Retaining only \hat{F}'_p of (45), \hat{Q}'_p in (50) we rewrite (43) in the form

$$\hat{F}'_p = \frac{1}{2E_N^2} \left[\frac{\bar{a}}{k_N} \int (\hat{F}'_p \cdot \nabla) \hat{p}_N d\Omega + \int \hat{Q}'_p \hat{p}_N d\Omega \right] \quad (53)$$

from which a simple formula may be derived for a linearized one-dimensional problem [5],

$$\frac{\hat{F}'_p}{\hat{F}_p} = \frac{1}{2} \frac{\tau_d}{1+\tau_d} \left[\frac{\tau_d^2}{1+(\tau_d^2)^2} + (6-1) \frac{C}{\bar{C}_p} \frac{\tau_d^2 \tau_t}{1+(\tau_t^2)^2} \right] \quad (54)$$

where τ_d and τ_t are the dynamic and thermal relaxation times, respectively,

$$\tau_d = \frac{s}{18\mu} \quad (55)$$

$$\tau_t = \frac{3}{2} \frac{C}{C_p} \Pr \tau_d \quad (56)$$

with ρ_s = density of the condensed material and d = average diameter of the particles.

To determine the effect of viscous and heat transfer losses arising from (48) and (49) we write

$$\alpha_p^{(b)} = \frac{-1}{2E_N^2} \left[\frac{\bar{a}}{k_N} \int_{\Omega} (\hat{S}'^{(I)} \cdot \nabla) \hat{p}_N d\Omega + \int_{\Omega} \hat{Q}' \hat{p}_N d\Omega \right] \quad (57a)$$

assuming an incompressible one-dimensional flow, we arrive at an analytical solution,

$$\alpha_p^{(b)} = \frac{2}{d} \sqrt{\frac{\omega_N u}{2\rho}} \left[1 + \frac{\gamma-1}{\sqrt{\Pr}} \right] \quad (57b)$$

The analytical integration of (43) is not possible and it is our approach to provide numerical integration via finite elements. In what follows we outline the detailed procedure.

3.2 Finite Element Formulation

The finite element formulation for the stability integral due to gas oscillations alone given by (44) was reported in [11]. Thus, our emphasis in this paper is concentrated on the stability integral representing only the particle damping as shown by (43).

Substituting (45) - (52) into (43), we obtain

$$\alpha_p = \alpha_{pH} + \alpha_{pS} + \alpha_{pQ} + \alpha_{pF} + \alpha_{pZ} \quad (58)$$

where

$$\begin{aligned} \alpha_{pH} &= \frac{1}{2E_N^2} \left[\frac{\bar{a}}{k_N} \rho_p \int_{\Gamma} ((\bar{u} \cdot \bar{u}_p) (\hat{u}'_p \cdot \nabla) \hat{p}_N + (\bar{u} \cdot \bar{u}') (\bar{u}_p \cdot \nabla) \hat{p}_N \right. \\ &\quad \left. - (\bar{u} \cdot \bar{u}) (\hat{u}' \cdot \nabla) \hat{p}_N - (\bar{u} \cdot \bar{u}') (\bar{u} \cdot \nabla) \hat{p}_N \right) d\Gamma \\ &\quad - \frac{\bar{a}}{k_N} \int_{\Omega} \rho_p \left((\bar{u}_p \cdot \bar{u}_p) (\hat{u}'_p \cdot \nabla) \cdot \nabla \hat{p}_N + \hat{u}'_p (\bar{u}_p \cdot \nabla) \cdot \nabla \hat{p}_N \right. \\ &\quad \left. - \bar{u}'_p (\hat{u}' \cdot \nabla) \nabla \hat{p}_N - \hat{u}' (\bar{u} \cdot \nabla) \cdot \nabla \hat{p}_N - (\bar{u}_p - \bar{u}) \hat{u}' \hat{p}_N \right. \\ &\quad \left. - (\hat{u}'_p - \bar{u}') \bar{u}_p \hat{p}_N \right) d\Omega \\ &\quad - \bar{a}^2 \rho_p \int_{\Omega} (\hat{u}'_p - \bar{u}') \cdot \nabla \left(\hat{p}_N d\Omega \right) \quad (I) \end{aligned} \quad (59)$$

$$\begin{aligned} \alpha_{pS} &= -\frac{u}{2E_N^2} \left[\frac{\bar{a}}{k_N} \int_{\Gamma} ((\bar{u} \cdot \bar{u}) (\hat{u}^* + \bar{u}') \cdot \nabla \hat{p}_N \right. \\ &\quad \left. + \frac{1}{3} (\bar{u} \cdot \bar{u}) \nabla \cdot (\hat{u}^* + \bar{u}') \hat{p}_N \right) d\Gamma \\ &\quad - \frac{\bar{a}}{k_N} \int_{\Omega} ((\hat{u}_i^* + \bar{u}_i') \cdot \nabla \hat{p}_N + \frac{1}{3} (\hat{u}^* + \bar{u}') \cdot \nabla \hat{p}_N) d\Omega \quad (II) \end{aligned} \quad (60)$$

$$\alpha_{pQ} = \frac{\zeta}{2E_N} \left[\int_{\Omega} (\mathbf{v} \cdot \nabla \hat{\mathbf{T}}') \hat{p}_N d\Omega - \int_{\Omega} (\nabla \hat{\mathbf{T}}' \cdot \nabla \hat{p}_N) d\Omega \right] \quad (61)$$

$$\begin{aligned} \alpha_{pS} &= \frac{\zeta p}{2E_N} \int_{\Omega} \left\{ \frac{1}{3} \mathbf{S} \cdot \hat{\mathbf{u}} \cdot (\hat{\mathbf{u}} + \hat{\mathbf{u}}^*) - 2 \frac{\partial \hat{\mathbf{u}}}{\partial \mathbf{x}_j} \frac{\partial (\hat{\mathbf{u}}_j + \hat{\mathbf{u}}_j^*)}{\partial \mathbf{x}_i} \right. \\ &\quad \left. - 2 \frac{\partial \hat{\mathbf{u}}_i}{\partial \mathbf{x}_j} \frac{\partial (\hat{\mathbf{u}}_j + \hat{\mathbf{u}}_j^*)}{\partial \mathbf{x}_j} \right\} \hat{p}_N d\Omega \quad (62) \end{aligned}$$

$$\begin{aligned} \alpha_{pZ} &= \frac{\zeta}{2E_N} \int_{\Omega} \left[(1+\beta) (\hat{\mathbf{e}}_p \cdot \hat{\mathbf{w}} + \hat{\mathbf{e}}_p \cdot \hat{\mathbf{w}}^*) - \beta C (\hat{\mathbf{T}}_p - \hat{\mathbf{T}}') \hat{\mathbf{w}}_p \right. \\ &\quad \left. - (\hat{\mathbf{S}} \cdot \hat{\mathbf{u}} + \hat{\mathbf{S}} \cdot \hat{\mathbf{u}}^*) - \hat{\rho} C p \left[\hat{\mathbf{a}} \cdot (\hat{\mathbf{T}}_p - \hat{\mathbf{T}}') + (\hat{\mathbf{u}} \cdot \nabla) \hat{\mathbf{T}}_p \right. \right. \\ &\quad \left. \left. + (\hat{\mathbf{u}} \cdot \nabla) \hat{\mathbf{T}}_p - (\hat{\mathbf{u}} \cdot \nabla) \hat{\mathbf{T}}' - (\hat{\mathbf{u}} \cdot \nabla) \hat{\mathbf{T}} \right] \right] \hat{p}_N d\Omega \quad (63) \end{aligned}$$

where the superscript (I) denotes the imaginary part. Note that the boundary terms in α_{pH} , α_{pS} , and α_{pQ} have appeared in addition to numerous other terms representing the viscous forces and thermal dissipation interacting with particles. Otherwise, the results are the same as in Culick[5].

To evaluate numerically these integrals, we introduce three-dimensional isoparametric finite elements. Any variable X may be interpolated as

$$X = \phi_{\alpha} X_{\alpha} \quad (64)$$

where ϕ_{α} is the interpolation function with α denoting the global node number.

The procedure for the solution of eigenvalues and eigenvectors for both acoustic and vortical motions are presented in [11]. Once the natural modes and frequencies of acoustic and vortical motions are determined, then the final form of the stability integral assumes the form

$$\begin{aligned} \alpha &= \int_{\Omega} F(\mathbf{r}) d\Omega + \int_{\Omega} G(\mathbf{z}) d\Omega = \int_{-1}^1 \int_{-1}^1 \int_{-1}^1 \hat{F}(\xi, \eta, \zeta) d\xi d\eta d\zeta \\ &\quad + \int_{-1}^1 \int_{-1}^1 \int_{-1}^1 \hat{G}(\xi, \eta, \zeta) d\xi d\eta d\zeta \quad (65) \end{aligned}$$

These integrals are then converted to Gaussian quadrature of the form

$$\begin{aligned} \alpha &= \sum_{i=1}^m \sum_{j=1}^m w_i w_j \hat{F}(\xi_i, \eta_j) \\ &\quad + \sum_{i=1}^m \sum_{j=1}^m \sum_{k=1}^m w_i w_j w_k \hat{G}(\xi_i, \eta_j, \zeta_k) \quad (66) \end{aligned}$$

where w_i represents the weights and ξ_i, η_j, ζ_k denote abscissa of the Gaussian quadrature [12].

4. Example Problems

To demonstrate the validity of the procedure, we consider a circular cylinder problem (Fig. 1) so that the results may be compared with the analytical solution given by (54).

The stability integral α_p is simplified to

$$\begin{aligned} \alpha_p &= - \frac{1}{2E_N^2} \left[\int_{\Omega} \hat{\mathbf{a}} \cdot \hat{\mathbf{r}}_p (\hat{\mathbf{u}}' - \hat{\mathbf{u}}^*) \hat{p}_N d\Omega \right. \\ &\quad \left. + \int_{\Omega} \zeta \rho C \hat{\mathbf{a}} \cdot \hat{\mathbf{k}}_N \hat{p}_p (\hat{\mathbf{T}}_p - \hat{\mathbf{T}}') \hat{p}_N d\Omega \right] \quad (67) \end{aligned}$$

In terms of the dynamic and thermal relaxation times, we obtain

$$\hat{\mathbf{u}}' - \hat{\mathbf{u}}^* = \left(\frac{1 + i\omega\tau_d}{1 + (\omega\tau_d)^2} - 1 \right) \frac{i}{\rho a k_N} \nabla \hat{p}_N \quad (68)$$

$$\hat{\mathbf{T}}_p - \hat{\mathbf{T}}' = \left(\frac{1 + i\omega\tau_t}{1 + (\omega\tau_t)^2} - 1 \right) \frac{(\gamma-1)}{\gamma \rho R} \hat{p}_N \quad (69)$$

The classical acoustic modes \hat{p}_N are of the form

$$\hat{p}_N = \cos(k_m z) \cos(m\theta) J_m(k_m r) \quad (70)$$

with

$$k_N^2 = k_\ell^2 + k_{mn}^2 \quad (71)$$

where $m = 0, 1, 2, \dots$, $k_\ell = \frac{\ell\pi}{L}$ with $\ell = 0, 1, 2, \dots$ and k_{mn} are the roots of the derivative of Bessel function $J_m(k_m r)$ such that

$$\frac{d}{dr} [J_m(k_m r)] = 0, \text{ at } r = R \quad (72)$$

Substituting (68) - (72) into (67) yields

$$\begin{aligned} \alpha_p &= - \frac{1}{2E_N^2} \frac{\beta}{1+\beta} \int_{\Omega} \left[\frac{\omega^2 \tau_d}{1 + (\omega\tau_d)^2} \nabla \hat{p}_N \right. \\ &\quad \left. + \frac{C(\gamma-1)}{C_p} \frac{\omega^2 \tau_t}{1 + (\omega\tau_t)^2} \hat{p}_N + \frac{C(\gamma-1)}{C_p} \hat{p}_N \right] r dr d\theta dz \quad (73) \end{aligned}$$

Numerical analyses have been carried out with the following assumptions: $\beta = 0.2$, $C(\gamma-1)/C_p = 1$, $\rho_s/\rho = 1$, $C_p/\rho = 1$, $P_r/(\gamma-1) = 1$. These assumptions yield $\tau_d = d^2/18$ and $\tau_t = d^2/12$. The results of calculations based on (54) and (73) for the first axial mode with various frequencies ($\omega = 300, 800, 1,800$ Hz) are shown in Fig. 2. Note here that the trend toward decrease in stability with a decrease in frequencies is evident for both one and two-dimensional geometries. However, the one-dimensional calculation overestimates (Fig. 3) the stability (particle damping) at higher frequencies ($\omega = 1,800$ Hz). The ranges for optimum diameters for the two-dimensional cylindrical system (3 microns for $\omega = 1,800$ Hz; 4 microns for $\omega = 800$ Hz; 6 microns for $\omega = 300$ Hz) are still maintained almost the same as in the one-dimensional approximations.

Referring to Fig. 4 for the first axial and tangential modes, the trends are significantly different from those of the axial mode. The two-dimensional cylindrical system is more stable than the one-dimensional system (Fig. 3) for all frequencies. Although the ranges of optimum diameters remain approximately the same as in the case of the axial mode, there is an indication that they shift toward

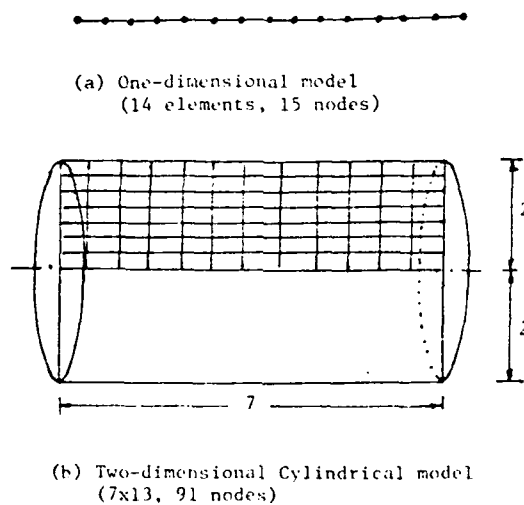


Fig. 1 Finite element models

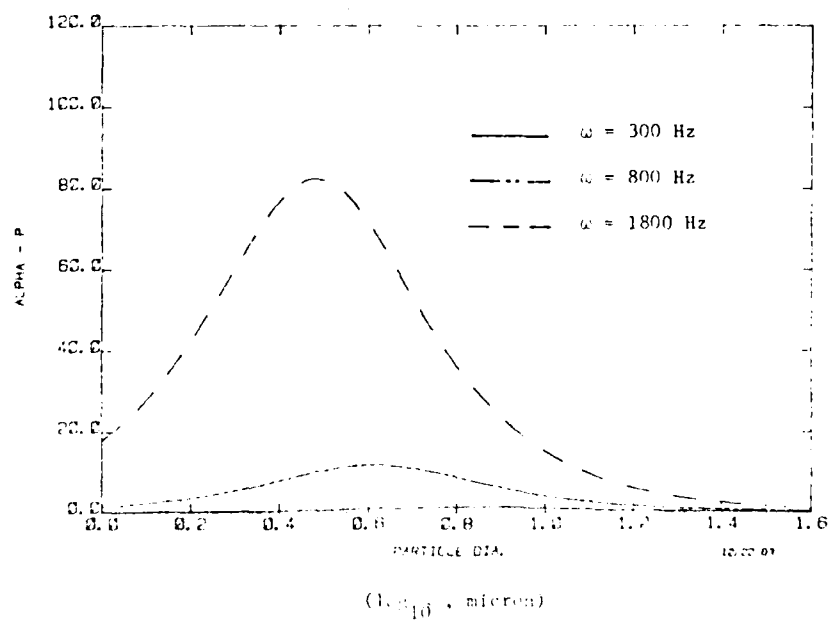


Fig. 2 Growth constants vs particle diameters, first axial mode for cylindrical geometry

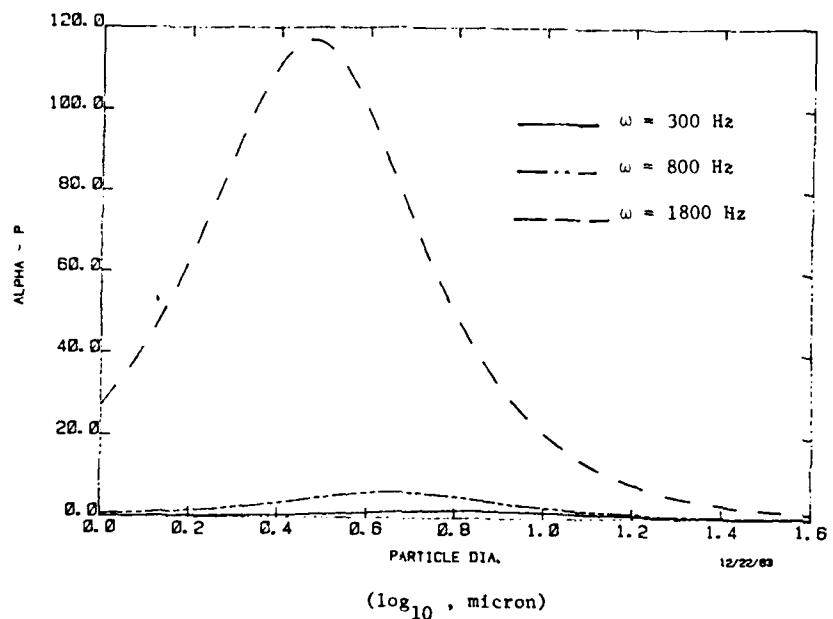


Fig. 3 Growth constants vs particle diameters, one-dimensional geometry

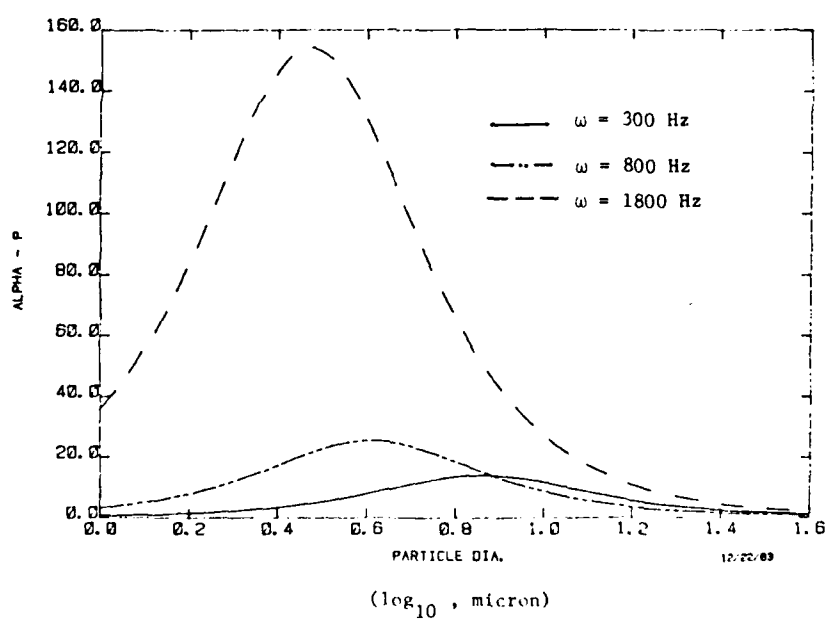


Fig. 4 Growth constants vs particle diameters for first axial and tangential mode for cylindrical geometry

larger sizes as the frequencies decrease.

In general, it is clear that one-dimensional approximations for the axisymmetric cylindrical geometries would lead to erroneous results. The trend of deviation depends on different modes of oscillations.

For more complete analysis, the flow field based on (1) through (22) and subsequent evaluations of the stability integrals (58-63) must be calculated. Note that there are seven variables: u_i , u_{pi} , T , T_{pi} , ρ_g , ρ_p , and p . Therefore, the required governing equations consist of (1), (2), (9), (12), (17), and (20). The drag forces are based on the Stokes law given by $F_{pi} = 3\pi\mu d(u_{pi} - u_i)$ and $Q_p = 2\pi\kappa d(T_p - T)$ where d denotes the average particle diameter and κ is the thermal conductivity. Initially, all incremental quantities, δu_{pi} , δT_p , δF_{pi} , δQ_p , $\delta \rho_p$, and δG are set equal to zero. Then these values are calculated from the initial solution and iterations continue until convergence. The results of this analysis will be reported elsewhere.

5. Concluding Remarks

A rigorous formulation of the governing equations involved in interactions of acoustic oscillations with vortical oscillations have been demonstrated. The finite element analyses for both flow field calculations and stability integral evaluations are shown to be convenient.

Simple example problems of two-dimensional axisymmetric geometries are solved and compared with one-dimensional approximations. It is shown that there is a trend toward decrease in stability with a decrease in frequencies. However, the one-dimensional calculation overestimates the stability at higher frequencies. The optimum ranges of diameters for stability, however, are approximately the same in both cylindrical and one-dimensional geometries. For the first axial and tangential modes, however, the trends are significantly different from those of the axial mode. The two-dimensional cylindrical system is more stable than the one-dimensional system for all frequencies. There is an indication that optimum particle diameters shift toward larger sizes as the frequencies decrease.

REFERENCES

1. Epstein, P. S. and Garhart, R.R. "The Absorption of Sound in Suspensions and Emulsions," *J. Acoustic Society of America*, Vol. 25, No. 3, 1953, pp. 552-565.
2. Dobbins, R. A. and Tempkin, S. "Measurement of Particulate Acoustic Attenuation," *AIAA J.*, Vol. 2, No. 6, 1964, pp. 1106-1111.
3. Tempkin, S. And Dobbins, R. R. "Measurements of Attenuation and Dispersion of Sound by an Aerosol," *J. Acoustic Society of America*, Vol. 40, No. 5, 1966, pp. 1016-1024.
4. Tempkin, S. and Dobbins, R. A. "Attenuation and Dispersion of Sound by Particulate Relaxation Processes," *J. Acoustic Society of America*, Vol. 40, 1966, pp. 317-324.
5. Culick, F. E. C. "T-Burner Testing of Metallized Solid Propellants," *AFRPL-TR-74-28*, October 1974.
6. Levine, J. N. and Culick, F. E. C. "Numerical Analysis of Nonlinear Longitudinal Combustion Instability in Metallized Propellant Solid Rocket Motors," *9th JANNAF Combustion Meeting*, Sept., 1972.
7. Culick, F. E. C. and Levine, J. N. "Comparison of Approximate and Numerical Analysis of Nonlinear Combustion Instability," *AIAA 12th Aerospace Science Meeting*, 1974, AIAA paper No. 74-201.
8. Culick, F. E. C. "Stability of Three-Dimensional Motions in a Combustion Chamber," *Combustion Science and Technology*, Vol. 10, 1975, pp. 109-124.
9. Derr, R. L., Kraeutle, K. J., Mathes, H. B., and Dehority, G. L. "Combustion Instability Studies Using Metallized Solid Propellants: Part I, Experimental Verification of Particle Damping Theory," *12th JANNAF Meeting*, 1975, CPIA No. 273, Vol. II pp. 155-165.
10. Kraeutle, K. J. and Derr, R. L. "Combustion Instability Studies Using Metallized Solid Propellants: Additional Experimental Evidence for the Validity of Particle Damping Theory," *13th JANNAF Combustion Meeting*, Vol. II Dec, 1976.
11. Chung, T. J., Hackett, R. M., and Kim, J. Y., "Recent Advances in Combustion Instability of Solid Propellant Rocket Motors," *AIAA Journal*, in press.
12. Chung, T. J. *Finite Element Analysis in Fluid Dynamics*, McGraw-Hill, 1978.

APPENDIX 3

UNSTEADY RESPONSE OF BURNING SURFACE
IN SOLID PROPELLANT COMBUSTION

T.J. Chung* and P.K. Kim**

Department of Mechanical Engineering
The University of Alabama in Huntsville
Huntsville, AlabamaAbstract

This paper is an update to the earlier paper concerning the multi-dimensional calculations of combustion response functions. Our ultimate goal is aimed at obtaining more precise information on combustion responses of heterogeneous solid propellants subjected to arbitrary cavity flow fields, i.e., pressure- and velocity-coupling with turbulent flames and possible effects of radiation. This paper is a first step toward such a goal. If multi-dimensional flow fields are allowed, the combustion responses can no longer be determined in a closed form, but they would require computerized numerical analyses for a large system of equations as a result of first and second order perturbations. All excited frequencies are calculated by means of eigenvalue analyses, and the combustion response functions corresponding to these frequencies are determined. For simplicity, the calculations are limited to homogeneous propellants and laminar flames. Effects of radiation, incident angles of impressed pressure waves, and velocity-coupling by means of the second order perturbation have been shown.

Nomenclature

a_0	mean local speed of sound
A	radiation boundary area (Eq. A-8)
A_b	admittance at burning surface
B	frequency factor
c	specific heat at constant pressure for gas
E^p	activation energy
f	fuel mass fraction
F	dimensional frequency
\hat{F}	response function
h	heat of combustion per unit mass of fuel
H	radiation function (Eq. A-8)
I	radiation intensity
k	gas thermal conductivity
K	dimensionless wave number
l	flame length
L	latent heat of vaporization, radiation
m	mean free path
M_b	Mach number at burning surface
n	constant exponent (Eq. 3, A-6), direction
	cosine
N	conduction to radiation parameter (Eq. 5)

P	pressure
Pr	Prandtl number
$q(R)$	radiative heat flux vector
r	burning rate
R	gas constant
R_c	dimensionless distance (Eq. 16)
Re	Reynolds number
Re	real part of complex variable (Eqs. 33,34)
t	time
T	temperature
u	gas velocity parallel to the flame surface
\bar{u}	gas velocity vector
\bar{u}_c	axial core velocity (Eq. 16)
v	gas velocity normal to the flame surface
w	radiation volumetric element (Eq. A-8)
x	reaction rate
y	coordinate parallel to the burning surface
z	coordinate normal to burning surface
α	oxidizer-fuel ratio
β	thermal diffusivity
δ	Eq. (3)
ϵ	constant exponent (Eq. A-6)
ζ	perturbation parameter
λ	Eq. (7)
λ_s	eigenvalue
λ_r	solid phase eigen function (Eq. B-17)
η	Lagrange multiplier
n	dimensionless radiation source function (Eq. A-9)
n_s	pressure index
ξ	Eq. (A-14)
ρ	mass density
τ	optical depth
ϕ	angle between normal vector to the surface (Eq. A-8)
ϕ	finite element interpolation function
θ	wave incidence angle
X	eigen vector
ω	frequency
Ω	albedo

Subscript and Superscript

$*$	dimensional quantity
i,j	vector quantity
o	mean or constant value
s	solid phase
∞	flame edge
w	radiative surface wall
α, β, γ	finite element global node number
(0)	zeroth order perturbation
(1)	first order perturbation
(2)	second order perturbation

*Professor

**Graduate Research Assistant

This research was supported partially by AFOSR
83-0084 with Dr Leonard Caveny as technical monitor.

I. Introduction

The response function as related to the combustion of solid propellants has been studied by numerous investigators. Some of the review articles include Culick [1] on homogeneous propellants [2-6] and Cohen [8] on heterogeneous propellants [9-14]. Both of them are limited to one-dimensional and quasi-steady situations. In recent years, some works toward non-steady problems have been attempted [15-17]. The majority of the discussions of response functions in the literature are concerned with pressure-coupling usually applicable in the linear stability. Computations of the response function for velocity-coupling important in a non-linear process, however, remain in a state of infancy, although some initial attempts toward this subject have been made [19].

As noted by Flandro [16], the velocity-coupling may be accommodated by second-order perturbations of multi-dimensional gas/solid governing equations. This approach deviates drastically from the one-dimensional analysis which has been adopted for nearly three decades. With modern computers and various tools of numerical analysis available, however, it seems possible to relax many undesirable restrictions. Observations indicate that combustion oscillations are time-dependent and often non-linear as influenced by turbulent flow fields, which may lead to erosive burning and unstable oscillations. Unfortunately, however, a computational tool for the most exact analysis of complicated physical phenomena such as these, even if developed, will not fit into the currently available computer. Thus, naturally, some approximations and simplifications must still be introduced to any theoretical formulations conducive to numerical analysis.

With this in mind, some additional materials and reassessments concerning the multi-dimensional calculations of combustion response functions are presented herein as an extension to the previous paper [17]. The influence of heterogeneity, surface roughness, particulate matter, or turbulence will not be considered at this time. We include the effect of radiation, adopt a simple, premixed, single-step laminar flame, expand the solid-gas governing equations into first and second order perturbations, and finally perform eigenvalue analyses. Complicated boundary conditions at the solid-gas interface and flame edges are imposed ideally by means of Lagrange multipliers together with finite elements. Calculations are carried out for various incident angles of impressed pressure waves at the flame edge boundaries [16].

Computed results show that the natural frequencies are clustered around low frequency range ($\omega < 10$). Spatial distributions of field variables corresponding to the computed frequencies indicate that the oscillatory behavior is pronounced at upstream and gradually diminishes toward downstream. Response functions oscillate in the axial direction with peaks occurring at the midstream, but diminishing toward flame edges for both first and second order perturbations. It is also shown that two-dimensional response functions are multi-peaked and may become negative as energy sinks. Finally, it is seen that the effect of radiation is more pronounced in the second order perturbation compared to the first order.

2. Governing Equations

The combustion of solid propellants is approximated by the Arrhenius law and a one-step forward chemical reaction. The flame of erosive burning is assumed to be a premixed laminar deflagration with a single species (fuel) [15,16].

The basic governing equations of the gas phase are composed of continuity, momentum, energy, species, and state. To non-dimensionalize these equations, we proceed as follows. Define the flame length as

$$l^* = k^*/c_p^* v^* \quad (1)$$

where $*$ denotes dimensional quantities, subscript o indicates the mean value in the chamber, k is the thermal conductivity, ρ is the density, c_p is the specific heat at constant pressure, and v is the gas speed normal to the surface.

Introduce, then, the following dimensionless quantities:

$$\begin{aligned} \rho &= \rho^*/\rho_o^*, \quad P = P^*/P_o^*, \quad T = T^*/T_o^* \\ u &= u^*/v_o^*, \quad t = t^*v_o^*/l^*, \quad x_i = x_i^*/l^* \\ M_b &= v^*/a_o^*, \quad h = h^*/c_p^* T^*, \quad E = E^*/RT \end{aligned} \quad (2)$$

where P is the pressure, T is the temperature, u is the mean flow velocity, t is the time, x is the length, subscript i denotes vector quantity, M_b is the Mach number at the burning surface, a_o^* is the speed of sound ($a_o^* = \sqrt{\gamma P_o^*/\rho_o^*}$ with $\gamma = c_v^*/c_p^*$), c_v is the specific heat at constant volume, h is the heat of combustion per unit mass of fuel, subscript ∞ denotes the flame edge, E is the activation energy, and R is the gas constant. From these, the governing equations for the gas phase are non-dimensionalized and the explicit forms are represented as in Appendix A (Eqs. A-1 through A-6). The dimensionless reaction rate explicitly involved in the equations of energy and species conservation is expressed as in Eq. (A-6). Note that the dimensionless frequency factor B is given by

$$B = \frac{B^* k^* T_o^* \rho^* n}{m^* c_p^* w'} \quad \text{with} \quad B = \frac{\rho^*}{\rho_o^*} \quad (3)$$

where B is the ratio of solid to gas density, n is the constant exponent, m is the mass flux, w' is the molecular weight of gas, z is the oxidizer-fuel ratio, * is the constant exponent and f is the fuel mass fraction. It is noted that Eq. (A-5) is valid under the assumption that the perfect gas law for the reference state holds,

$$P_o^* = \rho_o^* R T_o^* \quad (4)$$

The burning of solid propellants involves radiative heat transfer to some extent as the combustion chamber is an emitting, absorbing, and scattering media. It may be assumed that the boundary surfaces are gray and diffuse. Thus, the energy equation is given by

$$\begin{aligned} \rho [\frac{\partial T}{\partial t} + (u \cdot \nabla) T] - \frac{\gamma-1}{\gamma} \frac{\partial P}{\partial t} - \nabla^2 T + \frac{1-\Omega}{N} (T^4 \\ - \frac{1}{4\pi} H) - wh = 0 \end{aligned} \quad (5)$$

where Ω is the albedo, N is the conduction-to-radiation parameter, H is the radiation function, and η is the dimensionless radiation source function,

as defined in Eqs. (A-7) through (A-9).

For the solid phase, we assume that the mean burning rate is constant and the mean surface regression is given by

$$r^* = \rho_o^* v_o^* / \rho_s^* \quad (6)$$

where the subscript s indicates the solid phase. These and other variables are related as follows:

$$\begin{aligned} T_s^* &= T_o^* / T_s^* , \quad r = r^* / v_o^* , \quad y = y^* \rho_o^* v_o^* / k_o^* \\ t &= t^* \rho_o^* v_o^* / k_o^{*2} , \quad \zeta = k_s^* v_o^* / k_o^* c_s^* \end{aligned} \quad (7)$$

The dimensionless energy equation for the solid phase takes the form as in Eq. (A-10).

Conversion of solid to gas at the solid-gas interface may be governed by an Arrhenius law for the dimensional mass flux

$$m_s^* = B_s^* P_s^* n_s e^{-E_s} \quad (8)$$

with $E_s^* = E_s^* / RT_s^*$ being the dimensionless surface activation energy. The dimensionless mass, momentum, and energy balances across the interface are given in Appendix A-11 through A-13.

3. Perturbation Expansion

As proposed by Flandro [16], the perturbation expansion of all variables up to and including the second-order would enable the velocity-coupling, as well as the pressure-coupling, to be adequately modeled.

$$P = 1 + \epsilon P^{(1)} + \epsilon^2 P^{(2)} + \dots \quad (9)$$

$$\rho = \rho^{(0)} + \epsilon \rho^{(1)} + \epsilon^2 \rho^{(2)} + \dots \quad (10)$$

$$u = u^{(0)} + \epsilon u^{(1)} + \epsilon^2 u^{(2)} + \dots \quad (11)$$

$$T = T^{(0)} + \epsilon T^{(1)} + \epsilon^2 T^{(2)} + \dots \quad (12)$$

$$f = f^{(0)} + \epsilon f^{(1)} + \epsilon^2 f^{(2)} + \dots \quad (13)$$

$$T_s = T_s^{(0)} + \epsilon T_s^{(1)} + \epsilon^2 T_s^{(2)} + \dots \quad (14)$$

For simplicity, we may investigate an effect of an impressed pressure wave approaching the surface at arbitrary incidence given by

$$\begin{aligned} P &= 1 + \epsilon e^{i\omega t} [\cos K(x_o^* + x^*) \cos \theta + \cos K y \sin \theta] \\ &+ \epsilon^2 e^{i2\omega t} [\cos K(x_o^* + x^*) \cos \theta + \cos K y \sin \theta] + \dots \end{aligned} \quad (15)$$

where K is the dimensionless wave number ($K = 2\pi \cdot F/a_o^* v_o^*$), ω is the dimensionless frequency ($\omega = 2\pi \cdot F/v_o^*$), ϵ is the thermal diffusivity, F is the dimensionless frequency in Hertz, θ is the arbitrary incidence angle, and x_o^* is the antinode. It is also proposed [16] that a simple analytical model for the mean flow streamline in the vicinity of the surface be given by

$$u = u_c (1 - e^{-y/R_c}) \mathbf{i} + v \mathbf{j} \quad (16)$$

where u_c represents the axial core velocity, and R_c is the dimensionless distance from the surface.

Zeroth-Order System

All perturbation solutions begin with the zeroth-order system, which is one-dimensional and steady-state. Thus, we have

Continuity

$$\rho^{(0)} v^{(0)} = 1 \quad (17)$$

Energy

$$\frac{dT^{(0)}}{dy} - \frac{d^2 T^{(0)}}{dy^2} = w^{(0)} h \quad (18)$$

Species

$$\frac{df^{(0)}}{dy} - \frac{d^2 f^{(0)}}{dy^2} = -w^{(0)} \quad (19)$$

Reaction Rate

$$w^{(0)} = \frac{1}{h^2} Bz [\frac{1-T^{(0)}}{T^{(0)}}]^2 e^{-E/T^{(0)}} \quad (20)$$

State

$$\rho^{(0)} T^{(0)} = 1 \quad (21)$$

Solid Phase

$$\zeta \frac{d^2 T^{(0)}}{dy^2} - r^{(0)} \frac{dT_s^{(0)}}{dy} = 0 \quad (22)$$

$$\text{where } r^{(0)} = e^{-E_s(1/T_s^{(0)} - 1/\bar{T}_s)} \text{ with } E_s = E_s^* / RT_s^* \quad (23)$$

Solving (17) through (22) analytically results in

$$\rho^{(0)} = \frac{1}{T^{(0)}} \quad (24)$$

$$v^{(0)} = T^{(0)} \quad (25)$$

$$f^{(0)} = \frac{1}{h} (1-T^{(0)}) \quad (26)$$

$$T_s^{(0)} = (\bar{T}_s - T_\infty) e^{y/\zeta} + T_\infty \quad (27)$$

and the velocity distribution is given by (16). The temperature boundary conditions for the gas phase are obtained as follows:

at the flame edge ($y=\infty$)

$$T^{(0)}(\infty) = 1 \quad (28)$$

$$\frac{\partial T^{(0)}(\infty)}{\partial y} = 0 \quad (29)$$

at the solid-gas interface

$$T^{(0)}_+ = T^{(0)}_s - \bar{T}_s \quad (30)$$

$$\left(\frac{dT^{(0)}}{dy} \right)_+ = \frac{1}{\zeta} \left(\frac{dT_s^{(0)}}{dy} \right)_+ + L = \frac{\bar{T}_s - T_\infty}{\zeta} + L$$

Note that the temperature is continuous but its gradient is discontinuous at the interface.

Perturbation Systems

Perturbation expansions are performed by substituting Eqs. (9-14) into the governing equations using the following perturbed variables and Taylor

series expansion about the origin for the reaction rate and radiative terms.

$$(p^{(1)}, \dot{v}^{(1)}, \dot{u}^{(1)}, T^{(1)}, f^{(1)}, T_s^{(1)}) \\ = (\hat{p}^{(1)}, \dot{v}^{(1)}, \dot{u}^{(1)}, \hat{T}^{(1)}, \hat{f}^{(1)}) e^{i\omega t} \quad (31)$$

$$(p^{(2)}, \dot{v}^{(2)}, \dot{u}^{(2)}, T^{(2)}, f^{(2)}, T_s^{(2)}) \\ = (\hat{p}^{(2)}, \dot{v}^{(2)}, \dot{u}^{(2)}, \hat{T}^{(2)}, \hat{f}^{(2)}) e^{i2\omega t} \quad (32)$$

The results are listed in Eqs. (B-1 through B-9).

The boundary conditions corresponding to these perturbation equations include the flame edge ($y=\infty$), solid-gas interface ($y=0$), and the location deep in the solid ($y=-\infty$). At the flame edge, the mass fraction must vanish (Eq. B-10), and the impressed pressure wave, together with the equation of state (Eq. 5), will be specified. The temperature boundary condition (Eq. B-12) arises from the assumption that the flow is isentropic at the flame edge. On the other hand, the mass flux fractions of the fuel and oxidizer at the solid-gas interface are assumed to be fixed by the composition of the propellants (Eq. B-15). It also follows from Eq. (A-13) and Eq. (B-9) that the temperature boundary conditions at the solid-gas interface take an explicit form as shown in Eq. (B-16). Furthermore, as a consequence of mass and momentum balances across the interface, we arrive at the velocity boundary conditions (Eqs. B-20, B-21). For the location deep in the solid ($y=-\infty$), the temperature assumes a constant, independent of time, as defined in Eq. (B-24).

The second order perturbation system and the corresponding boundary conditions can be derived in a similar manner, and the results are listed in Eq. C-1 through C-9 and Eq. C-10 through C-25, respectively.

Finally, the response functions for the first and second order systems are calculated from

$$F^{(1)} = \text{Re} \left(\frac{A_b^{(1)}}{M_b} + \frac{\dot{v}^{(1)}/\dot{v}^{(0)}}{p^{(0)}/p^{(1)}} \right) \quad (33)$$

and

$$F^{(2)} = \text{Re} \left(\frac{A_b^{(2)}}{M_b} + \frac{\dot{v}^{(2)}/\dot{v}^{(0)}}{p^{(2)}/p^{(1)}} \right) \quad (34)$$

where $A_b^{(1)}$ and $A_b^{(2)}$ denote the admittance of the first and second order systems, respectively.

4. Finite Element Calculations

Fig. 1 shows the domain of study of the flame zone ($0 < y < \infty$) with the boundary conditions to be specified at the flame edge ($y=\infty$) and at the solid-interface ($y=0$). The solid phase ($0 < y < -\infty$) is eliminated from the calculation by providing the solid-interface boundary conditions.

The finite element equations, by means of isoparametric four-node linear elements, are constructed in the form

$$(i\omega A_{\xi\eta} + B_{\xi\eta}) X_{\eta} = F_{\xi} \quad (35)$$

where X_{η} denotes the solution vector consisting of nodal values of the density, velocity, temperature, mass fraction, and radiation function, i.e.,

$$X_{\eta} = [\rho_{\beta}, u_{\beta}, T_{\beta}, f_{\beta}, H_{\beta}] \quad (36)$$

In this formulation, the governing equations (Eqs. B-1 through B-8) are used for the first order system and Eqs. C-1 through C-8 are used for the second order system. Note that the pressure degree of freedom is excluded from computational processes through the equation of state. All boundary conditions (Eqs. B-10 through B-22 for the first order system; Eqs. C-10 through C-25 for the second order system) are cast in the form of the boundary matrix equation,

$$q_{rn} X_{\eta} = b_r \quad (37)$$

where $r=1, 2, \dots, m$, m being the total number of boundary conditions ($m=5$ in this case). Introducing the concept of Lagrange multipliers λ_r and minimization of variational principles, we now arrive at the finite element matrix equations with all boundary conditions properly imposed.

$$\begin{bmatrix} i\omega A_{\xi\eta} + B_{\xi\eta} & q_{r\xi} \\ q_{rn} & 0 \end{bmatrix} \begin{bmatrix} X_{\eta} \\ \lambda_r \end{bmatrix} = \begin{bmatrix} F_{\xi} \\ b_r \end{bmatrix} \quad (38)$$

This represents a system of complex characteristic equations lending itself to eigenvalue problems.

$$\begin{bmatrix} i\omega A_{\xi\eta} + B_{\xi\eta} & q_{r\xi} \\ q_{rn} & 0 \end{bmatrix} = 0 \quad (39)$$

These expressions (Eq. 38 and Eq. 39), of course, represent either the first or the second order perturbation system. Explicit forms of these equations are shown in Ref. [17]. Complex eigenvalues and eigenvectors can be calculated from Eq. (39). However, the system given by Eq. (38) represents forced oscillations with F_{ξ} and b_r serving as forcing functions. Thus, the actual amplitudes corresponding to each eigenvalue (natural frequency) can then be calculated from Eq. (38). From this information, it is now possible to determine the response functions corresponding to the first and second order perturbation systems. Finite element equations are summarized in Appendices D, E, and F.

5. Discussions

Additional calculations beyond the previous paper [17] are carried out. In particular, first order eigenvalue solutions and amplitudes corresponding to each of the natural frequencies are presented. The eigenvalue calculations for the second order perturbation system are not included at this time, although the amplitudes for the second order system corresponding to arbitrarily selected frequencies are computed. The computational domain is as shown in Fig. 1, and the various constants used are as follows: $E=10$, $E_s=4$, $L=0.15$, $T_s=0.35$, $T_{\infty}^{(0)}=1.0$, $M_b=0.01$, $B=1000$, $z=1$, $\zeta=\xi=1$, $n_s=0.75$, $k=1$, $\gamma=1.27$, $x_o^*=0$, $u_c=1$, $R_c=10$, $Pr=1.0$.

The results of the eigenvalue analysis, as shown in Fig. 2, represent 135 frequencies (corresponding to all variables over 135 finite element nodes). Note that most of these frequencies are clustered around a low frequency range ($\omega < 10.0$) with peaks occurring at approximately $\omega = 10^{-6}$ and

10^{-3} . This trend appears to be true for both radiative and non-radiative cases, although clustering peaks occur at slightly different frequencies.

As reported earlier [17], the spatial distributions of variables corresponding to the computed frequencies indicate that the oscillatory behavior is pronounced at upstream and gradually diminishes toward downstream.

Spatial distributions of the calculated response functions for the first and second order systems are shown, respectively, in Figs. 3 and 4 ($\omega=1.83$, $\beta=0.50$, $N=0.1$, $\theta=\pi/2$ and $M_b=0.01$). Although it is premature to make any reasonable assessments, response functions tend to oscillate in the axial direction with peaks occurring at mid-stream but diminishing toward flame edges. This trend appears to hold true for both first and second order perturbations. It is certain that this phenomenon is due to the presence of mean flow.

Fig. 5 shows the frequency dependence of response function for the first and second order systems at location M. It is clear that two-dimensional response functions are multi-peaked and may become negative as observed by T'ien [15]. The notion of energy sink in connection with negative response functions was suggested by Flandro [16], and this may perhaps be possible for an oscillatory system. The effect of radiation is more pronounced for the second order perturbation compared to the first order. In general, damping appears to prevail at low frequencies for the first order system. This trend is reversed for high frequencies. Large negative peaks develop for the second order system due to radiation at very low and very high frequencies, with intermediate ranges being subdued.

Effects of albedoes on response functions are shown in Fig. 6. It is clear that response functions increase with a decrease of albedoes for the first order response, whereas this trend is not obvious for the second order response. On the other hand, for low frequencies, this behavior is reversed for the case of the first order response (Fig. 7). Somewhat erratic behavior is observed for the second order response, although it increases negatively with a decrease of albedoes.

In Fig. 8, a directional dependency of response functions for the first order perturbation system (at location M) is shown in polar coordinates. As the incidence angle increases counter-clockwise, response functions decrease exponentially to the minimum at $\theta=\pi/2$, and start to increase again in the second quadrant. It may be reasoned that the wave incidence parallel to the burning surface may enhance the combustion response as opposed to the case of normal incidence. Furthermore, the influence of incidence directed upstream appears to be stronger than the incidences directed downstream. Similar trends prevail for the case of a second order perturbation system (Fig. 9), except that the response diminishes quickly as this angle approaches $\theta=\pi$.

6. Conclusions

Eigenvalue solutions to the first order perturbation system associated with rocket propellant combustion have been carried out. Based on this information, amplitudes of field variables in the flame zone are determined and response functions for selected frequencies are computed for both first and second order perturbation systems.

The following conclusions are summarized:

- (a) Most of the natural frequencies are clustered around low frequency range ($\omega < 10.0$).
- (b) Spatial distributions of field variables corresponding to the computed frequencies indicate that the oscillatory behavior is pronounced at upstream and gradually diminishes toward downstream.
- (c) Response functions oscillate in the axial direction with peaks occurring at mid-stream, but diminishing toward flame edges for both first and second order perturbations.
- (d) Two-dimensional response functions are multi-peaked and may become negative as energy sinks.
- (e) The effect of radiation is more pronounced in the second order perturbation compared to the first order.
- (f) Response functions are smallest at a normal wave incidence and increase toward parallel to the surface.

References

1. Culick, F.E.C., "A Review of Calculations for Unsteady Burning of a Solid Propellant", AIAA J., Vol. 7, No. 12, Dec. 1968, pp. 2241-2255.
2. Crad, H., "Resonant Burning in Rocket Motors", Commun. in Pure Appl. Math. 2, Mar. 1949, pp. 79-102.
3. Hart, R.W. and McClure, F.T., "Combustion Instability: Acoustic Interaction with a Burning Propellant Surface", J. Chem. Phys., 30, Sept. 1959, pp. 1501-1514.
4. Cheng, Sin-I., "Unstable Combustion in Solid Propellant Rocket Motors", in 8th Symposium on Combustion, Williams and Wilkins, 1962, pp. 81-96.
5. Denison, M.R. and Baum, E., "A Simplified Model of Unstable Burning on Solid Propellants", ARS J. 31, Aug. 1961, pp. 1112-1122.
6. Beckstead, M.W. and Price, E.W., "Non-acoustic Combustion Instability", AIAA J., Vol. 5, No. 11, Nov. 1967, pp. 1989-1996.
7. Williams, F.A., "Response of a Burning Solid to Small Amplitude Pressure Oscillations", J. of Applied Phys., Vol. 33, No. 1962, p. 3151.
8. Cohen, N.S., "Response Function Theories that Account for Size Distribution Effects - A Review", AIAA J., Vol. 19, No. 7, July 1981, pp. 907-912.
9. Williams, F.A. and Lengelle, G., "Simplified Model for Effect of Solid Heterogeneity on Oscillatory Combustion", Astronautica Acta, Vol. 14, Jan. 1968, pp. 97-118.
10. Law, C.K. and Williams, F.A., "A Theory for the Influence of Solid Heterogeneity on L* Instability", Combustion Science and Technology, Vol. 6, Feb. 1973, pp. 335-345.
11. Beckstead, M.W., Derr, R.L. and Price, C.F., "A Model of Solid Propellant Combustion

Based on Multiple Flames", AIAA J., Vol. 8, Dec. 1970, pp. 2200-2207.

12. Condon, J.A., Osborn, J.R. And Glick, R.L., "Statistical Analysis of Polydisperse, Heterogeneous Propellant Combustion: Non-steady-State", 13th JANNAF Combustion Meeting, CPIA publication 281, Vol. 2, 1976, pp. 209-223.
13. Beckstead, M.W., "Combustion Calculations for Composite Solid Propellants", 13th JANNAF Combustion Meeting, CPIA publication 281, Vol. 2, 1976, pp. 299-312.
14. Cohen, N.S. and Bower, J.M., "Combustion Response Modeling for Composite Solid Propellants", AFRPL-TR-78-39, Jet Propulsion Laboratory, Pasadena, Calif., June 1978.
15. T'ien, J.S., "Oscillatory Burning of Solid Propellants Including Gas Phase Time Lag", Combustion Science and Technology, Vol. 5, 1972.
16. Flandro, G.A., "Non-Linear Time-Dependent Combustion of a Solid Rocket Propellant", 19th JANNAF Combustion Meeting, Greenbelt, MD, Oct., 1982.
17. Chung, T.J. and Kim, P.K., "Finite Element Approach to Response Function Calculations for Solid Propellant Rocket Motors", AIAA Paper 84-1433, AIAA/SAE/ASME 20th Joint Propulsion Conf., June 11-13, 1984.
18. Cohen, N.S. and Strand, L.D., "Non-Steady Combustion of Composite Solid Propellants", JPL D-1602, May 1984.

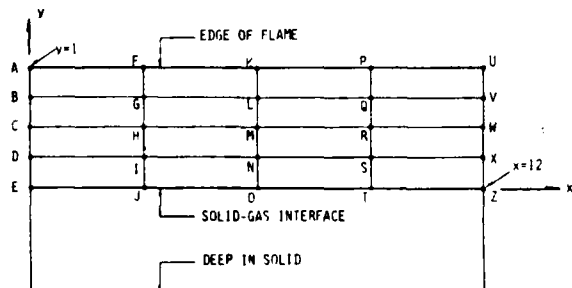


FIG. 1 FINITE ELEMENT GEOMETRY FOR GAS PHASE, 7 DEGREES OF FREEDOM (PRESSURE, DENSITY, TWO COMPONENTS OF VELOCITY, TEMPERATURE, FUEL MASS FRACTION, RADIATION FUNCTION)

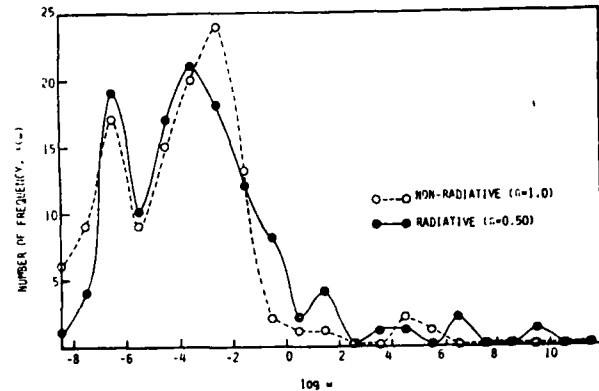


FIG. 2 NATURAL FREQUENCY DISTRIBUTIONS OF FLAME ZONE COMBUSTION, $R_b=0.01$, $N=0.001$, FIRST ORDER PERTURBATION SYSTEM

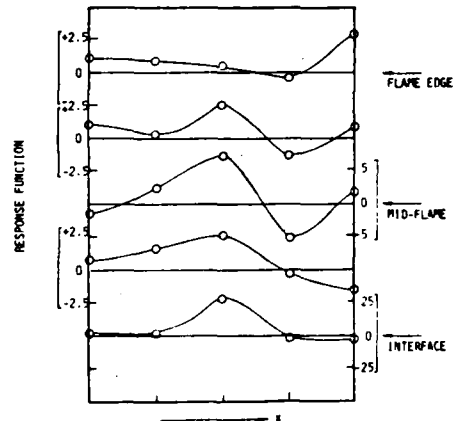


FIG. 3 SPATIAL DISTRIBUTION OF FIRST ORDER RESPONSE FUNCTION, $w=1.83$, $a=0.50$, $\theta=\pi/2$, $N=0.1$, $R_b=0.01$

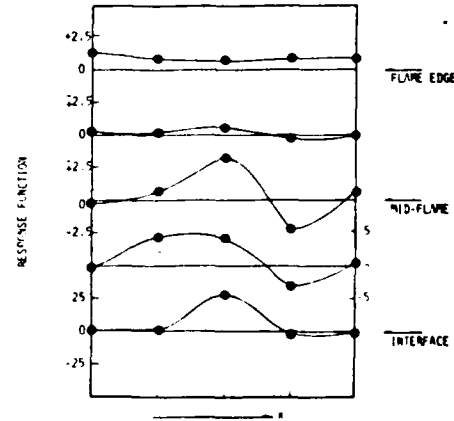


FIG. 4 SPATIAL DISTRIBUTIONS OF SECOND ORDER RESPONSE FUNCTION, $w=1.83$, $a=0.50$, $\theta=\pi/2$, $q=0.1$, $R_b=0.01$

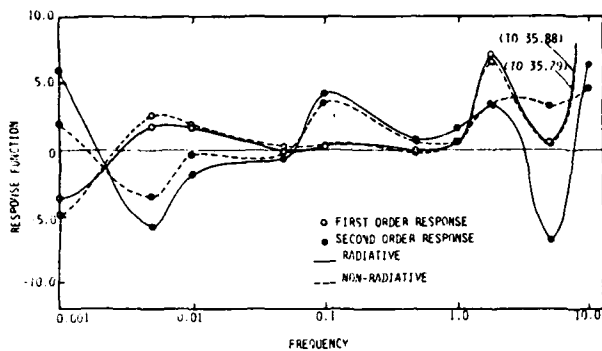


FIG. 5 FREQUENCY DEPENDENCE OF RESPONSE FUNCTIONS FOR FIRST AND SECOND ORDER SYSTEMS AT LOCATION $M_1 = 0.1\pi/2$, $M_2 = 0.01$, $N = 0.1$, $\alpha = 0.5$

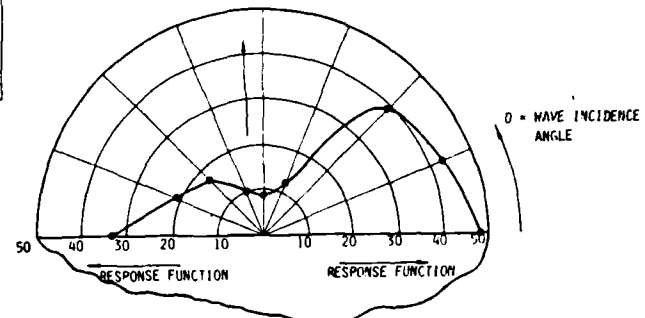


FIG. 8 DIRECTIONAL DEPENDENCE OF RESPONSE FUNCTIONS IN FIRST ORDER PERTURBATION SYSTEM AT LOCATION $M_1 = 0.1\pi/2$, $M_2 = 0.01$, $N = 0.1$, $\alpha = 0.75$

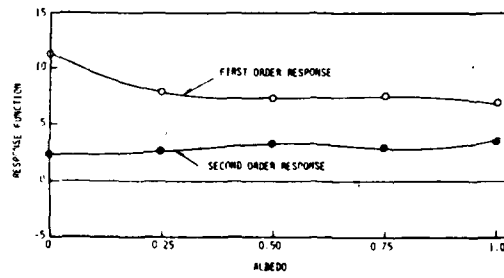


FIG. 6 ALBEDO EFFECTS ON RESPONSE FUNCTIONS FOR FIRST AND SECOND ORDER PERTURBATIONS AT LOCATION $M_1 = 0.1\pi/2$, $M_2 = 0.01$, $N = 0.1$, $\alpha = 0.5$

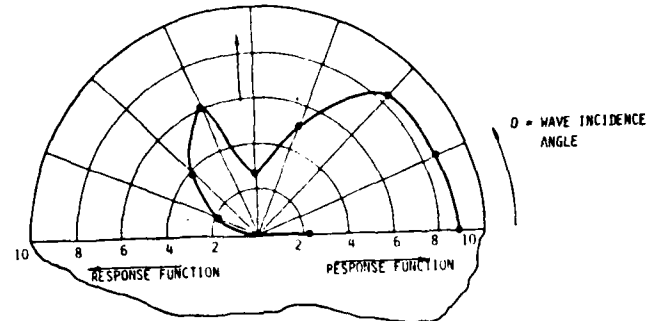


FIG. 9 DIRECTIONAL DEPENDENCE OF RESPONSE FUNCTION IN SECOND ORDER PERTURBATION SYSTEM AT LOCATION $M_1 = 0.1\pi/2$, $M_2 = 0.01$, $N = 0.1$, $\alpha = 0.75$

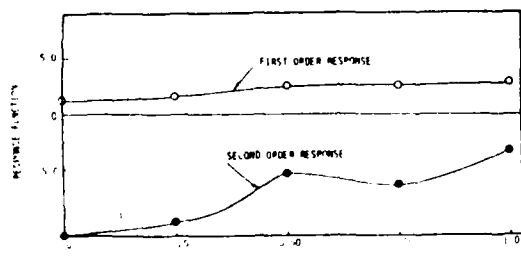


FIG. 7 ALBEDO EFFECTS ON RESPONSE FUNCTIONS FOR FIRST AND SECOND ORDER PERTURBATIONS AT LOCATION $M_1 = 0.1\pi/2$, $M_2 = 0.01$, $N = 0.1$, $\alpha = 0.5$

Appendix A - Governing Equations

(Gas Phase)

Continuity

$$\frac{\partial \rho}{\partial t} + \nabla \cdot (\rho \underline{u}) = 0 \quad (A-1)$$

Momentum

$$\rho \left[\frac{\partial \underline{u}}{\partial t} + (\underline{u} \cdot \nabla) \underline{u} \right] + \frac{1}{\gamma M_b^2} \nabla p - \Pr \nabla^2 \underline{u} + \frac{1}{3} \nabla (\nabla \cdot \underline{u}) = 0 \quad (A-2)$$

Energy

$$\rho \left[\frac{\partial T}{\partial t} + (\underline{u} \cdot \nabla) T \right] - \frac{\gamma-1}{\gamma} \frac{\partial p}{\partial t} - \nabla^2 T + \nabla \cdot \underline{q}_{(R)} - w h = 0 \quad (A-3)$$

Species Conservation

$$\rho \left[\frac{\partial f}{\partial t} + (\underline{u} \cdot \nabla) f \right] - \nabla^2 f + w = 0 \quad (A-4)$$

State

$$p = \rho T \quad (A-5)$$

Reaction Rate

$$w = B z T \left(\frac{p}{T} \right)^n f^n e^{-E/T} \quad (A-6)$$

Radiative Heat Transfer

$$\nabla \cdot \underline{q}_{(R)} = \frac{1-\Omega}{N} (T^4 - \frac{1}{4\pi} H) \quad (A-7)$$

$$H = \int_V \tau \frac{e^{-\tau}}{\tau^2} dV + \int_A T_w \frac{e^{-\tau_w}}{\tau_w^2} \cos \theta dA \quad (A-8)$$

$$\tau = (1-\Omega) T^4 + \frac{\Omega}{4\pi} H \quad (A-9)$$

(Solid Phase)

Energy

$$\frac{\beta}{\zeta} \frac{\partial T_s}{\partial t} + \frac{r}{\zeta} \frac{\partial T_s}{\partial y} - \nabla^2 T_s = 0 \quad (A-10)$$

(Solid-Gas Interface)

Mass Balance

$$m_s = \rho_s r = \rho v \quad (A-11)$$

$$\beta \left(\frac{\partial u}{\partial t} \right)_+ = (r \frac{\partial u}{\partial y})_+ \quad (A-12)$$

$$\frac{1}{\xi} \left(\frac{\partial T}{\partial y} \right)_- - \left(\frac{\partial T}{\partial y} \right)_+ = -rL \quad (A-13)$$

$$L = \frac{L^*}{\epsilon_p^* T_{\infty}^*} = \frac{h_p^* - h_s^*}{c_p^* T_{\infty}^*}, \quad \xi = k_o^* / k_s^* \quad (A-14)$$

Appendix B - First Order Perturbation System

(1) Governing Equations

Continuity

$$i\omega \hat{u}^{(1)} + \nabla \cdot (\rho^{(0)} \hat{u}^{(1)} + \hat{\rho}^{(1)} \underline{u}^{(0)}) = 0 \quad (B-1)$$

Momentum

$$i\omega \rho^{(0)} \hat{u}^{(1)} + \rho^{(0)} (\underline{u}^{(0)} \cdot \nabla) \hat{u}^{(1)} + \rho^{(0)} (\hat{u}^{(1)} \cdot \nabla) \underline{u}^{(0)} + \hat{\rho}^{(1)} (\underline{u}^{(0)} \cdot \nabla) \underline{u}^{(0)} + \frac{1}{\gamma M_b^2} \nabla p^{(1)} - \Pr \nabla^2 \underline{u}^{(1)} + \frac{1}{3} \nabla (\nabla \cdot \hat{u}^{(1)}) = 0 \quad (B-2)$$

Energy

$$i\omega \rho^{(0)} \hat{T}^{(1)} + \rho^{(0)} (\underline{u}^{(0)} \cdot \nabla) \hat{T}^{(1)} + \rho^{(0)} (\hat{u}^{(1)} \cdot \nabla) T^{(0)} + \hat{\rho}^{(1)} (\underline{u}^{(0)} \cdot \nabla) T^{(0)} - i\omega \frac{\gamma-1}{\gamma} \hat{p}^{(1)} - \nabla^2 \hat{T}^{(1)} + \nabla \hat{q}_{(R)}^{(1)} - \hat{w}^{(1)} h = 0 \quad (B-3)$$

Species Conservation

$$i\omega \rho^{(0)} \hat{f}^{(1)} + \rho^{(0)} (\underline{u}^{(0)} \cdot \nabla) \hat{f}^{(1)} + \rho^{(0)} (\hat{u}^{(1)} \cdot \nabla) f^{(0)} + \hat{\rho}^{(1)} (\underline{u}^{(0)} \cdot \nabla) f^{(0)} - \nabla^2 \hat{f}^{(1)} + \hat{w}^{(1)} = 0 \quad (B-4)$$

State

$$\hat{p}^{(1)} = \rho^{(0)} \hat{T}^{(1)} + \hat{\rho}^{(1)} T^{(0)} \quad (B-5)$$

Reaction Rate

$$\hat{w}^{(1)} = w^{(0)} \left[\frac{ET^{(1)}}{T^{(0)2}} + 2\hat{p}^{(1)} - 2\frac{\hat{T}^{(1)}}{T^{(0)}} + 2\frac{\hat{f}^{(1)}}{f^{(0)}} \right] \quad (B-6)$$

Radiative Heat Transfer

$$\nabla \hat{q}_{(R)}^{(1)} = \frac{1-\Omega}{N} [4(T^{(0)})^3 \hat{T}^{(1)} - \frac{1}{4\pi} \hat{H}^{(1)}] \quad (B-7)$$

$$\hat{H}^{(1)} = \int_V [4(1-\Omega)(T^{(0)})^3 \hat{T}^{(1)} + \frac{\Omega}{4\pi} \hat{H}^{(1)}] \frac{e^{-\tau}}{\tau^2} dV \quad (B-8)$$

Solid Phase Energy

$$i\omega \frac{\beta}{\zeta} \hat{T}_s^{(1)} + \frac{r^{(0)}}{\zeta} \frac{\partial \hat{T}_s^{(1)}}{\partial y} + \frac{\hat{r}^{(1)}}{\zeta} \frac{\partial T_s^{(0)}}{\partial y} - \nabla^2 \hat{T}_s^{(1)} = 0 \quad (B-9)$$

(2) Boundary Conditions

Flame Edge ($y=\infty$)

$$\hat{f}^{(1)}(\infty) = 0 \quad (B-10)$$

$$\rho^{(0)}(\infty) \hat{T}^{(1)}(\infty) + \hat{\rho}^{(1)}(\infty) T^{(0)}(\infty) = \cos K(x_o^* + x) \cos \theta + \cos K \ell^* \sin \theta \quad (B-11)$$

$$\hat{T}^{(1)}(\infty) = \frac{\gamma-1}{\gamma} \hat{p}^{(1)} - \frac{i}{\omega} \frac{\partial \hat{T}^{(1)}}{\partial y} \Big|_{y=\ell^*} \quad (B-12)$$

$$\hat{u}^{(1)}(\infty) = -\frac{1}{\gamma M_b} \sin K(x_o^* + x^*) \cos \theta \quad (B-13)$$

$$\hat{v}^{(1)}(\infty) = -\frac{1}{\gamma M_b} \sin K \ell^* \sin \theta \quad (B-14)$$

Solid-Gas Interface ($y=0$)

$$\hat{f}^{(1)}_+ = \left(\frac{\partial \hat{f}^{(1)}}{\partial y} \right)_+ + \left(\frac{\partial \hat{f}^{(0)}}{\partial y} \right)_+ \left[\frac{\hat{v}^{(1)}}{\bar{T}_s} \pm 1 - \frac{\hat{T}^{(1)}}{\bar{T}_s} \right] \quad (B-15)$$

$$\hat{T}^{(1)}_+ = \left(\frac{\partial \hat{T}^{(1)}}{\partial y} \right)_+ + \eta_s \left[\frac{1}{\beta\omega} A - \frac{1}{\beta\omega} B \lambda_1 - L \right] - \frac{\lambda_1}{\xi} \left(1 + \frac{1}{\beta\omega} \frac{E_s}{T_s} B \right) + \frac{E_s L}{T_s} - \frac{1}{\beta\omega} \frac{E_s}{T_s} A \quad (B-16)$$

$$\text{where } \lambda_1 = \frac{1}{2\xi} [1 + (1 + 4i\beta\xi)^{1/2}] \quad (B-17)$$

$$A = - \frac{\bar{T}_s - T_\infty}{\zeta\xi} \quad (B-18)$$

$$B = - \frac{\bar{T}_s - T_\infty}{\zeta\xi} \quad (B-19)$$

$$\hat{u}^{(1)}_+ = - \frac{1}{\beta\omega} \left(\frac{E_s}{T_s} \hat{T}^{(1)}_+ + \eta_s \left(\frac{\partial \hat{u}^{(0)}}{\partial y} \right)_+ \right) [\cos K(x_o^* + x^*) \cos \theta + \sin \theta] \quad (B-20)$$

$$\hat{v}^{(1)}_+ = \left\{ \left[(E_s + 1) \hat{T}^{(1)}_+ + (\eta_s - 1) \bar{T}_s \right] - \frac{1}{\beta\omega} \left(\frac{E_s}{T_s} \hat{T}^{(1)}_+ + \eta_s \left(\frac{\bar{T}_s - T_\infty}{\zeta} \right) \right) \right\} [\cos K(x_o^* + x^*) \cos \theta + \sin \theta] \quad (B-21)$$

$$\hat{\rho}^{(0)} \hat{T}^{(1)}_+ + \hat{\rho}^{(1)} \hat{T}^{(0)}_+ = \cos K(x_o^* + x^*) \cos \theta + \sin \theta \quad (B-22)$$

Deep in Solid ($y=-\infty$)

$$\hat{T}_s^{(1)}(-\infty) = 0 \quad (B-23)$$

$$\frac{\partial \hat{T}_s^{(1)}}{\partial x} \Big|_{x=-\infty} = \frac{\partial \hat{T}_s^{(1)}}{\partial y} \Big|_{y=-\infty} = 0 \quad (B-24)$$

Appendix C - Second Order Perturbation System(1) Governing EquationsContinuity

$$12\omega \hat{\rho}^{(2)} + \nabla \cdot (\hat{\rho}^{(0)} \hat{u}^{(2)} + \hat{\rho}^{(1)} \hat{u}^{(1)} + \hat{\rho}^{(2)} \hat{u}^{(0)}) = 0 \quad (C-1)$$

Momentum

$$12\omega \hat{\rho}^{(0)} \hat{u}^{(2)} + \hat{\rho}^{(0)} \left[(\hat{u}^{(0)} \cdot \nabla) \hat{u}^{(2)} + (\hat{u}^{(1)} \cdot \nabla) \hat{u}^{(1)} + (\hat{u}^{(2)} \cdot \nabla) \hat{u}^{(0)} \right] + \hat{\rho}^{(1)} \left[(\hat{u}^{(0)} \cdot \nabla) \hat{u}^{(1)} + (\hat{u}^{(1)} \cdot \nabla) \hat{u}^{(0)} \right] + \hat{\rho}^{(2)} \left[(\hat{u}^{(0)} \cdot \nabla) \hat{u}^{(0)} + \frac{1}{\gamma M_b^2} \nabla \hat{p}^{(2)} - \Pr \left(\nabla^2 \hat{u}^{(2)} + \frac{1}{3} \nabla (\nabla \cdot \hat{u}^{(2)}) \right) \right] = 0 \quad (C-2)$$

Energy

$$12\omega \hat{\rho}^{(0)} \hat{T}^{(2)} + \hat{\rho}^{(0)} \left[(\hat{u}^{(0)} \cdot \nabla) \hat{T}^{(2)} + (\hat{u}^{(1)} \cdot \nabla) \hat{T}^{(1)} + (\hat{u}^{(2)} \cdot \nabla) \hat{T}^{(0)} \right] + \hat{\rho}^{(1)} \left[(\hat{u}^{(0)} \cdot \nabla) \hat{T}^{(1)} + (\hat{u}^{(1)} \cdot \nabla) \hat{T}^{(0)} \right] + \hat{\rho}^{(2)} \left[(\hat{u}^{(0)} \cdot \nabla) \hat{T}^{(0)} + 12\omega \frac{\gamma-1}{\gamma} \hat{p}^{(2)} - \nabla^2 \hat{T}^{(2)} + \nabla \hat{q}_{(R)}^{(2)} - \hat{w}^{(2)} h \right] = 0 \quad (C-3)$$

Species Conservation

$$12\omega \hat{\rho}^{(0)} \hat{f}^{(2)} + \hat{\rho}^{(0)} \left[(\hat{u}^{(0)} \cdot \nabla) \hat{f}^{(2)} + (\hat{u}^{(1)} \cdot \nabla) \hat{f}^{(1)} + (\hat{u}^{(2)} \cdot \nabla) \hat{f}^{(0)} \right] + \hat{\rho}^{(1)} \left[(\hat{u}^{(0)} \cdot \nabla) \hat{f}^{(1)} + (\hat{u}^{(1)} \cdot \nabla) \hat{f}^{(0)} \right] + \hat{\rho}^{(2)} \left[(\hat{u}^{(0)} \cdot \nabla) \hat{f}^{(0)} - \nabla^2 \hat{f}^{(2)} + \hat{w}^{(2)} \right] = 0 \quad (C-4)$$

State

$$\hat{p}^{(2)} = \hat{\rho}^{(0)} \hat{T}^{(2)} + \hat{\rho}^{(1)} \hat{T}^{(1)} + \hat{\rho}^{(2)} \hat{T}^{(0)} \quad (C-5)$$

Reaction Rate

$$\begin{aligned} \hat{w}^{(2)} = w^{(0)} & \left\{ \frac{E \hat{T}^{(2)}}{(T^{(0)})^2} + \frac{E \hat{T}^{(1)}}{(T^{(0)})^2} [2\hat{p}^{(1)} - 2 \frac{\hat{T}^{(1)}}{T^{(0)}} \right. \\ & + 2 \frac{\hat{f}^{(1)}}{f^{(0)}}] + (\hat{p}^{(1)})^2 + 2\hat{p}^{(2)} + \left(\frac{\hat{T}^{(1)}}{T^{(0)}} \right)^2 \\ & - 2 \frac{\hat{T}^{(2)}}{T^{(0)}} + \frac{(\hat{f}^{(1)})^2}{f^{(0)}} + 2 \frac{\hat{f}^{(2)}}{f^{(0)}} \\ & + 2\hat{p}^{(1)} \left[-2 \frac{\hat{T}^{(1)}}{T^{(0)}} + 2 \frac{\hat{f}^{(1)}}{f^{(0)}} + \frac{E \hat{T}^{(1)}}{(T^{(0)})^2} \right] \\ & - 2 \frac{\hat{T}^{(1)}}{T^{(0)}} [2\hat{p}^{(1)} + 2 \frac{\hat{f}^{(1)}}{f^{(0)}} + \frac{E \hat{T}^{(1)}}{(T^{(0)})^2}] \\ & + 2 \frac{\hat{f}^{(1)}}{f^{(0)}} [2\hat{p}^{(1)} - 2 \frac{\hat{T}^{(1)}}{T^{(0)}} + \frac{E \hat{T}^{(1)}}{T^{(0)}}] \\ & \left. + \frac{E \hat{T}^{(1)}}{(T^{(0)})^2} [2\hat{p}^{(1)} - 2 \frac{\hat{T}^{(1)}}{T^{(0)}} + 2 \frac{\hat{f}^{(1)}}{f^{(0)}}] \right\} \end{aligned} \quad (C-6)$$

Radiative Heat Transfer

$$\nabla \hat{q}_{(R)}^{(2)} = \frac{1-\Omega}{N} [4(T^{(0)})^3 \hat{T}^{(2)} + 6(T^{(0)})^2 (\hat{T}^{(1)})^2 - \frac{1}{4\pi} \hat{H}^{(2)}] \quad (C-7)$$

$$\hat{H}^{(2)} = \int_V [4(1-\Omega)(T^{(0)})^3 \hat{T}^{(2)} + 6(T^{(0)})^2 (\hat{T}^{(1)})^2 + \frac{\Omega}{4\pi} \hat{H}^{(2)}] \frac{e^{-\tau}}{\tau^2} dV \quad (C-8)$$

Solid Phase Energy

$$12\omega \frac{\beta}{\zeta} \hat{T}_s^{(2)} + \frac{r^{(0)}}{\zeta} \frac{\partial \hat{T}_s^{(2)}}{\partial y} + \frac{r^{(1)}}{\zeta} \frac{\partial \hat{T}_s^{(1)}}{\partial y} \quad (C-9)$$

$$+ \frac{\hat{r}^{(2)}}{\zeta} \frac{\partial \hat{T}_s^{(0)}}{\partial y} - \nabla^2 \hat{T}_s^{(2)} = 0 \quad (C-9)$$

(2) Boundary Condition

Flame Edge ($y=\infty$)

$$\hat{f}^{(2)}(\infty) = 0 \quad (C-10)$$

$$\rho^{(0)}(\infty) \hat{T}^{(2)}(\infty) + \hat{\rho}^{(1)}(\infty) \hat{T}^{(1)}(\infty) + \hat{\rho}^{(2)}(\infty) T^{(0)}(\infty)$$

$$= \cos K(x_o^* + x^*) \cos \theta + \cos K \ell^* \sin \theta \quad (C-11)$$

$$\hat{T}^{(2)}(\infty) = \frac{\gamma-1}{\gamma} \hat{p}^{(2)} - \frac{i}{\omega} \frac{\partial \hat{T}^{(2)}}{\partial y} \Big|_{y=\ell^*} \quad (C-12)$$

$$\hat{u}^{(2)}(\infty) = -\frac{1}{\gamma M_b} \sin K(x_o^* + x^*) \cos \theta \quad (C-13)$$

$$\hat{v}^{(2)}(\infty) = -\frac{1}{\gamma M_b} \sin K \ell^* \sin \theta \quad (C-14)$$

Solid-Gas Interface ($y=0$)

$$\begin{aligned} \hat{f}^{(2)}_+ &= (\frac{\partial \hat{f}^{(2)}}{\partial y})_+ + (\frac{\partial \hat{f}^{(1)}}{\partial y})_+ [\frac{\hat{v}^{(1)}_+}{\bar{T}_s} + 1 \\ &\quad - \frac{\hat{T}^{(1)}_+}{\bar{T}_s}] + (\frac{\partial \hat{f}^{(0)}}{\partial y})_+ [\frac{\hat{v}^{(2)}_+}{\bar{T}_s} - (\frac{\hat{v}^{(1)}_+}{\bar{T}_s})^2 \\ &\quad - \frac{\hat{T}^{(2)}_+}{\bar{T}_s} + (\frac{\hat{T}^{(1)}_+}{\bar{T}_s})^2] \end{aligned} \quad (C-15)$$

$$\begin{aligned} \hat{T}^{(2)}_+ &= (\frac{\partial \hat{T}^{(2)}}{\partial y})_+ + \frac{1}{\beta \omega} CG - \frac{1}{(\beta \omega)^2} D(G + \eta_s) - LG \\ &\quad \frac{\lambda_1}{\xi} + L \frac{E_s}{\bar{T}_s} - \frac{1}{\beta \omega} \frac{E_s}{\bar{T}_s} C \end{aligned} \quad (C-16)$$

$$\text{where } C = \frac{\bar{T}_s - T_\infty}{\zeta \xi} (\lambda_1 - \frac{1}{\zeta}) \quad (C-17)$$

$$D = \frac{C}{\zeta} \quad (C-18)$$

$$\begin{aligned} G &= (\frac{E_s}{\bar{T}_s} \hat{T}^{(1)}_+)^2 + 2\eta_s \frac{E_s}{\bar{T}_s} \hat{T}^{(1)}_+ \\ &\quad + \eta_s (\eta_s - 1) \end{aligned} \quad (C-19)$$

$$\begin{aligned} \hat{u}^{(2)}_+ &= -\frac{1}{\beta \omega} \{ [\frac{E_s}{\bar{T}_s} \hat{T}^{(1)}_+ + \eta_s] (\frac{\partial \hat{u}^{(1)}_+}{\partial y})_+ \\ &\quad + [2\eta_s \frac{E_s}{\bar{T}_s} \hat{T}^{(1)}_+ + \eta_s (\eta_s - 1) + (\frac{E_s}{\bar{T}_s} \hat{T}^{(1)}_+)^2 \\ &\quad + \frac{E_s}{\bar{T}_s} \hat{T}^{(2)}_+] (\frac{\partial u^{(0)}}{\partial y})_+ \} [\cos K(x_o^* + x^*) \cos \theta \\ &\quad + \sin \theta]^2 \end{aligned} \quad (C-20)$$

$$\hat{v}^{(2)}_+ = (R - \frac{1}{\beta \omega} I) [\cos K(x_o^* + x^*) \cos \theta + \sin \theta]^2 \quad (C-21)$$

where

$$\begin{aligned} R &= (E_s + 1) \hat{T}^{(2)}_+ + \frac{E_s (E_s + 1)}{\bar{T}_s} (\hat{T}^{(1)}_+)^2 \\ &\quad + [E_s (2\eta_s - \frac{1}{\bar{T}_s^2}) + (\eta_s - 1)] \hat{T}^{(1)}_+ \end{aligned}$$

$$+ (\eta_s - 1) [\eta_s \bar{T}_s - \frac{1}{\bar{T}_s}] \quad (C-22)$$

$$\begin{aligned} I &= (\frac{E_s}{\bar{T}_s} \hat{T}^{(1)}_+ + \eta_s) (\frac{\partial \hat{v}^{(1)}_+}{\partial y})_+ + [2\eta_s \frac{E_s}{\bar{T}_s} \hat{T}^{(1)}_+ \\ &\quad + \eta_s (\eta_s - 1) + (\frac{E_s}{\bar{T}_s} \hat{T}^{(1)}_+)^2 + \frac{E_s}{\bar{T}_s} \hat{T}^{(2)}_+ + \frac{\bar{T}_s - T_\infty}{\zeta}] \end{aligned} \quad (C-23)$$

$$\begin{aligned} \rho^{(0)} \hat{T}^{(2)}_+ &+ \hat{\rho}^{(1)} \hat{T}^{(1)}_+ + \hat{\rho}^{(2)} T^{(0)}_+ \\ &= \cos K(x_o^* + x^*) \cos \theta + \sin \theta \end{aligned} \quad (C-24)$$

Deep in the Solid

$$\hat{T}_s^{(2)}(-\infty) = 0 \quad (C-25)$$

$$\frac{\partial \hat{T}_s^{(2)}}{\partial x} \Big|_{y=-\infty} = \frac{\partial \hat{T}_s^{(2)}}{\partial y} \Big|_{y=-\infty} = 0 \quad (C-26)$$

Appendix D -Finite Element Equations of First Order System

(1) Governing Equations

Continuity

$$(i\omega A_{\alpha\beta} + \bar{B}_{\alpha\beta}) \rho_\beta^{(1)} + \bar{C}_{\alpha\beta i} u_\beta^{(1)} = 0 \quad (D-1)$$

Momentum

$$(i\omega A_{\alpha\beta} + \bar{D}_{\alpha\beta}) u_\beta^{(1)} + \bar{E}_{\alpha\beta i} \rho_\beta^{(1)} + \bar{F}_{\alpha\beta i} T_\beta^{(1)} = 0 \quad (D-2)$$

Energy

$$\begin{aligned} (i\omega G_{\alpha\beta} + \bar{H}_{\alpha\beta} + \bar{R}A_{\alpha\beta}) T_\beta^{(1)} &- (i\omega \bar{D}_{\alpha\beta} + \bar{P}_{\alpha\beta}) \rho_\beta^{(1)} \\ &- \bar{R}B_{\alpha\beta} H_\beta^{(1)} = 0 \end{aligned} \quad (D-3)$$

Species

$$(i\omega \bar{A}_{\alpha\beta} + \bar{Q}_{\alpha\beta}) f_\beta^{(1)} + \bar{R}_{\alpha\beta} T_\beta^{(1)} + \bar{S}_{\alpha\beta} \rho_\beta^{(1)} = 0 \quad (D-4)$$

Radiation Function

$$\bar{R}C_{\alpha\beta} T_\beta^{(1)} + (\bar{R}D_{\alpha\beta} - A_{\alpha\beta}) H_\beta^{(1)} = 0 \quad (D-5)$$

Note that explicit forms of these matrices are shown in Appendix F.

(2) Boundary Conditions

Flame Edge

$$f_\beta^{(1)} = 0 \quad (D-6)$$

$$(\frac{i}{\omega} A_\beta + B_\beta) T_\beta^{(1)} = \bar{A} \quad (D-7)$$

$$T^{(0)} B_\beta \rho_\beta^{(1)} + \rho^{(0)} B_\beta T_\beta^{(1)} = \bar{B} \quad (D-8)$$

$$B_\beta u_\beta^{(1)} = i\bar{R} \quad (D-9)$$

$$B_\beta v_\beta^{(1)} = i\bar{I} \quad (D-10)$$

where

$$v_\beta = \frac{\partial \phi_\beta}{\partial y} \Big|_{y=\ell^*} \quad (D-11)$$

$$B_\beta = \phi_\beta \Big|_{y=\ell^*} \quad (D-12)$$

$$\bar{A} = \frac{\gamma-1}{\gamma} [G1]_\beta B_\beta \quad (D-13)$$

$$\bar{B} = [G1]_\beta B_\beta \quad (D-14)$$

$$G1 = \cos K(x_o^* + x^*) \cos \theta + \cos K l^* \sin \theta \quad (D-15)$$

$$\bar{H} = -\frac{1}{\gamma M_b} [\sin K(x_o^* + x^*) \cos \theta]_\beta B_\beta \quad (D-16)$$

$$\bar{I} = -\frac{1}{\gamma M_b} \sin K l^* \sin \theta \quad (D-17)$$

Solid-Gas Interface

$$(E_\beta - F_\beta) f_\beta^{(1)} - (\bar{C} \frac{E_\beta}{T_s}) v_\beta^{(1)} + (\bar{C} \frac{E_\beta}{T_s}) T_\beta^{(1)} = \bar{C} \quad (D-18)$$

$$\left\{ \frac{i}{\omega} \frac{E_\beta}{\beta T_s} \left(\frac{\lambda_1}{\zeta} B - A \right) E_\beta + \left[\left(\frac{\lambda_1}{\zeta} + \frac{E_s}{T_s} L \right) E_\beta - F_\beta \right] \right\} T_\beta^{(1)} = \frac{i}{\omega} \frac{\eta_s}{\beta} (A - B \lambda_1) - \eta_s L \quad (D-19)$$

$$E_\beta u_\beta^{(1)} + \left\{ \frac{i}{\omega} \frac{u_c}{\beta R_c} \frac{E_s}{T_s} \bar{D} E_\beta \right\} T_\beta^{(1)} = \frac{i}{\omega} \frac{\eta_s}{\beta} \frac{u_c}{R_c} \bar{D} \quad (D-20)$$

$$E_\beta v_\beta^{(1)} = \bar{D} \left[(E_s + 1) - \frac{1}{\beta \omega} \frac{E_s}{T_s} \left(\frac{\bar{T}_s - T_\infty}{\zeta} \right) \right] E_\beta T_\beta^{(1)} = -\frac{i}{\omega} \frac{\eta_s}{\beta} \frac{\bar{T}_s - T_\infty}{\zeta} \bar{D} + (\eta_s - 1) \bar{T}_s \quad (D-21)$$

$$(T_\beta^{(0)} + E_\beta) \rho_\beta^{(1)} + (\rho_\beta^{(0)} + E_\beta) T_\beta^{(1)} = \bar{D} \quad (D-22)$$

where

$$E_\beta = \phi_\beta \Big|_{y=0} \quad (D-23)$$

$$F_\beta = \frac{\partial \phi_\beta}{\partial y} \Big|_{y=0} \quad (D-24)$$

$$\bar{C} = \left(\frac{\partial f^{(0)}}{\partial y} \right)_\beta E_\beta \quad (D-25)$$

$$\bar{D} = [G2]_\beta E_\beta \quad (D-26)$$

$$G2 = \cos K(x_o^* + x^*) \cos \theta + \sin \theta \quad (D-27)$$

Appendix E -

Finite Element Equations of Second Order System

(1) Governing Equations

Continuity

$$(12\omega A_{\alpha\beta} + \bar{B}_{\alpha\beta}) \rho_\beta^{(2)} + \bar{C}_{\alpha\beta 1} u_{\beta 1}^{(2)} = F A_1 \quad (E-1)$$

Momentum

$$(12\omega A_{\alpha\beta} + \bar{B}_{\alpha\beta}) u_{\beta 1}^{(2)} + (E_{\alpha\beta 1} + \bar{C}_{\alpha\beta 1}) \rho_\beta^{(2)} + \bar{F}_{\alpha\beta 1} T_\beta^{(2)} = -i\omega F B_\alpha - F C_{\alpha 1} \quad (E-2)$$

Energy

$$(i \frac{2\omega}{\gamma} A_{\alpha\beta} + \bar{G} G_{\alpha\beta} + \bar{H} H_{\alpha\beta} + \bar{R} R_{\alpha\beta}) T_\beta^{(2)} - \bar{O} O_{\alpha\beta} f_\beta^{(2)} - \bar{R} \bar{B}_{\alpha\beta} H_\beta^{(2)} - (i2\omega S_{\alpha\beta} + T_{\alpha\beta}) \rho_\beta^{(2)} = -i\omega F D_\alpha + F E_\alpha \quad (E-3)$$

Species

$$(i2\omega A_{\alpha\beta} + \bar{G} G_{\alpha\beta} + \bar{O} O_{\alpha\beta}) f_\beta^{(2)} + \bar{H} H_{\alpha\beta} T_\beta^{(2)} + \bar{W}_{\alpha\beta} \rho_\beta^{(2)} = i\omega F G_\alpha + F H_\alpha \quad (E-4)$$

Radiation Function

$$\bar{R} \bar{C}_{\alpha\beta} T_\beta^{(2)} + (\bar{R} \bar{B}_{\alpha\beta} - A_{\alpha\beta}) H_\beta^{(2)} = -F Z_\alpha \quad (E-5)$$

Note that explicit forms of these matrices are shown in Appendix F.

(2) Boundary Conditions

Flame Edge

$$f_\beta^{(2)} = 0 \quad (E-6)$$

$$(i \frac{1}{\omega} A_\beta + B_\beta) T_\beta^{(2)} = \bar{A} \quad (E-7)$$

$$\bar{B} \bar{1}_\beta T_\beta^{(2)} + \bar{B} \bar{2}_\beta \rho_\beta^{(2)} = \bar{B} \quad (E-8)$$

$$B_\beta u_\beta^{(2)} = i\bar{H} \quad (E-9)$$

$$B_\beta v_\beta^{(2)} = i\bar{I} \quad (E-10)$$

where

$$A_\beta = \frac{\partial \phi_\beta}{\partial y} \Big|_{y=\ell^*} \quad (E-11)$$

$$B_\beta = \phi_\beta \Big|_{y=\ell^*} \quad (E-12)$$

$$\bar{B} \bar{1}_\beta = \rho^{(0)} \bar{B}_\beta \quad (E-13)$$

$$\bar{B} \bar{2}_\beta = T^{(0)} \bar{B}_\beta \quad (E-14)$$

$$\bar{A} = \frac{\gamma-1}{\gamma} [G1]_\beta B_\beta \quad (E-15)$$

$$\bar{B} = [G1 - \rho^{(1)} T^{(1)}]_\beta B_\beta \quad (E-16)$$

$$G1 = \cos K(x_o^* + x^*) \cos \theta + \cos K l^* \sin \theta \quad (E-17)$$

$$\bar{H} = -\frac{1}{\gamma M_b} [\sin K(x_o^* + x^*) \cos \theta]_\beta B_\beta \quad (E-18)$$

$$\bar{I} = -\frac{1}{\gamma M_b} \sin K l^* \sin \theta \quad (E-19)$$

Solid-Gas Interface

$$(E_B - F_B) f_B^{(2)} = \bar{C} \quad (E-20)$$

$$E_B u_B^{(2)} - \bar{C}_B T_B^{(2)} = \bar{D} \quad (E-21)$$

$$E_B v_B^{(2)} + \bar{D}_B T_B^{(2)} = \bar{E} + \bar{D} \quad (E-22)$$

$$(\bar{P}_B + i \frac{\bar{D}_B}{\omega}) T_B^{(2)} = i \bar{S} + \bar{T} \quad (E-23)$$

$$\bar{E}_{1B} \theta_B^{(2)} + \bar{E}_{2B} T_B^{(2)} = \bar{H} \quad (E-24)$$

where

$$E_B = \Phi_B \Big|_{y=0} \quad (E-25)$$

$$\bar{E}_{1B} = T^{(0)}(0) E_B \quad (E-26)$$

$$\bar{E}_{2B} = \rho^{(0)}(0) E_B \quad (E-27)$$

$$F_B = \frac{\partial \Phi_B}{\partial y} \Big|_{y=0} \quad (E-28)$$

$$\bar{C}_B = - \frac{u_c}{R_c} \frac{E_s}{\bar{T}_s} (C_3)^2 E_B \quad (E-29)$$

$$\bar{D}_B = \left\{ \frac{1}{\beta \omega} \frac{\bar{T}_s - T_\infty}{\zeta} \frac{E_s}{\bar{T}_s} - (E_s + 1) \right\} (C_3)^2 E_B \quad (E-30)$$

$$\bar{P}_B = \left\{ i \frac{b_1}{\zeta} + \frac{a_1}{\zeta} + L \frac{E_s}{\bar{T}_s} \right\} E_B - F_B \quad (E-31)$$

$$\bar{D}_B = \left\{ -i(a_1 - \frac{1}{\zeta}) + b_1 \right\} \frac{E_s}{\beta \bar{T}_s} \frac{\bar{T}_s - T_\infty}{\zeta \xi} E_B \quad (E-32)$$

$$\bar{C} = \left[\frac{\partial f^{(1)}}{\partial y} \frac{v^{(1)}}{\bar{T}_s} + 1 - \frac{T^{(1)}}{\bar{T}_s} \right] B_E B \quad (E-33)$$

$$\bar{D} = \frac{1}{\beta \omega} (C_3)^2 \frac{u_c}{R_c} \left[\left(\frac{E_s}{\bar{T}_s} T^{(1)} + \eta_s \right) \frac{\partial u^{(1)}}{\partial y} + C_3 \right] B_E \quad (E-34)$$

$$\bar{E} = - \frac{1}{\beta \omega} (C_3)^2 \left[\left(\frac{E_s}{\bar{T}_s} T^{(1)} + \eta_s \right) \frac{\partial v^{(1)}}{\partial y} + C_3 \frac{\bar{T}_s - T_\infty}{\zeta} \right] B_E \quad (E-35)$$

$$\bar{D} = (C_3)^2 \left[\bar{T}_s G_3 + G_4 \right] B_E \quad (E-36)$$

$$S = \frac{1}{\beta \omega} \frac{\bar{T}_s - T_\infty}{\zeta \xi} \left[(a_1 - \frac{1}{\zeta}) [G_3] B_E - \frac{1}{\beta \omega \zeta} b_1 [G_3] + \eta_s [G_3] \right] \quad (E-37)$$

$$T = - \frac{1}{\beta \omega} \frac{\bar{T}_s - T_\infty}{\zeta \xi} \left\{ b_1 [G_3] B_E + \frac{1}{\beta \omega \zeta} [a_1 - \frac{1}{\zeta}] [G_3] + \eta_s [G_3] - L [G_3] B_E \right\} \quad (E-38)$$

$$\bar{H} = [C_3 - c^{(1)} T^{(1)}] B_E \quad (E-39)$$

$$a_1 = \frac{1}{2\zeta} \left\{ 1 + (1 + 16\beta^2 \omega^2 \zeta^2)^{1/4} \cos \frac{\theta_p}{2} \right\} \quad (E-40)$$

$$b_1 = \frac{1}{2\zeta} \left\{ (1 + 16\beta^2 \omega^2 \zeta^2)^{1/4} \sin \frac{\theta_p}{2} \right\} \quad (E-41)$$

$$C_3 = \cos K(x_0^* + x^*) \cos \theta + \sin \theta \quad (E-42)$$

$$G_3 = 2\eta_s \frac{E_s}{\bar{T}_s} T^{(1)} + \eta_s (\eta_s - 1) + \left(\frac{E_s}{\bar{T}_s} T^{(1)} \right)^2 \quad (E-43)$$

$$G_4 = \frac{E_s}{\bar{T}_s} (T^{(1)})^2 + \left\{ - \frac{E_s}{\bar{T}_s^2} + (\eta_s - 1) \right\} T^{(1)} - \frac{(\eta_s - 1)}{\bar{T}_s} \quad (E-44)$$

Note that θ_p denotes the principal angle of the solid phase eigenfunction λ_1 .

Appendix F -
Matrices for Appendices E and F

$$\bar{A}_{\alpha\beta} = \rho^{(0)} A_{\alpha\beta}$$

$$\bar{B}_{\alpha\beta} = B_{\alpha\beta} + C_{\alpha\beta}$$

$$\bar{C}_{\alpha\beta i} = \rho^{(0)} C_{\alpha\beta i}$$

$$\bar{D}_{\alpha\beta} = \rho^{(0)} B_{\alpha\beta} + \rho^{(0)} C_{\alpha\beta} + \frac{4}{3} \Pr D_{\alpha\beta}$$

$$\bar{E}_{\alpha\beta i} = E_{\alpha\beta i} + \frac{T^{(0)}}{\gamma M_b} C_{\alpha\beta i}$$

$$\bar{F}_{\alpha\beta i} = \frac{\rho^{(0)}}{\gamma M_b^2} C_{\alpha\beta i}$$

$$\bar{G}_{\alpha\beta i} = \frac{T^{(0)}}{\gamma M_b^2} C_{\alpha\beta i}$$

$$\bar{G}_{\alpha\beta} = \frac{\rho^{(0)}}{\gamma} A_{\alpha\beta}$$

$$\bar{H}_{\alpha\beta} = \rho^{(0)} C_{\alpha\beta} + D_{\alpha\beta} - h \bar{H} H_{\alpha\beta}$$

$$\bar{O}_{\alpha\beta} = \frac{\gamma - 1}{\gamma} T^{(0)} A_{\alpha\beta}$$

$$\bar{P}_{\alpha\beta} = 2h w^{(0)} T^{(0)} A_{\alpha\beta}$$

$$\bar{Q}_{\alpha\beta} = \rho^{(0)} C_{\alpha\beta} + D_{\alpha\beta}$$

$$\bar{R}_{\alpha\beta} = w^{(0)} \left[\frac{E}{T^{(0)2}} - \frac{2}{T^{(0)}} + 2\rho^{(0)} \right] A_{\alpha\beta}$$

$$\bar{W}_{\alpha\beta} = 2w^{(0)} T^{(0)} A_{\alpha\beta}$$

$$\bar{G} G_{\alpha\beta} = \rho^{(0)} C_{\alpha\beta} + D_{\alpha\beta}$$

$$\bar{H} H_{\alpha\beta} = \bar{R}_{\alpha\beta}$$

$$\bar{O} O_{\alpha\beta} = h \bar{O} O_{\alpha\beta}$$

$$\bar{R} A_{\alpha\beta} = 4 \frac{1-\Omega}{N} T^{(0)} A_{\alpha\beta}$$

$$\bar{R} B_{\alpha\beta} = \frac{1}{4\pi} \frac{1-\Omega}{N} A_{\alpha\beta}$$

$$\bar{R} C_{\alpha\beta} = 4(1-\Omega) T^{(0)} Z_{\alpha\beta}$$

$$\begin{aligned}
\overline{RD}_{\alpha\beta} &= \frac{\Omega}{4\pi} Z_{\alpha\beta} \\
\overline{S}_{\alpha\beta} &= 2w^{(0)} T^{(0)} A_{\alpha\beta} \\
A_{\alpha\beta} &= \int_{\Omega} \phi_{\alpha} \phi_{\beta} d\Omega \\
B_{\alpha\beta} &= \int_{\Omega} u_{1,i}^{(0)} \phi_{\alpha} \phi_{\beta,i} d\Omega \\
C_{\alpha\beta} &= \int_{\Omega} u_{1,i}^{(0)} \phi_{\alpha} \phi_{\beta,i} d\Omega \\
C_{\alpha\beta i} &= \int_{\Omega} \phi_{\alpha} \phi_{\beta,i} d\Omega \\
D_{\alpha\beta} &= \int_{\Omega} \phi_{\alpha,j} \phi_{\beta,j} d\Omega \\
E_{\alpha\beta i} &= \int_{\Omega} u_{1,j}^{(0)} u_{1,i}^{(0)} \phi_{\alpha} \phi_{\beta} d\Omega \\
S_{\alpha\beta} &= \frac{\gamma-1}{\gamma} T^{(0)} A_{\alpha\beta} \\
T_{\alpha\beta} &= 2hw^{(0)} T^{(0)} A_{\alpha\beta} \\
Z_{\alpha\beta} &= 2 \int_{\Omega} \phi_{\beta} \phi_{\gamma} [RTT]_{\gamma} d\Omega' \int_{\Omega} \phi_{\alpha} d\Omega \\
RTT &= \int_0^{\pi/2} \frac{e^{-\tau/\cos\phi_z}}{\tau} d\phi_z \\
OO_{\alpha\beta} &= \frac{2w^{(0)}}{f^{(0)}} A_{\alpha\beta} \\
FA_{\alpha} &= - \int_{\Omega} [\rho^{(1)} u_{1,i}^{(1)} + \rho^{(1)} u_{1,i}^{(1)}]_{\gamma} \phi_{\gamma} \phi_{\alpha} d\Omega \\
FB_{\alpha} &= \int_{\Omega} [\rho^{(1)} u_{1,i}^{(1)}]_{\gamma} \phi_{\gamma} \phi_{\alpha} d\Omega \\
FC_{\alpha i} &= \int_{\Omega} \phi_{\gamma} [\rho^{(0)} u_{1,j}^{(1)} u_{1,j}^{(1)} + \rho^{(1)} u_{1,j}^{(0)} u_{1,j}^{(1)} \\
&\quad + \rho^{(1)} u_{1,j}^{(1)} u_{1,j}^{(0)} + \frac{1}{\gamma M_b} \rho^{(1)} T_{,i}^{(1)} \\
&\quad + \frac{1}{\gamma M_b^2} \rho^{(1)} T_{,i}^{(1)}]_{\gamma} \phi_{\alpha} d\Omega \\
FD_{\alpha} &= - \int_{\Omega} [\rho^{(1)} T_{,i}^{(1)}]_{\gamma} \phi_{\gamma} \phi_{\alpha} d\Omega \\
FE_{\alpha} &= \int_{\Omega} [hw^{(0)} \bar{X} - Y]_{\gamma} \phi_{\gamma} \phi_{\alpha} d\Omega \\
FG_{\alpha} &= - \int_{\Omega} [\rho^{(1)} f^{(1)}]_{\gamma} \phi_{\gamma} \phi_{\alpha} d\Omega \\
FH_{\alpha} &= - \int_{\Omega} [w^{(0)} \bar{X} + Z]_{\gamma} \phi_{\gamma} \phi_{\alpha} d\Omega \\
FZ_{\alpha} &= 12T^{(0)^2} \int_{\Omega} \phi_{\gamma} [RTT]_{\gamma} d\Omega' \int_{\Omega} \phi_{\eta} [T^{(1)^2}]_{\eta} \phi_{\alpha} d\Omega \\
\bar{X} &= \frac{ET^{(1)}}{(T^{(0)})^2} [2P^{(1)} - 2 \frac{T^{(1)}}{T^{(0)}} + 2 \frac{f^{(1)}}{f^{(0)}}] + 2\rho^{(1)} T^{(1)}
\end{aligned}$$

END

FILMED

10-85

DTIC